Nonlinear wave effects in laboratory plasmas: A comparison between theory and experiment

M. Porkolab

Department of Physics, Massachusetts Institute of Technology, Cambridge, Massachusetts 02139

R. P. H. Chang

Bell Laboratories, Murray Hill, New Jersey 07974

The rich nonlinear phenomena that occur in plasmas are reviewed in a systematic way. The foundations of turbulence theory (both weak and strong) and experiments performed in the past decade to verify such theories are presented. The aim is to emphasize those experiments that demonstrate clearly the validity (or failure) of some of the theories. In particular, we discuss experiments that demonstrate the validity and/or limits of weak turbulence theory, strong turbulence theory, parametric instabilities, echoes, trapping of particles in large-amplitude waves, and electrostatic ion acoustic shocks. We present concluding remarks in each section regarding the present status of each of these phenomenon.

CONTENTS

I. INTRODUCTION

By its very nature, plasma is a highly nonlinear dielectric medium. When permeated by an external magnetic field, it can support a multitude of electrostatic and electromagnetic waves, in the form of either thermal fluctuations or suprathermal turbulence. The latter may be generated by a variety of instabilities, which are usually present in a hot plasma, or may be induced by externally injected beams or microwave power. The waves (or fluctuations) may strongly interact and scatter each other. In addition, the turbulent fluctuations may strongly interact with charged particles and trap, accelerate, heat, or diffuse them. This is particularly true in hot plasmas where collisions are rare. Thus the macroscopic properties of hot plasmas will depend on collisionless, turbulent processes. By such processes nature attempts to establish thermodynamic equilibrium. In order for us to understand or predict the outcome of such processes, the underlying fundamental nonlinear mechanisms must be understood. This constitutes one of the central problems of modern plasma physics.

During the past decade, a significant growth in the field of nonlinear plasma physics has taken place. While initially most of the work done was theoretical, more recently experimental tests of these theories became available. In many cases the experimental tests led to improvements and/or modifications of the existing theories. In the present paper we wish to review some of these experiments and briefly outline the underlying theories. While a number of excellent books are already available on nonlinear plasma theory (Kadomtsev, 1965; Sagdeev and Galeev, 1969; Tsytovich, 1970, 1972; Davidson,

1972), there is as yet no comprehensive review of experimental nonlinear plasma physics. There are, however, some review articles on specific topics (Gentle, 1972; Porkolab, 1976). For the sake of completeness we shall try to incorporate these topics into the present article. The list of references given is representative, but not exhaustive. We also note that only experiments that can be explained by theory will be discussed in this paper (although some other experiments are listed as references).

Let us now discuss some of the fundamental properties of turbulence theories. We may define two parameters that are of importance (Drummond and Ross, 1973):

(i) $\epsilon_1 = W/nT$ defines the ratio of wave energy to thermal energy [where $W=(E_W^2+B_W^2)/8\pi$ plus particle kinetic energy; n is the particle density, and T is the temperature measured in units of energy].

(ii) $\epsilon_2=\tau_{ac}/\tau_{int}$ is the ratio of the autocorrelation time of the waves to the interaction time of waves and particles. We may then characterize turbulence as weak or strong, depending upon the values of ϵ_1 and ϵ_2. In particular, weak turbulence is defined as the state where $\epsilon_1 \ll 1, \epsilon_2 \ll 1$. The first of these conditions requires that the wave energy be smaller than the thermal energy. The second condition requires that the turbulence be characterized by the presence of a broad spectrum of small-amplitude waves which can be identified with the eigenmodes of the linear equations, and which produce relatively small deviations of the particles from their unperturbed orbits. Assuming the random-phase approximation (i.e., the "golden rule"), a perturbation theory has been developed to describe this state. All other regimes are characterized as strong turbulence and/or strongly nonlinear waves; for example, if $\epsilon_1 \gtrsim 1$, we have large-amplitude turbulent fluctuations and if $\epsilon_2 \gtrsim 1$, we are dealing with a large-amplitude single wave. Particles may be trapped in the troughs of the waves, and the state cannot be described by a perturbation expansion. In addition, the large-amplitude wave may decay into other waves, and on a longer time scale may thus produce a broad spectrum. Weak-turbulence theory is well developed (up to fourth order in the electric field amplitudes), but its validity depends upon very stringent conditions, and hence only a few very careful and delicate experiments are able to satisfy them. In general, it is easier to produce strong turbulence experimentally. Strong turbulence may be defined as a "stochastic collection of nonlinear eigenmodes." However, in the absence of rigorous theories, it is not easy to know what physical quantities one should measure in such an experiment. It is hoped that theories of strong turbulence and experimental measurements will be developed together. In any case, it is likely that different ways of producing turbulence will require different theoretical approaches for a full explanation. It is also likely (or at least hoped) that computer simulation will aid considerably in a complete understanding of strong turbulence.

Let us now examine in more detail ϵ_2, the ratio of the autocorrelation time $\tau_{ac}=[k\Delta(\omega/k)]^{-1}$ and the interaction time τ_{int}. The autocorrelation time is the duration during which a particle feels a force exerted by the waves with wave number $k\pm\Delta k$. On the other hand, we may define $\tau_{int}=\min(\tau_{tr},\tau_D)$, where $\tau_{tr}=(m/e\phi)^{1/2}/k=(m/(ekE_k))^{1/2}$ is the trapping time, and $\tau_D=(k^2D)^{-1/3}$ is the diffusion time. Thus we see that the trapping time is the period of oscillation of a particle with velocity $v=\omega/k$, in the trough of a wave of frequency ω and wave number k. If $\tau_{ac} \ll \tau_{tr}$, a particle is unable to decide whether it is trapped or not. So, instead, it undergoes a random walk in velocity space, diffusing with a characteristic time scale τ_D. As we shall see later $D \propto \tau_{ac} W$, and so $\tau_D \propto \tau_{tr}^{4/3}/\tau_{ac}^{1/3}$, or $\tau_{ac}^{4/3}/\tau_{tr}^{4/3} \propto \tau_{ac}/\tau_D$. Thus the condition $\tau_{ac} \ll \tau_{tr}$ means $\tau_{ac} \ll \tau_D$, so that the diffusion must be slow compared with the loss of wave correlation.

We note that in some experiments, such as in a beam-plasma system, large-amplitude waves exist for several τ_{tr} times, and then we may have to talk about "coherent turbulence." Also, in the case of parametric instabilities due to a long-wavelength pump wave with a small wave number, τ_{tr} is long, and we may have $\epsilon_2 < 1$ while $\epsilon_1 \gtrsim 1$. Again, we expect strong turbulence due to an initially coherent pump wave. On the other hand, if $\epsilon_1 \ll 1$ (small-amplitude pump wave) we can deal with the system by perturbation techniques. Thus there are additional cases one has to consider when at least one large-amplitude wave is present in the system. Such single, large-amplitude waves may also modify the plasma equilibrium itself by the ponderomotive force: this may lead to filamentation and/or soliton formation. This again requires a different theoretical treatment. Thus we wee that the "turbulent" state of plasma may contain both coherent large-amplitude waves and random-phase turbulence. Furthermore, particles will interact with this system of waves in various ways. Our aim here is to present experimental data demonstrating the existence of some of these phenomena under actual laboratory conditions. Clearly, a complete understanding of plasma turbulence will require much more work, both theoretically and experimentally, than has been done up until now. Let us now outline some of the topics which we shall discuss in this paper.

First, in Sec. II we shall discuss weak-turbulence theory and some relevant experiments. In particular, we shall cover quasilinear effects, mode-mode coupling, and nonlinear Landau damping. In Sec. III we cover plasma wave echoes. In Sec. IV we discuss parametric instabilities and solitons. In Sec. V we present attempts at improving weak-turbulence theory by "renormalization," namely, orbit diffusion and the concept of "clumps." In Sec. VI we present results concerning large-amplitude waves and trapping, and in Sec. VII we discuss some experiments on ion acoustic shocks. We have deliberately avoided or discuss only briefly experiments that (in our opinion) are not yet well understood in terms of quantitative comparison with theories (e.g., nonlinear drift waves, turbulent resistivity experiments, nonlinear tearing modes, magnetic reconnection, etc.).

II. WEAK-TURBULENCE THEORY AND EXPERIMENTS

A. Foundations of weak-turbulence theory

The first comprehensive theory of plasma turbulence, what we today call "weak-turbulence theory," was devel-

oped more than a decade ago (Vedenov *et al.*, 1962; Drummond and Pines, 1962; Aamodt and Drummond, 1964, 1965; Dikasov *et al.*, 1965; Aamodt and Sloan, 1967; Ross, 1969; Nishikawa, 1970; Dum and Ott, 1971). Only recently have experimental tests of these theories become available (Cano *et al.*, 1967; Ellis and Porkolab, 1968; Porkolab and Chang, 1969; Chang and Porkolab, 1970(a), 1970(b); Gentle and Malein, 1971; Gentle and Roberson, 1971; Roberson *et al.*, 1971; Franklin *et al.*, 1971; Chang and Porkolab, 1972). Weak-turbulence theory assumes a set of random waves making wave packets, each satisfying a linear dispersion relation, weakly interacting among themselves and with background particles. It consists of the following identifiable processes:

A. Quasilinear theory
B. Resonant mode–mode coupling
C. Nonresonant mode–mode coupling (or nonlinear Landau damping)
D. Four-wave scattering.

Note that in the random-phase approximation process (A) contains terms up to $|E|^2$ in the electric field amplitudes, processes (B) and (C) contain terms of the order of $|E|^4$, and process (D) contains terms of order $|E|^6$. When we consider coherent waves, it turns out that process (B) changes considerably; in particular, for coherent waves it becomes of order $|E|^2$, whereas process (C) remains of order $|E|^4$ (where in each case we assume proper normalization to the thermal energy). Physically, process (A) takes into account the linear stage of the instability, including modification of the background equilibrium distribution function, due to the presence of the fluctuations. Process (B) considers transformation and scattering of wave packets among themselves, while process (C) takes into account nonlinear scattering of waves and particles. Higher-order effects, such as frequency shifts, are taken into account by process (D). Some of these processes are illustrated in Fig. 1 in terms of the Feynman diagrams. We must emphasize that in all of these calculations, in the integrations over velocity space, unperturbed particle orbits are used. Only in more modern theories, which we discuss in the next section, are orbit perturbations included.

Let us now outline how the foregoing processes are calculated in weak-turbulence theories. This can be done by a rigorous multiple time scale expansion (Davidson, 1968, 1969, 1972) or a WKB-type solution (Aamodt and Drummond, 1964; Aamodt, 1965). We shall start from the Vlasov equation and Poisson's equation, and assume electrostatic perturbations only

$$\frac{\partial f}{\partial t}+\mathbf{v}\cdot\frac{\partial f}{\partial \mathbf{x}}+\frac{q_j}{m_j}\frac{(\mathbf{v}\times\mathbf{B})}{c}\cdot\frac{\partial f}{\partial \mathbf{v}}+\frac{q_j}{m_j}\mathbf{E}\cdot\frac{\partial f}{\partial \mathbf{v}}=0\,, \tag{2.1}$$

$$\nabla\cdot\mathbf{E}=4\pi\sum_j q_j\int d^3v f(\mathbf{v})\,, \tag{2.2}$$

where B is the external magnetic field, f is the particle distribution function, q_j is the charge of particles of species j, and m_j is the particle mass. Let us now expand terms in a Fourier series

$$E(\mathbf{x},t)=\sum_k E_k\exp[i(\mathbf{k}\cdot\mathbf{x}-\omega t)]\,, \tag{2.3}$$

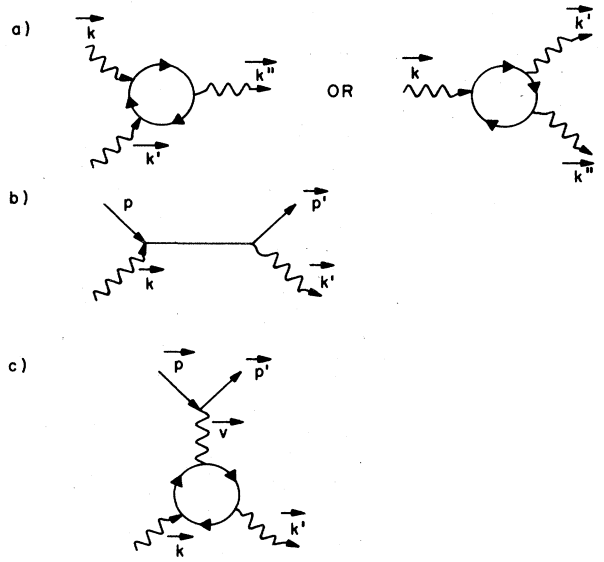

FIG. 1. Feynman diagrams of (a) resonant mode-mode coupling, (b) nonlinear wave-particle (Compton) scattering, (c) scattering from a shielded (dressed) particle.

$$f(\mathbf{x},t)=g(\mathbf{x},t)+\sum_{k\neq 0}f_{\mathbf{k}}\exp[i(\mathbf{k}\cdot\mathbf{x}-\omega t)]\,, \tag{2.4}$$

where in the last expression we separated the $k=0$ term. In the following we shall ignore the external magnetic field, and assume one-dimensional perturbations only. The techniques outlined below can easily be extended to more complicated systems where the magnetic field plays an important role (Aamodt, 1965; Rosenbluth *et al.*, 1969; Porkolab and Chang, 1972; Johnston, 1976).

B. Quasilinear theory

Substituting Eqs. (2.3) and (2.4) into (2.1) and (2.2), we get

$$\frac{\partial g}{\partial t}=\frac{-q_j}{m_j}\sum_{k'}E_{-k'}\frac{\partial f_{k'}}{\partial v}\,, \tag{2.5}$$

$$\frac{\partial f_k}{\partial t}+v\frac{\partial f_k}{\partial x}+\frac{q_j}{m_j}E_k\frac{\partial g}{\partial v}=\frac{-q_j}{m_j}\sum_{k\neq 0}E_{k-k'}\frac{\partial f_{k'}}{\partial v}\,, \tag{2.6}$$

$$ikE_k=4\pi\sum_j q_j\int dv f_k\,, \tag{2.7}$$

where in Eq. (2.6) the $k=0$ term has been separated out again. Substituting Eq. (2.6) into (2.5) gives us to order $|E_k|^2$ the quasilinear diffusion equation

$$\frac{\partial g}{\partial t}=\frac{\partial}{\partial v}D\frac{\partial g}{\partial v}\,, \tag{2.8}$$

where

$$D=\left(\frac{q_j}{m_j}\right)^2\sum_{k'}\frac{|E_{k'}|^2}{(ik'v-i\omega)} \tag{2.9}$$

is the diffusion coefficient. Treating the singularity by

the usual techniques, i.e.,

$$\lim_{\delta\to 0+}\frac{1}{\omega_k - kv + i\delta} = \frac{P}{\omega_k - kv} - i\pi\delta(\omega_k - kv)\,, \tag{2.10}$$

where P designates the principle part, and δ designates the Dirac delta function. We can split Eq. (2.9) into two parts, namely one that corresponds to resonant particles

$$D_R = 8\pi\left(\frac{q}{m}\right)^2 \int dk \epsilon_k \pi\delta(\omega - kv)\,, \tag{2.11a}$$

and one that is associated with nonresonant particles (i.e., "sloshing" energy)

$$D_{NR} = 8\pi\left(\frac{q}{m}\right)^2 \int dk\, \frac{\epsilon_k \gamma_k}{(\omega - kv)^2}\,, \tag{2.11b}$$

where $\epsilon_k = |E_k|^2/8\pi$ is the wave energy. In the usual case Eq. (2.11a) is used in conjunction with Eq. (2.8) and the WKB equation

$$\partial\epsilon_k/\partial t = 2\gamma_k\epsilon_k. \tag{2.11c}$$

These equations describe the diffusion of the resonant particles in the background distribution function due to the presence of the waves.

C. Mode-mode coupling

Let us now continue with our calculation of the higher-order wave scattering terms. In the WKB sense (Aamodt, 1965) we shall consider $g(v,t)$ stationary on this time scale. Expanding $f_k(v,\omega)$ and $E_k(\omega)$ by a perturbation series, and using the electrostatic assumption

$$E_k = -\nabla\phi_k = -ik\phi_k\,, \tag{2.12}$$

where $\phi_{-k} = \phi_k^*$ and $\omega_{-k} = -\omega_k^*$ (i.e., the reality conditions), we obtain an iterative solution of Eqs. (2.6) and (2.7):

First-order solution:

$$\epsilon(\omega,k)\phi_k^{(1)}(t) = 0. \tag{2.13}$$

Second-order solution:

$$\epsilon(\omega,k)\phi_k^{(2)}(t) = -\sum_j\sum_{k'}\frac{4\pi q^3 n_0}{k^2m^2}\int d^3v\int_0^\infty d\tau\int_0^\infty d\tau' G_k(\tau)\left[(k-k')\frac{\partial}{\partial v(\tau)}G_{k'}(\tau')k'\frac{\partial g}{\partial v(\tau')} + k'\frac{\partial}{\partial v(\tau)}G_{k-k'}(\tau')(k-k')\frac{\partial g}{\partial v(\tau')}\right]\phi_{k'}\phi_{k-k'}\,. \tag{2.14}$$

Third-order solution:

$$\begin{aligned}\epsilon(\omega,k)\phi_k^{(3)}(t) = -\sum_j\sum_k\frac{4\pi q^3 n_0^2}{k^2m^2}\int d^3v\Bigg(&\int_0^\infty d\tau\int_0^\infty d\tau' G_k(\tau)(k-k')\frac{\partial}{\partial v(\tau)}G_{k'}(\tau')\,k'\frac{\partial g}{\partial v(\tau')}\left[\phi^{(2)}_{k-k'}\phi_{k'} + \phi_{k-k'}\phi^{(2)}_{k'}\right]\\ &+\sum_{k''}\frac{iq}{m}\int_0^\infty d\tau\int_0^\infty d\tau'\int_0^\infty d\tau''\, G_k(\tau)(k-k')\frac{\partial}{\partial v(\tau)}G_{k'}(\tau')(k'-k'')\\ &\times\frac{\partial}{\partial v(\tau')}G_{k''}(\tau'')k''\,\frac{\partial g}{\partial v(\tau'')}\phi_{k-k'}\phi_{k'-k''}\phi_{k''}\Bigg).\end{aligned} \tag{2.15}$$

Here $G_k(\tau)$ is the propagation operator (Green's function), which in the weak-turbulence approximation is given by unperturbed orbits, i.e.,

$$G_k(\tau) = \exp[ik(x'-x) + \omega\tau]\,, \tag{2.16}$$

where

$$x' = x - v\tau,\quad \tau = t - t'. \tag{2.17}$$

Here $\epsilon(\omega,k)$ is the linearized quasilinear dispersion relation, namely,

$$\epsilon(\omega,k) = 1 + \sum_j\frac{\omega_p^2}{k^2}\sum_{m=-\infty}^{\infty}\int_{-\infty}^{\infty} dv\frac{\partial g/\partial v}{(\omega - kv)}, \tag{2.18}$$

where again the $\omega = kv$ singularity is to be treated according to Eq. (2.10). In Eq. (2.14) there are two types of terms: namely, those associated with resonant mode–mode coupling [i.e., $\epsilon_R(\omega,k) = 0$] and those due to nonresonant wave–wave scattering [i.e., $\epsilon(\omega,k) \neq 0$]. The latter are also called "virtual" waves, and more recently the name "quasimodes" has also been applied in connection with parametric instabilities. In obtaining a wave kinetic equation valid up to fourth order on ϕ_k, we substitute the appropriate expressions for virtual waves, $\phi_{k'}^{(2)}$ and $\phi_{k-k'}^{(2)}$ from Eq. (2.14) into Eq. (2.15). Then assuming a resonant wave at (ω,k) on the left-hand side, we expand the dielectric function $\epsilon(\omega,k)$. Using the WKB result, $\gamma\phi \simeq \partial\phi/\partial t$ (Aamodt, 1965), we obtain the

following equation:

$$\frac{\partial\epsilon(\omega,k)}{\partial\omega}\frac{\partial\phi_k(t)}{\partial t}=\gamma_k\frac{\partial\epsilon(\omega,k)}{\partial\omega}\phi_k+\sum_{k'} iQ_{k-k',k'}\phi_{k-k'}\phi_{k'}$$

$$+\mathrm{Im}[P_{k,k'}\phi_k|\phi_{k'}|^2+R_{k,k-k'}\phi_k|\phi_{k-k'}|^2+S_{k,k-k'}\phi_k|\phi_{k-k'}|^2], \tag{2.19}$$

where the term proportional to $Q_{k-k',k'}$ represents resonant mode–mode coupling, and the terms proportional to P,R,S represent nonlinear Landau damping.

D. Resonant mode-mode coupling

Let us first discuss the mode–mode coupling term $Q_{k-k',k'}$. To obtain a wave kinetic equation we have to distinguish between fixed phase waves and incoherent waves, and we shall treat them separately.

1. Fixed phase waves

For fixed phase waves the following equations govern three-wave coupling:

$$iS_k(dA_k/dt)=V_{k,k',k''}A_{k'}A_{k''}\,, \tag{2.20a}$$

$$iS_{k'}(dA_{k'}/dt)=V^*_{k,k',k''}A_kA_{-k''}\,, \tag{2.20b}$$

$$iS_{k''}(dA_{k''}/dt)=V^*_{k,k',k''}A_kA_{-k'}\,, \tag{2.20c}$$

where we have defined

$$A_k(t)=\phi_k(t)[(k^2/8\pi)\,|\partial\epsilon/\partial\omega|]^{1/2} \tag{2.21a}$$

and

$$s_k=\mathrm{sign}(\partial\epsilon_k/\partial\omega_k). \tag{2.21b}$$

The definition of the matrix element $V_{k,k',k''}$ follows from a calculation of Q in Eq. (2.19), and in an unmagnetized plasma it is given by

$$V_{k,k',k''}=\frac{1}{H}\sum_j\frac{4\pi e_j^3}{m_j^2}\int_{-\infty}^{\infty}d^3v\,\frac{1}{\omega_1-k_1v+i\delta}\times\left[k_2\frac{\partial}{\partial v}\frac{k_3\partial f_{j0}/\partial v}{\omega_3-k_3v+i\delta}+\left(\begin{matrix}k_2\rightarrow k_3\\ \omega_2\rightarrow\omega_3\end{matrix}\right)\right]_{\delta\to 0^+}, \tag{2.22}$$

where

$$H=16\pi\left|\frac{k^2}{8\pi}\frac{\partial\epsilon_k}{\partial\omega_k}\frac{k'^2}{8\pi}\frac{\partial\epsilon_{k'}}{\partial\omega_{k'}}\frac{k''^2}{8\pi}\frac{\partial\epsilon_{k''}}{\partial\omega_{k''}}\right|^{1/2}.$$

Here we assumed that the selection rules

$$\Delta\omega=-\omega_k+\omega_{k'}+\omega_{k''}=0\,, \tag{2.23}$$

$$\Delta k=-k+k'_k+k''=0\,,$$

are satisfied. One can also show that the following symmetry relations are satisfied

$$V_{k,k',k''}=V_{k,k'',k'}=V_{-k,-k',-k''}\,, \tag{2.24a}$$

$$V_{k,k',k''}=V_{-k',-k,k''}=V_{-k'',k',-k}.$$

From the foregoing relationships a number of conservation laws can be deduced. In particular, the sum of wave energy W and momentum P is conserved in the scattering process

$$\frac{d}{dt}\sum_k W_k=0;\quad \frac{d}{dt}\sum_k P_k=0; \tag{2.25}$$

where

$$W_k=\omega_k s_k N_k,\quad P_k=s_k kN_k\,, \tag{2.26}$$

and where $N_k=|A_k|^2$ is the occupation number density.

Let us now consider the stability of the three-wave system. This can be studied by rewriting Eqs. (2.20a)–(2.20c) in the following form:

$$d^2A_k/dt^2=-|V_{k,k',k''}|^2(s_ks_{k'}|A_{k''}|^2+s_ks_{k''}|A_{k'}|^2)A_k\,, \tag{2.27a}$$

$$d^2A_{k'}/dt^2=-|V_{k,k',k''}|^2(s_{k'}s_k|A_{k''}|^2-s_{k'}s_{k''}|A_k|^2)A_{k'}\,, \tag{2.27b}$$

$$d^2A_{k''}/dt^2=-|V_{k,k',k''}|^2(s_{k''}s_k|A_{k'}|^2-s_{k'}s_{k''}|A_k|^2)A_{k''}\,. \tag{2.27c}$$

It is easy to show from Eqs. (2.27) that if at least one (but not all) of the waves is negative energy (i.e., $s<0$) explosive instability results. This means that for nontrivial initial conditions, all amplitudes $A_k,A_{k'},A_{k''}$ grow without bound (i.e., to infinite level) within a finite time. Sometimes this is also called the "nonlinear instability." We note that such an instability may occur even if linearly the system (i.e., each individual wave) is stable. On the other hand, if all waves are either positive energy or negative energy, nonlinear stability results. However, if at least one of the waves is considerably larger than the other two waves (i.e., a "pump" wave), initially a decay instability may result: namely, the other two waves will grow exponentially in time until pump depletion occurs. This is a complete analog of parametric instabilities discussed in more detail in a separate section. However, here the pump wave is an

electrostatic wave with a finite k_0. For example, if in Eq. (2.27) at $t=0$

$$0<|A_{k'}|^2 \ll |A_k|^2,$$

$$0<|A_{k''}|^2 \ll |A_k|^2,$$

and $\omega_k=\omega_0>(\omega_{k'},\omega_{k''})$, then near $t\gtrsim 0$, Eqs. (2.27) reduce to

$$\frac{1}{|A_{k'}|^2}\frac{d^2|A_{k'}|^2}{dt^2}\cong |V_{k,k',k''}|^2|A_k|^2, \tag{2.28a}$$

$$\frac{1}{|A_{k''}|^2}\frac{d^2|A_{k''}|^2}{dt^2}\cong |V_{k,k',k''}|^2|A_k|^2, \tag{2.28b}$$

which shows exponential growth (initially) of $|A_{k'}|^2$, $|A_{k''}|^2$; clearly, $|A_k|^2$ acts as a pump wave. Note that the growth rate is

$$\gamma\propto |V_{k,k',k''}||A_0| \tag{2.29}$$

as in the case of resonant parametric decay instability.

On a larger time scale, as $A_{k'}, A_{k''}$ grow and become comparable to A_k, a more exact solution of Eq. (2.27) is needed. This can be best obtained by introducing the relative phases of the waves in Eqs. (2.20a)–(2.20c). The solutions are obtained in terms of elliptic integrals (Sagdeev and Galeev, 1969) which predict a cylical exchange of wave energies among the three waves. The characteristic period of pump depletion is given by

$$t_0\simeq\frac{1}{2V_{k,k',k''}|A_0|}\ln\frac{A_0(0)}{A_1(0)} \tag{2.30a}$$

so that within a numerical factor $t_0\propto\gamma^{-1}$. Similarly, if a negative energy wave exists in the system, the "explosion" time is

$$t_0\simeq\frac{1}{|A_0|V_{k,k',k''}}. \tag{2.30b}$$

2. Random-phase waves

To obtain a wave kinetic equation for random-phase waves, we multiply Eq. (2.19) on the left-hand side by ϕ_k^*, and apply the random-phase approximation. This is equivalent to saying that in an ensemble of systems the only difference among wave packets is in the phases, that an average over those phases yields a nonzero value only to products of the form

$$\langle\phi_k\phi_k^*\rangle=|\phi_k|^2\delta(k-k'), \tag{2.31}$$

and that

$$\langle\phi_k\rangle=0.$$

In particular, $|k\phi_k|^2$ measures the spectral density of the mean energy of the electric field in the wave packet

$$\langle E^2\rangle=\int|A_k|^2dk=\int N_k dk,$$

where A_k and N_k have been defined earlier. Using time-dependent perturbation theory, after a considerable amount of algebra (Rosenbluth *et al.*, 1969), the following kinetic equation is obtained

$$\frac{d}{dt}N_k=4\pi_{k'}\sum_{k'}|V_{k,k',k''}|^2\delta_{k,k'+k''}\delta(\omega_k^\alpha-\omega_{k'}^\beta-\omega_{k''}^\gamma)$$

$$\times[N_{k'}N_{k''}-N_kN_{k''}S_kS_{k'}-N_kN_{k'}S_kS_{k''}]+2\gamma_kN_k \tag{2.32}$$

where $2\gamma_kN_k$ is due to quasilinear growth. Equation (2.32) may be repeated for $N_{k'}$ and $N_{k''}$ by rotating indices. We note that the terms $N_kN_{k''}$ and $N_kN_{k'}$ on the right-hand side are due to spontaneous emission, and for an unstable system may be neglected. Unfortunately, in three dimensions an exact solution of Eq. (2.32) does not exist. We note, however, the work of Vedenov and Rudakov (1965) and Davidson and Goldman (1968), who attempted an approximate three-dimensional solution of the interaction of two electron plasma waves in an ion wave background, which reduced to a diffusion equation. On the other hand, in one dimension Davidson (1972) presents a solution which predicts that if all three waves are positive energy waves the system is nonlinearly stable. Again, similarly to fixed phase waves, if one packet is considerably larger than the others it tends to decay with a characteristic time scale $\tau\propto|V_{k,k',k''}|^{-2}$, while the other waves grow so that a new equilibrium state is achieved. However, oscillating solutions, as in the case of fixed phase waves, do not exist. Similarly to fixed phase waves, if one of the wave packets is negative energy, nonlinear ("explosive") instability results. The explosion time is $\tau\propto|V_{k,k',k''}|^{-2}$ (unlike fixed phase waves). In general, for wave packets the same conservation relations and symmetry relations hold as for fixed phase waves.

E. Nonlinear Landau damping

The kinetic equations governing nonlinear Landau damping are obtained from the last three terms (P,R,S) of Eq. (2.19). In particular, by multiplying Eq. (2.19) by ϕ_k^*, and averaging over phases we obtain the following kinetic equations

$$dN_k/dt=2\gamma_kN_k+\sum_{k''}S_kL_{k,k''}N_kN_{k''}, \tag{2.33a}$$

$$dN_{k''}/dt=2\gamma_{k''}N_{k''}-\sum_{k''}S_{k''}L_{k,k''}N_kN_{k''}. \tag{2.33b}$$

For an unmagnetized plasma we have the following expression for the matrix element

$$L_{k,k''}=\sum_j\int d^3v\,2\pi\,\delta(\omega'-k'v)\frac{\omega_{pj}^2}{k'^2}\left|\frac{\partial\epsilon(\omega',\vec{k}')}{\partial\omega'}\right|k'\frac{\partial g}{\partial v}\tilde{L}_{k,k''}, \tag{2.34a}$$

where

$$\tilde{L}_{k,k''}=\left|\frac{2V_{k,k'',k'}}{\epsilon(\omega',k')}-\frac{2e_j^2k'^2(kk'')}{m_j(\omega-kv)(\omega''-k''v)H}\right|, \tag{2.34b}$$

and where $V_{k,k'',k'}$ and H have been defined earlier in Eq. (2.22). Note that by assumption $\omega\neq kv$, $\omega''\neq k''v$, and the selection rules are

$$\omega - \omega'' - (k - k'')v = 0, \tag{2.35a}$$

$$\omega' = \omega - \omega'', \quad k' = k - k''. \tag{2.35b}$$

This result was obtained in this form by Sloan and Drummond (1970). We note that exactly the same kinetic equations are obtained for fixed phase waves (Porkolab and Chang, 1972). Assuming two narrow packets, Eqs. (2.33a) and (2.33b) can be solved for $\gamma_k = \gamma_{k''}$ and the result is

$$N_k(t) = \frac{\exp\{2\gamma_k t - Z[1 - \exp(2\gamma_k t)]\}}{1 + [S_{k''}N_k(0)/(N_{k''}(0) + S_{k''}N_k(0))](\exp[-L(1 - \exp(2\gamma_k))] - 1)} \tag{2.36}$$

where

$$Z = (L_{k,k''}/2\gamma_k)(N_{k''}(0) + S_{k''}N_k(0))$$

It is easy to see that for one negative energy wave (i.e., $S_{k''} = -1$) and one positive energy wave (i.e., $S_k = 1$) and $L_{k,k''} > 0$ explosive instability results at time

$$t_e^* = \frac{1}{2\gamma_k} \ln\left[1 + \frac{2\gamma_k \ln(N_{k''}(0)/N_k(0))}{L_{k,k''}(N_{k''}(0) - N_k(0))}\right]. \tag{2.37}$$

Note that in the limit $\gamma_k = \gamma_{k''} = 0$,

$$t_e^* = \frac{\ln(N''(0)/N(0))}{L_{k,k''}(N''(0) - N(0))}.$$

It can be shown that energy and momentum are conserved only if the particles are included in the system; this is a consequence of Eq. (2.35).

Let us now discuss Eq. (2.34) in more detail. As we see, there are two terms in Eq. (2.34b): the first term represents scattering of a wave from the screened potential of a charged particle [the shielding term is proportional to $\epsilon(\omega', k')^{-1}$], and the second term corresponds to four-wave scatter from a bare particle (or Compton scattering). These terms tend to cancel, except for short-wavelength waves [i.e., terms often cancel to $0(k^2\lambda_D^2)$, and the first surviving term is of $0(k^4\lambda_D^4)$; Aamodt and Drummond, 1966; Sloan and Drummond, 1970; Drummond and Sloan, 1971; Ott and Dum, 1971].

Another case when the terms do not cancel is in a magnetic field, where the waves propagate almost perpendicularly to the magnetic field and have short wavelengths, of order $k_\perp r_c \simeq 1$, where $r_c = v_t/\Omega$ is the Larmor radius of particles. For such a case the matrix element is given by Rosenbluth *et al.* (1969) and Porkolab and Chang (1972) as follows:

$$L^l_{k,k''} = \sum_j \frac{4\pi\omega_p^4 I\Omega}{|\partial\epsilon/\partial\omega||\partial\epsilon/\partial\omega''|M_j n_0} \tilde{L}^l_{k,k''}, \tag{2.38a}$$

where

$$\tilde{L}^l_{k,k''} = \sum_{s,p}\left(\int_0^\infty dv_\perp \frac{\partial g}{\partial v_\perp} \frac{J_s(x)J_p(x'')J_{s-m}(x'')J_{p-m}(x'')}{[(\omega - s\Omega)^2 - \Omega^2][(\omega - p\Omega)^2 - \Omega^2]} - \frac{\left(\int_0^\infty dv_\perp \frac{\partial g}{\partial v_\perp} \frac{J_m(x')J_{s-m}(x'')J_s(x)}{(\omega - s\Omega)^2 - \Omega^2}\right)\left(\int_0^\infty dv_\perp \frac{\partial g}{\partial v_\perp} \frac{J_m(x')J_{p-m}(x'')J_p(x)}{(\omega - p\Omega)^2 - \Omega^2}\right)}{\int_0^\infty dv_\perp \frac{\partial g}{\partial v_\perp} J_m^2(x')}\right). \tag{2.38b}$$

Here j represents particle species, l, m, s, p represent integers, J's are the ordinary Bessel functions, M is the particle mass, n_0 is the density, $x = k_\perp v_\perp/\Omega$, and ω_p is the angular plasma frequency. Chang and Porkolab (1970) have verified Eq. (2.38b) experimentally.

Finally, we note that the effect of nonlinear Landau damping upon the distribution function is similar to Landau damping, namely diffusion. In general, the total diffusion is the sum of quasilinear diffusion, as given by Eqs. (2.8) and (2.11b), and nonlinear diffusion. For example, for an unmagnetized plasma in one dimension, the nonlinear Landau damping diffusion coefficient D_{NLD} can be written as follows:

$$D_{\mathrm{NLLD}} = \frac{4\pi}{M^2}\int d^3k \int d^3k'' \frac{N_k N_{k''} 4\pi\omega_p^4 k(\omega' - kv')}{|\partial\epsilon/\partial\omega||\partial\epsilon/\partial\omega''|k^2k''^2Mn_0}\left|\frac{kk''}{(\omega - kv)^2} - \frac{H^2 V_{k,k'',k} n_0}{k'^2 eM}\right|^2 \tag{2.39}$$

where all the symbols have been defined earlier.

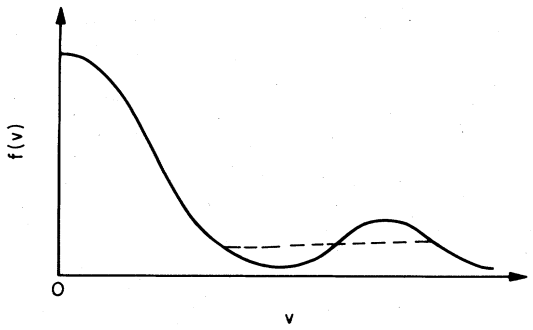

FIG. 2. Electron distribution function with a "gentle bump" on the tail. The solid line is the initial distribution, and the dashed line is the final state.

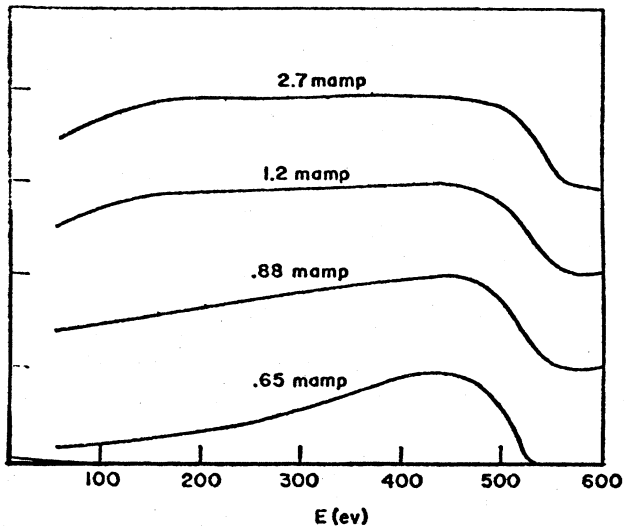

FIG. 4. Electron distribution function after the beam has traversed the plasma column. Only the beam electrons are collected. (After Roberson *et al.*, 1971.)

F. Experiments on quasilinear effects

The first quantitative test of quasilinear theory was carried out by Roberson *et al.*, (1971) and Arunasalam *et al.* (1971). These authors studied the saturation of an unstable spectrum of electron plasma waves excited by a "gentle bump" on the tail of the electron distribution function. Such a distribution function, which is shown in Fig. 2, was used in the theoretical papers of Drummond and Pines (1962) and Vedenov *et al.*, (1962) to study the growth and eventual saturation of electron plasma waves in a low-density beam-plasma system ($n_b \ll n_0$). According to the theory of Landau (1946), electron plasma waves with phase velocities coinciding with the positive slope of the beam part grow until their amplitude is sufficiently large to cause appreciable diffusion, thereby reducing the slope (and hence the growth rate, which is proportional to $\partial g/\partial v$). The wave growth and diffusion continue until $\partial g/\partial v = 0$ (dashed curve). Although the growth rate becomes zero, the diffusion coefficient remains large because the electric fields are still present. Experimentally, the beam is injected into a plasma column from one end, and the instability grows spatially (rather than in time) along the length of the column. As the beam particles diffuse, the growth rate is reduced until saturation occurs. In Fig. 3 we show the results of Roberson *et al.* (1971). As the beam current (density) is increased, saturation occurs in increasingly shorter distances. In Fig. 4 the tail of the associated electron dis-

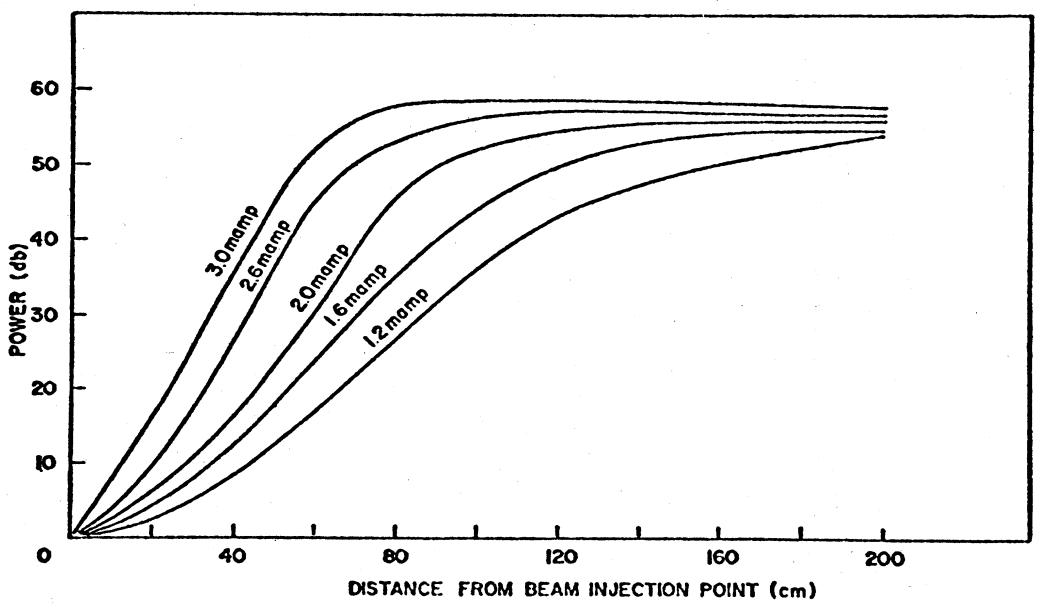

FIG. 3. Total wave energy as a function of distance from the point of beam injection for different beam currents, $n_e = 1.3 \times 10^9$ cm^{-3}, $T_e = 15$ eV, $V = 500$ V. (After Roberson *et al.*, 1971.)

tribution is shown, demonstrating the flattening of the "gentle bump" as the beam density (current) is increased so that saturation occurs within the length of the machine. Both the absolute magnitude of the saturated wave energy and the shape of the spectrum $E^2(\omega)$ were found to agree with theoretical predictions.

In the experiments of Arunasalam *et al.* (1971) a relatively monoenergetic beam was injected at one end of a linear device; thus, initially, quasilinear theory would not hold. However, after the instability develops, the beam energy should spread, and according to the theory of Shapiro (1963) the beam spread should be sufficiently large for the quasilinear theory to hold. Arunasalam *et al.* (1971) used elegant microwave scattering techniques to detect the spectrum of unstable waves along the plasma column. Assuming the Shapiro theory to hold, the authors found good agreement with quasilinear theory, including the angular spread of wave vectors. Unfortunately, in this experiment the electron beam distribution function was not measured. However, the authors invoked the results of Kharchenko *et al.* (1962), who observed flattening of an injected monoenergetic beam in similar experiments. Hence it is reasonable to assume that similar effects should have occurred in the experiments of Arunasalam *et al.* (1971).

G. Experiments on mode-mode coupling

Some of the first experiments on resonant mode–mode coupling were done by Cano *et al.* (1967), Ellis and Porkolab (1968), Porkolab and Chang (1969), Chang and Porkolab (1970), Hai and Wong (1970), Franklin *et al.* (1971), and Mix *et al.* (1972). In some of these experiments only the frequency selection rules were verified. The first experiment to show wave-vector selection rules was that of Porkolab and Chang (1969), while the first experiment in which not only all the selection rules, but also the matrix elements were measured quantitatively was that of Chang and Porkolab (1970a). These authors studied a backscatter type of decay of electron Bernstein waves, and in Figs. 5 and 6 we show the decay spectrum and interferometer traces of the waves detected in these experiments. From the figures we see that both the frequency and the wave-vector selection rules (Eq. 2.23) for resonant mode–mode coupling are satisfied. The nonlinear matrix elements were also determined, and

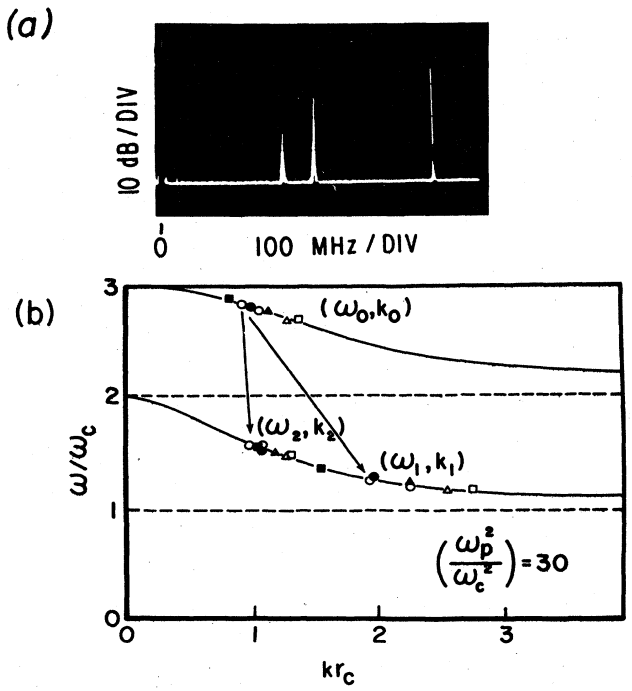

FIG. 5. (a) Typical decay spectrum; $f_1 = 335$ MHz, $f_2 = 420$ MHz, $f_0 = 758$ MHz. The pump signal (f_0) is greatly attenuated by a filter. ω_c (cyclotron frequency). (b) Dispersion relation and decay modes. Each set of three identical symbols represents a pair of decay modes like that indicated by the arrows. There are seven pairs of decay modes shown in the figure. (After Chang and Porkolab, 1970.)

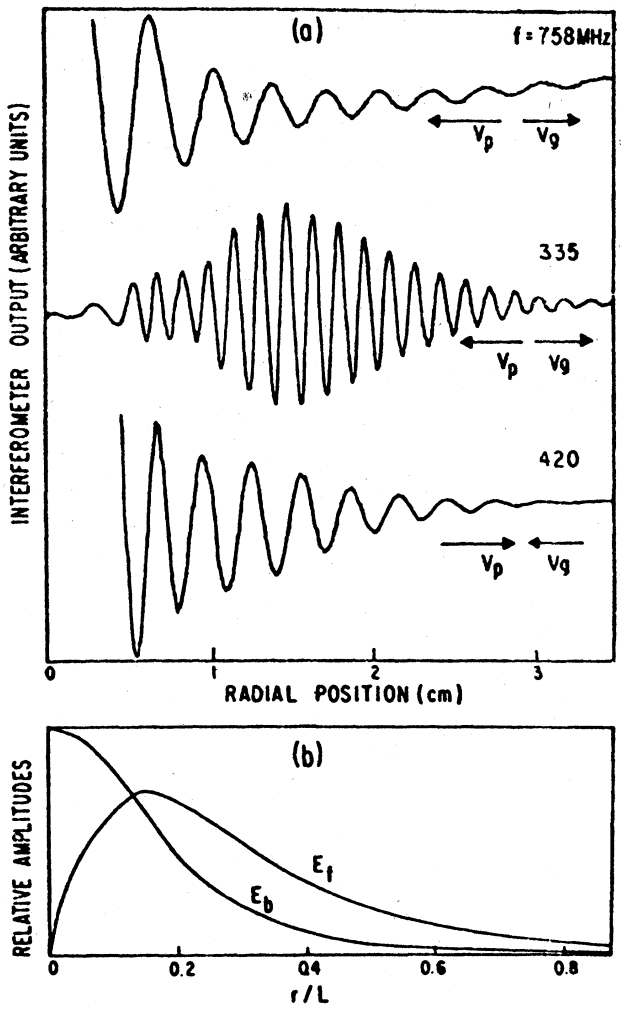

FIG. 6. (a) Interferometer traces of the finite-amplitude wave (758 MHz greatly attenuated by a filter) and perturbed waves (335 and 420 MHz) during decay. $k_0(758) = 19.0$ cm^{-1}; $k_b(420) = 20.6$ cm^{-1}; $k_f(335) = 39.8$ cm^{-1}. The transmitter is the T probe at $r = 0$. (b) Spatial variation of the perturbed-wave amplitudes as predicted by theory. Relative amplitudes in (a) and (b) are normalized for convenient display. (After Chang and Porkolab, 1970.)

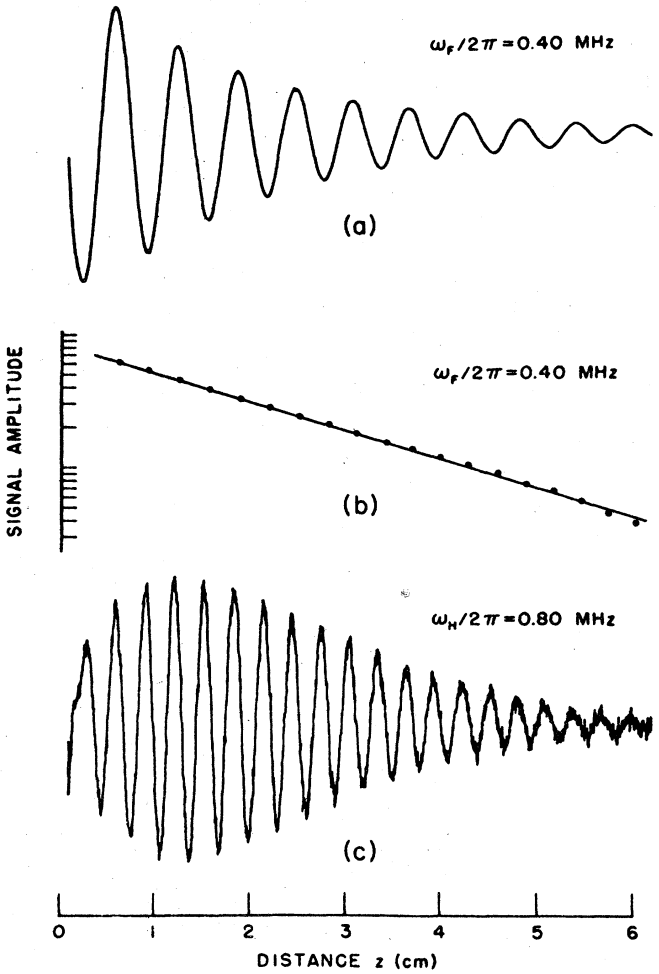

FIG. 7. Chart-recorder traces showing the spatial behavior of the fundamental wave [diagram (a)] and of the corresponding second harmonic wave [diagram (c)]. The peak amplitude of the second harmonic wave is ~ 0.05 of the peak amplitude of the fundamental. Diagram (b) illustrates the exponential damping of the fundamental wave. The damping distance normalized to the wavelength $(\delta/\lambda)_F$ has in this instance a value equal to 3.2. (After Mix *et al.*, 1972.)

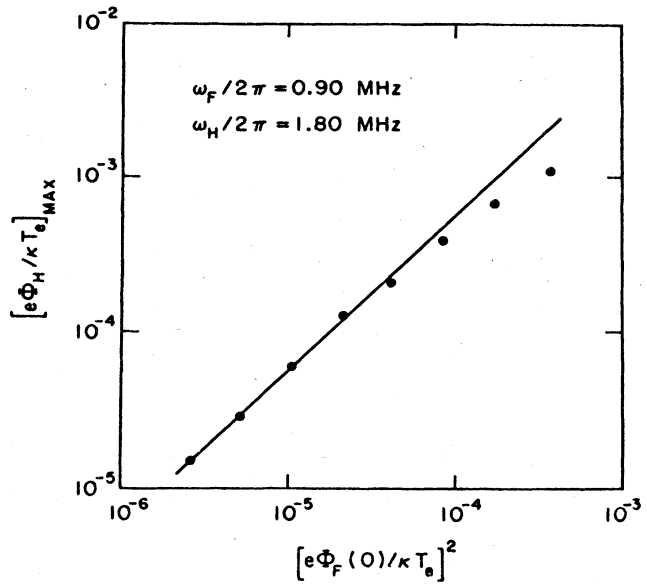

FIG. 8. Amplitude of the harmonic wave as a function of the amplitude of the fundamental. The solid circles are from experiment. The straight line is at 45° to the axis, as is demanded by second-order perturbation theory [see Eq. (22)]. The parameter $[e\Phi_H/kT_e]_{max}$ refers to the peak amplitude of the harmonic wave (see, for example, Fig. 7). (After Mix *et al.*, 1972.)

were found to agree with theory within experimental error.

In Figs. 7 and 8 we show the results of Mix *et al.* (1972), who studied harmonic generation of an ion acoustic wave propagating along a magnetized plasma column. In particular, harmonic generation can be regarded as forward scattering of a wave with itself, so that the selection rules become $k(2\omega) \simeq 2k(\omega)$. We see from Fig. 7, that this is well satisfied, and Fig. 8 shows that $E(2\omega) \propto E^2(\omega)$, which is again as expected for a second-order scattering of a wave with itself. These authors also found good agreement with theory for the coupling coefficient (matrix element) as long as $E(2\omega) \ll E(\omega)$. At large pump levels a saturation in the level of nonlinearly generated waves is observed in both of the foregoing experiments, which indicates pump depletion and/or a breakdown of weak-turbulence theory.

H. Experiments on nonlinear Landau damping

There have been a number of experiments which verified the strong interaction between the beat of two waves and resonant particles, i.e., nonlinear Landau damping and/or growth (Chang and Porkolab, 1970, 1972; Gentle and Malein, 1971; Ikezi and Kiwamoto, 1971). While Chang and Porkolab studied the resonance between two electron cyclotron harmonic waves (Bernstein waves) and the electron gyro frequency or its harmonics, Gentle and Malein studied the resonance between two electron plasma waves and electrons, and Ikezi and Kiwamoto studied the nonlinear ion Landau damping of two ion acoustic waves. In Figs. 9–11 we show the results of Chang and Porkolab, which demonstrate (a) decay instability associated with nonlinear cyclotron damping so that $\omega_2 - \omega_1 = n\Omega_e$, $n = 1, 2$ (Fig. 9); (b) amplification of a test wave with frequency ω_1 in the presence of a pump wave with frequency ω_2 so that $\omega_2 - \omega_1 \simeq n\Omega_e$ (Fig. 10); (c) amplification rate of the test wave which gave good agreement with Eq. (2.38b), the matrix element (Fig. 11). Note also the sudden breakdown of theory at high pump levels. In Fig. 12 we show the matrix elements for nonlinear Landau damping obtained by Gentle and Malein for electron plasma waves; also shown are the theoretical estimates. These authors found particularly strong interaction when $\Delta\omega/\Delta k \simeq v_{te}$, as expected from theory. Note the good agreement between theory and experiment. In Fig. 13 we show from the experiments of Ikezi and Kiwamoto that a test wave with frequency ω_1 is damped in the presence of a pump wave with frequency ω_2 if $\omega_2 < \omega_1$, and grows if $\omega_2 > \omega_1$ (assuming $\Delta\omega/\Delta k$

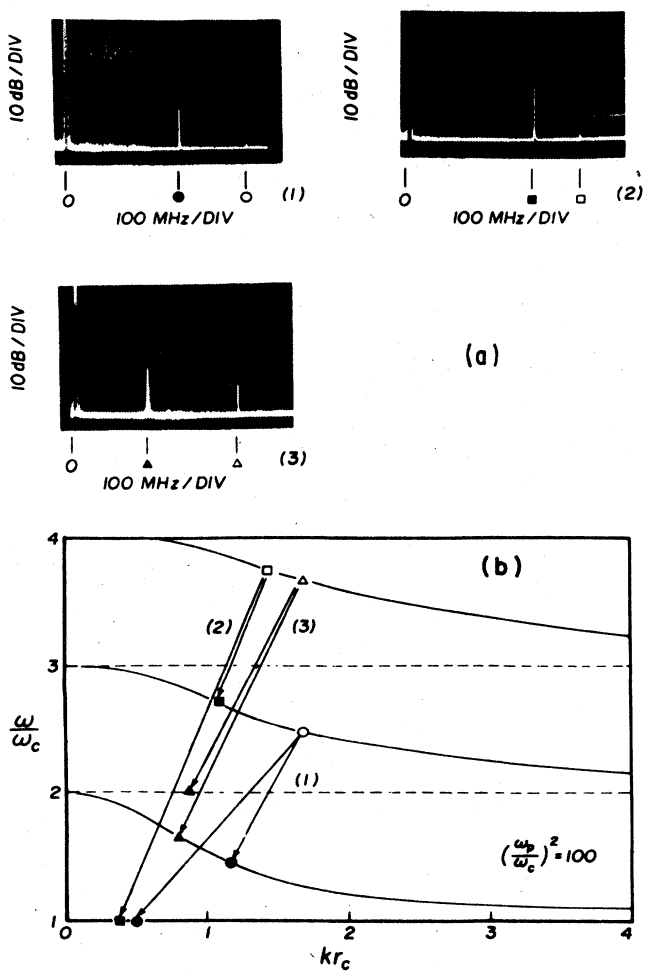

FIG. 9. (a) Spectra for three distinct cases of nonresonant decay. The finite-amplitude wave signal (hollowed symbols) is greatly attenuated by filtering. (b) Location of spectra (1), (2), and (3) on the linear dispersion diagram, with $k_{\parallel} = 0$. (In the experiment, $k_{\parallel}/k_{\perp} < 0.04$; thus these curves are a good approximation.) (After Chang and Porkolab, 1970, 1972.)

$\simeq v_{ti}$), as predicted by theory [see Eqs. (2.23a) and (2.23b)].

While the foregoing experiments were carried out using coherent waves, Matthieussent and Olivain (1975) studied nonlinear Landau damping using a broadband spectrum of bounded electron plasma waves which they injected into a linear device by a probe. They found that while there was clear evidence of broadening of the spectrum toward lower frequencies as the level of the externally injected spectrum was increased, there was also evidence of heating of the whole distribution of electrons rather than only those electrons which resonate with the group velocity of the wave packet. Thus it was concluded that, in addition to nonlinear Landau damping, resonance broadening (which we discuss in the next section) may have played an important role. Indeed, the conditions for the occurrence of such a phenomenon were satisfied (i.e., for the fluctuations the autocorrelation length was of the order of the trapping length).

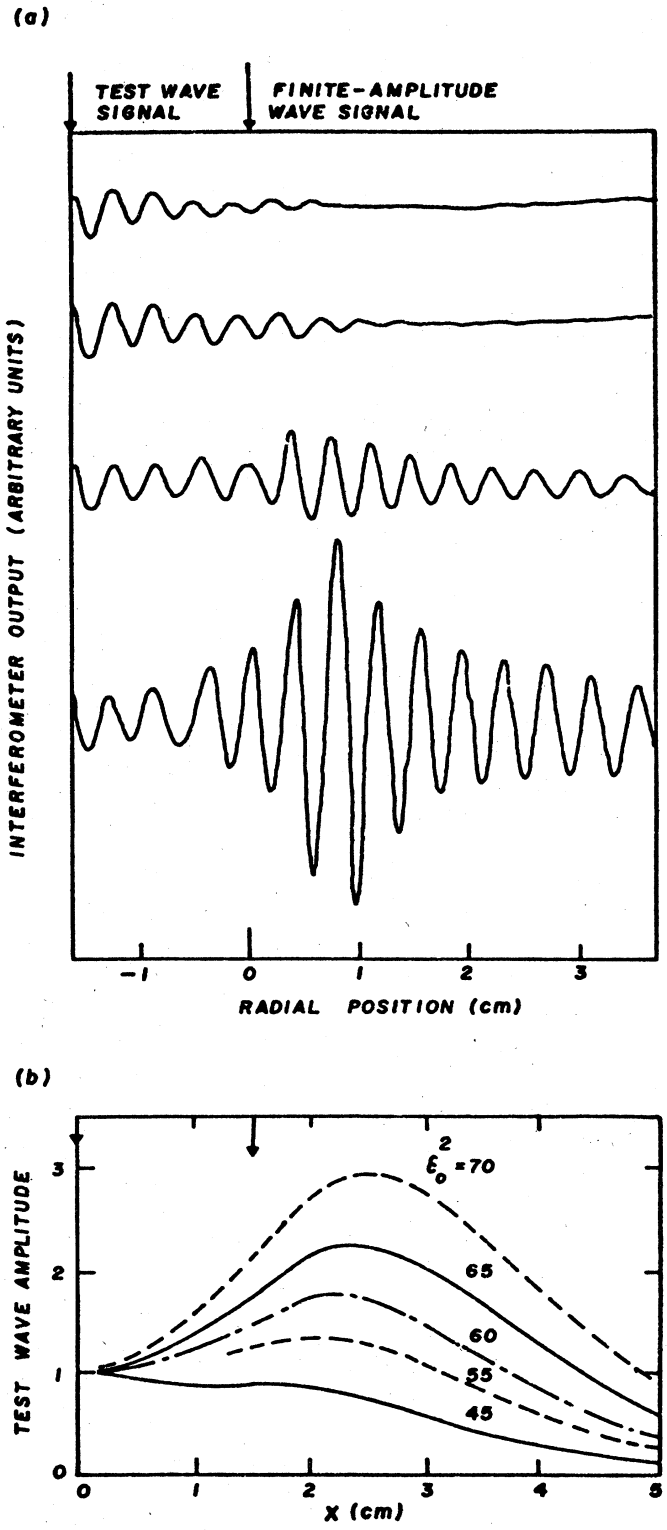

FIG. 10. (a) Interferometer traces showing the amplification of an externally excited test wave for case (2) of Fig. 2. The arrows indicate the locations of the wave sources. (b) Test wave amplitude (normalized to 1 at $x = 0$) as a function of distance, with the finite-amplitude wave power as a parameter. The arrows indicate the locations of the transmitting probes. (After Chang and Porkolab, 1970,1972.)

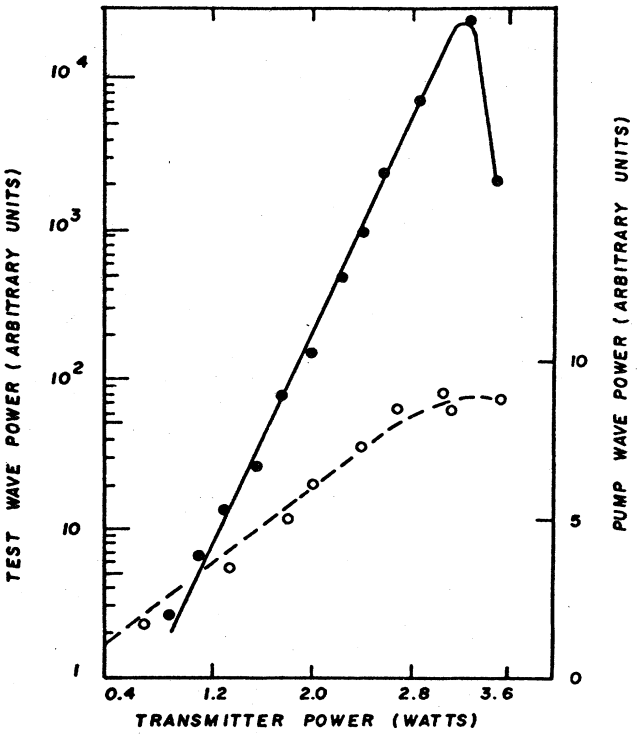

FIG. 11. $E^2_{\omega,k}$ (solid curve) and $E^2_{\omega'',k''}$ (dashed curve) vs transmitter power. (After Chang and Porkolab, 1970, 1972.)

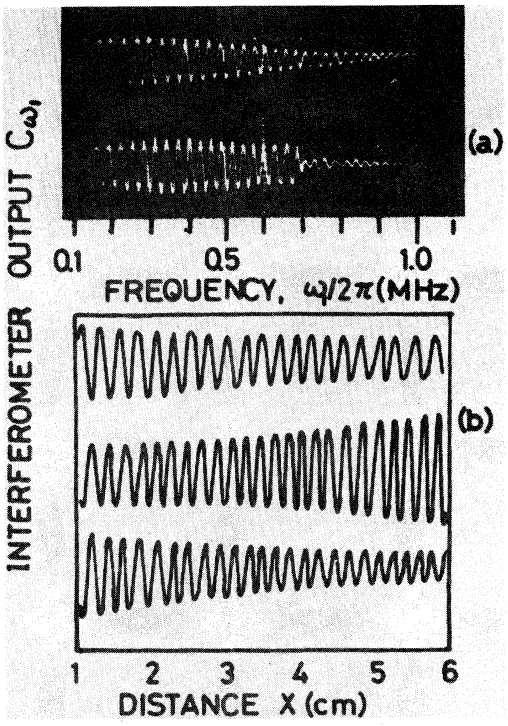

FIG. 13. (a) Interferometer output C_{ω_1} as a function of frequency ω_1. No wave ω_2 is excited in the top trace. The wave ω_2 is excited on the bottom trace and has a frequency 0.7 MHz. $\omega_{pi}/2\pi = 1.2$ MHZ. (b) Interferometer traces showing nonlinear growth and damping of wave $\omega_1/2\pi = 0.9$ MHz. Top trace, no wave ω_2. Middle trace, with wave $\omega_2/2\pi = 1.0$ MHz. Bottom trace, with wave $\omega_2/2\pi = 0.8$ MHz. $\omega_{pi}/2\pi = 1.3$ MHz. (After Ikezi and Kiwamoto, 1971.)

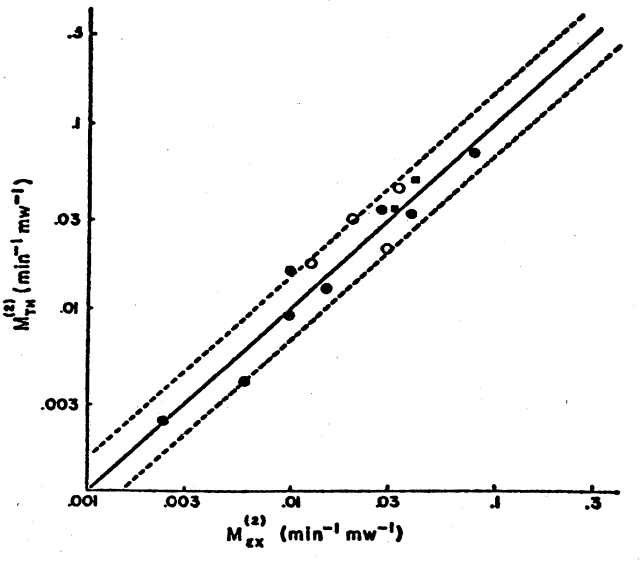

FIG. 12. Matrix elements $M^{(2)}$ for nonlinear Landau damping. Observed values are plotted against theoretical predictions for several waves. The dashed lines are experimental error bars. (After Gentle and Malein, 1971.)

In summary, the predictions of weak-turbulence theory have been verified experimentally to a limited extent. While quasilinear theory has been verified in one or two instances for a broad wave packet, mode coupling theories have been verified mostly for coherent waves. Thus, while the calculated mode coupling matrix elements agree with experimental measurements using fixed phase waves, the assumptions of the random-phase approximation in mode coupling still remain to be tested experimentally.

III. ECHOES

A. Theory of collisionless echoes

Landau's treatment of the dampling of plasma waves shows that macroscopic quantities, such as the electric field and the charge density, are damped exponentially, but that perturbations in the electron phase-space distribution $f(x,v,t)$ oscillate indefinitely (Landau, 1946). Since the electron density is given by the integral of $f(x,v,t)$, one may think of the damping as arising from the phase mixing of various parts of the distribution function. However, as we shall see in this section, the direction of the phase evolution of the perturbed dis-

tribution function can be reversed by the application of a second electric field at a later time (in pulsed experiments) or a different location (in spatial propagation experiments). This results in the subsequent reappearance of a macroscopic field, i.e., an echo. The echo occurs several Landau damping periods after the application of the second pulse, or at a different location from the second pulse in the case of spatial echo (Gould *et al.*, 1967; O'Neil and Gould, 1968).

Let us now see how echoes are formed. When an electric field of spatial dependence $\exp(-ik_1x)$ is excited in the plasma, it Landau damps away; however, it modulates the distribution function and leaves a perturbation of the form $f_1(v)\exp(-ik_1x+ik_1vt)$. For a time t sufficiently long there is no electric field associated with this perturbation, since an integral over velocity will phase mix to zero. Now let us consider an experimental situation where after a time τ a wave of spatial dependence $\exp(ik_2x)$ is excited, and then damps away with its own linear damping rate. At the same time it will modulate the unperturbed part of the distribution, leaving a first-order term of the form $f_2(v)\exp[ik_2x-ik_2v(t-\tau)]$, but it also will modulate the perturbation due to the first wave; the result is a second-order term of the form $f_1(v)f_2(v)\exp[i(k_2-k_1)x+ik_2v\tau-i(k_2-k_1)vt]$. Thus we see that at a time t^*, where

$$t^*=(k_2\tau/k_2-k_1), \tag{3.1}$$

the coefficient of v in the exponential will vanish, and at this time an integral of this nonlinear term over velocities will not phase mix to zero. Hence, at time t^* a net electric field will reappear in the plasma. Furthermore, if τ is long compared to a collisionless damping period and $k_2/(k_2-k_1)$ is of order unity, then this third electric field will appear long after the first two waves have damped away, i.e., it will be an echo. Of course, higher-order echoes may also be possible. For example, a third-order echo is produced when the velocity space perturbation from the first pulse is modulated by the second spatial harmonic of the electric field from the second pulse. The echo will then occur at a time (O'Neil and Gould, 1968)

$$t^*=2k_2\tau/(2k_2-k_1). \tag{3.2}$$

For example, when $k_2=k_1$, the echo occurs at time $t^*=2\tau$. Higher-order echoes may also form at times $t^*=\tau nk_2/k_{mn}$, where $k_{mn}=(nk_2-mk_1)$.

It is also possible to have spatial echoes, and these are easier to observe experimentally than the temporal ones (O'Neil and Gould, 1968). If an electric field of frequency ω_1 is excited continuously at a particular location x_1 in the plasma, and if an electric field of frequency $\omega_2>\omega_1$ is excited continuously at a distance (x_1+l), then a second-order spatial echo of frequency $(\omega_2-\omega_1)$ is produced at a location

$$l^*=l\omega_2/(\omega_2-\omega_1), \tag{3.3}$$

where $l^*=(x-x_1)$ is the relative distance from the point where the first field was excited. This result follows from an integral over v of the second-order perturbation $f_1(k_1,v_z)f_2(k_z,v)\exp[i\omega_3t+i\omega_2(d/v_z)-i\omega_3(z/v_z)]$, where $\omega_3=\omega_2-\omega_1$.

In a magnetic field the situation is more complicated if the perturbation has a finite value of $k_\perp$. In that case the free streaming perturbations will also depend on Ω, the cyclotron frequency. For example, for two perturbations of the form $f_1^{(1)}(k,v_z)\exp[-i\omega_1t+i(\omega_1-l\Omega)z/v_z]$ and $f_2^{(1)}(k,v_z)\exp[i\omega_2t-i(\omega_2-n\Omega)(z-d)/v_z]$ an echo is produced due to the beat when the integral over v_z does not vanish, namely at a location

$$z^*=d(\omega_2-n\Omega)/(\omega_2-\omega_1-p\Omega), \tag{3.4}$$

where the velocity-dependent term in the exponential will vanish. Here v_z is the particle velocity along the magnetic field line, l,n,p are integers, and d is the relative location of the two initial excitations (Porkolab and Sinnis, 1968; Porkolab, 1969). Thus additional shifts of echo position (time) due to the finite cyclotron motion are expected.

While the foregoing picture is based on a free streaming type of ballistic picture, more rigorous kinetic theory descriptions have also been obtained (O'Neil and Gould, 1968). This analysis is similar to second-order resonant mode–mode coupling theory, except that wave-particle interactions are also retained. These wave-particle interactions are different, however, from nonlinear Landau damping; the interaction is associated with the poles corresponding to the ballistic terms, which are usually discarded in weak-turbulence (mode–mode coupling) theories. Nevertheless, the kinetic theory allows one to include collective phenomena, such as Landau damping of the individual waves, and thus the theory can also predict the shape of the echo. For example, for two external pulses of the form

$$\phi_{ext}=\Phi_1\cos(k_1x)\delta(\omega_pt)+\Phi_2\cos(k_2x)\delta[\omega_p(t-\tau)] \tag{3.5}$$

kinetic theory predicts the following expression for the echo O'Neil and Gould, 1968:

$$\Phi_e=\frac{-ik_1k_3}{4}\left(\frac{e}{m}\right)\frac{\Phi_1\Phi_2}{k_3^2}\int_{-\infty}^{\infty}dv\,\frac{\partial f_0}{\partial v}\,\frac{(t-\tau)\exp[-ik_3v(t-\tau)+ik_1v\tau)]}{\epsilon(k_3,-ik_3v)\epsilon(k_2,-ik_2v)\epsilon(-k_1,ik_1v)} \tag{3.6}$$

Here Φ_1,Φ_2 are the externally applied potentials, and $\epsilon(k_j,ik_jv)$ are the dielectric functions associated with the two pulses and the echo. Thus, if we let $t-\tau=\tau(k_1/k_3)$, the exponential nearly vanishes, and we get an echo. Note that since $k_3=k_2-k_1$, this condition is the same as $t^*=\tau k_2/k_3$ which we obtained earlier. In Fig. 14 we exhibit from the work of O'Neil and Gould (1968) a numerical representation of Eq. (3.6). Note that the echo is asymmetric, that is, the rise and fall time of the echo are different. We also note that, in general, the n,mth

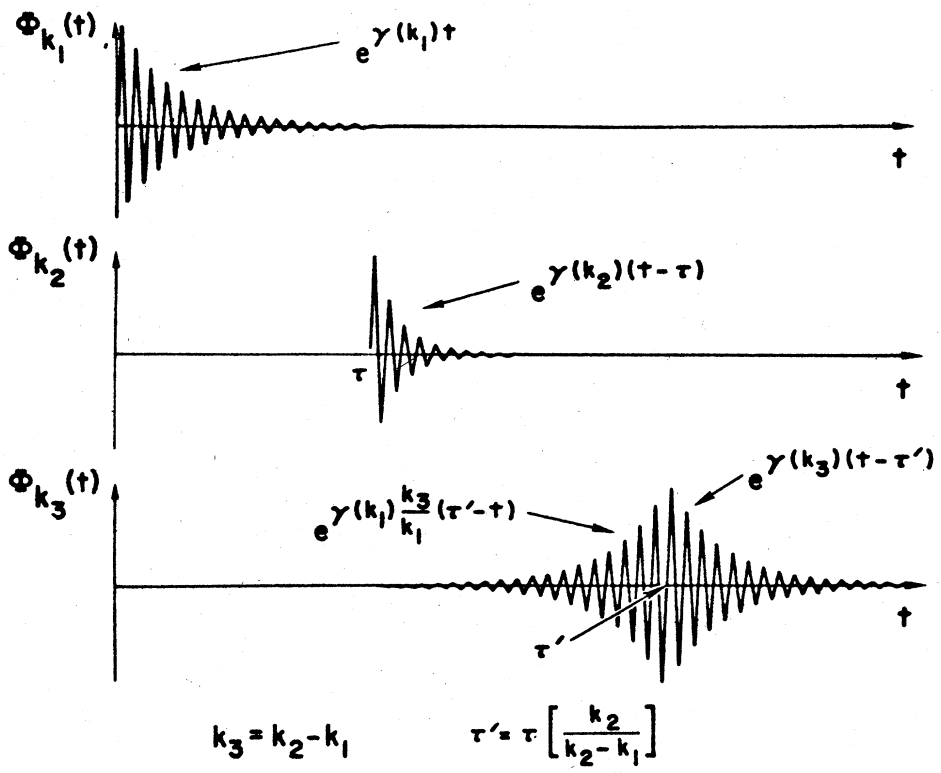

FIG. 14. Approximate variation of the principal Fourier coefficients of the self-consistent field for the case $k_3 \cong k_1 \cong \frac{1}{2}k_2$. Upper line: response to the first pulse. Middle line: response to the second pulse. Lower line: echo. (After Gould *et al.*, 1967.)

echo amplitude varies as $\Phi_e \propto \Phi_1^n \Phi_2^m$. Asymptotic forms of Eq. (3.6) can be found in the original papers of O'Neil and Gould.

Additional studies of echoes have been carried out by Kamimura (1970), who obtained a Langmuir wave echo from the pulsing of two cyclotron waves, and Sitenko *et al.* (1970), who obtained ion acoustic echoes from pulsing two Langmuir waves.

B. Collisional effects

It was noted by O'Neil and Gould (1968), Su and Oberman (1968), O'Neil (1968), and Hinton and Oberman (1968) that echoes may be particularly sensitive to Coulomb collisions and microturbulence. This can be seen by the following physical picture. The effective collision frequency acting upon the echo perturbation $\exp(ikvt)$ due to 90° collision is

$$\nu_{\text{eff}} = \nu_{90°} v_{te}^2 \frac{\partial^2}{\partial v^2} \exp(ikvt) \simeq \nu_{90°}(\omega_p t)^2 , \tag{3.7}$$

where we used $kv_{te} \simeq \omega_{pe}$ (v_{te} is the thermal velocity, and ω_{pe} is the electron plasma frequency). Therefore the effective damping is $\exp(-\nu_{\text{eff}} t)$, and for echo formation we want

$$\nu_{\text{eff}} t = \nu_{90°}\omega_p^2 t^3 < 1 \tag{3.8a}$$

or

$$t < (\nu_{90°}\omega_p^2)^{-1/3} , \tag{3.8b}$$

or the echo will be washed out. Thus the echo is washed out in a time short compared with a 90° collision time (since usually $\omega_p \gg \nu_{90°}$). Similarly, by replacing $t \to l/v_t$, we find that a spatial echo is washed out in a distance

$$l < \lambda_{90°}\left(\frac{\lambda_D}{\lambda_{90°}}\right)^{2/3} , \tag{3.9}$$

where $\lambda_{90°} = v_{te}/\nu_{90°}$ is the mean free path for 90° collisions, and $\lambda_D = v_{te}/\omega_{pe}$ is the Debye length.

One may argue that in a turbulent plasma a turbulent diffusion coefficient would produce a similar loss of "particle memory" in a time

$$\tau \simeq (\delta v)^2/D , \tag{3.10a}$$

where δv is the change in velocity due to scattering by the turbulent fluctuations. Using the relation $\delta v \simeq 1/k\tau$, we get from Eq. (3.10a)

$$k^2 D\tau^3 \simeq 1 \tag{3.10b}$$

or

$$\tau \simeq 1/(k_2 D)^{1/3} \tag{3.10c}$$

as the time within which an echo would be destroyed. Thus we see that both Coulomb collisions and microturbulence are very effective in damping echo formation. According to O'Neil (1968), for spatial echoes the damping factor varies as

$$\phi_e \propto l^2 \exp[-D(v_3)\tfrac{2}{3} l^3 k_3^5/\omega_3^3] , \tag{3.11}$$

where $D(v_3)$ is the diffusion coefficient evaluated at the phase velocity of the echo. Because of the above, it is hoped that echoes may be particularly useful as a diagnostic tool to study microturbulence in plasmas.

C. Trapped particle echoes

Echoes may be associated with trapped particles, and such trapped particle echoes have been studied both theoretically (Liu and Wong, 1970) and experimentally (Wong and Taylor, 1969; Chatelier, 1974). For example, consider particles trapped in a magnetic well or in a potential well. First apply a pulse at $t=0$, and as a result some of the particles will be accelerated. Then apply a second pulse at time $t=\tau$; some of the previously accelerated particles return in phase, and are "marked" again by the new pulse. These particles then keep regrouping at times $t=2\tau$ (l and in general at $n\tau$). Again, if turbulence or collisions are present, the phase is washed out according to the relationship

$$\nu_{\text{eff}} \simeq \nu_{90^\circ}(\omega_b \tau)^2, \tag{3.12}$$

where ω_b is the "bounce frequency" of the trapped particles. Thus, by increasing the pulse separation time so that

$$\tau > (\nu_{90^\circ}\omega_b^2)^{-1/3}, \tag{3.13}$$

we cause the echo to be washed out.

D. Experimental results

Let us now consider the experimental evidence for the formation of echoes. The first experimental observation of electron plasma wave echoes was by Malmberg *et al.* (1968). The geometry of their experimental setup is shown in Fig. 15, and the results are shown in Figs. 16, 17, and 18. In Fig. 16 we show interferometer forces of two electron plasma waves launched by wire antennas in a low-density, low-temperature plasma ($n \simeq 10^8$ cm^{-3}, $T_e \simeq 9$ eV) with frequencies $f_{1,2}=120$, 130 MHz; the echo is produced at $f_e=140$ MHz. This a third-order spatial echo, namely, $f_3=2f_2-f_1$. The variation of echo position with frequency and transmitter separation is shown in Fig. 17. In the experiments the plasma is confined by a 300 G magnetic field so that $\omega_{pe} \ll \Omega_e$, and the plasma-waves can be considered one dimensional. Note the linear variation of l^*/l, as predicted by theory for a fixed set of frequencies. There is some discrepancy between theory and experiment at the position $l=0$. However, the authors claim that this is not important since the finite intercept is within the damping length of the waves. We also note that second-order echo formation using electron plasma waves is, in general, difficult since the resonant mode coupling conditions for such waves cannot be satisfied. Finally, in Fig. 18 we show variation of the echo wave power as the primary wave amplitude are varied. Note the power dependence $\Phi_e^4 \propto \Phi_2^2\Phi_1^4$, which is as expected for a third-order echo.

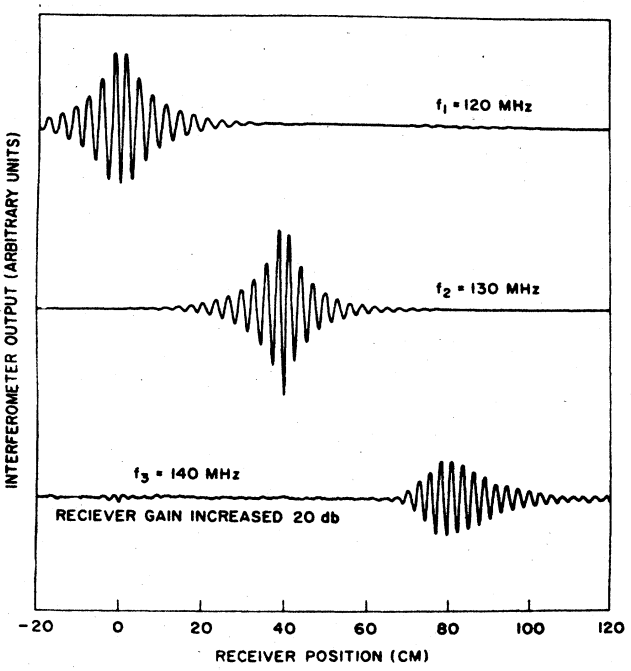

FIG. 16. Third-order echo. The transmitter probes are at 0 and 40 cm. Upper curve, receiver tuned to f_1; second curve, receiver tuned to f_2; third curve, receiver tuned to f_3 and gain increased 20 dB. (After Malmberg *et al.*, 1968.)

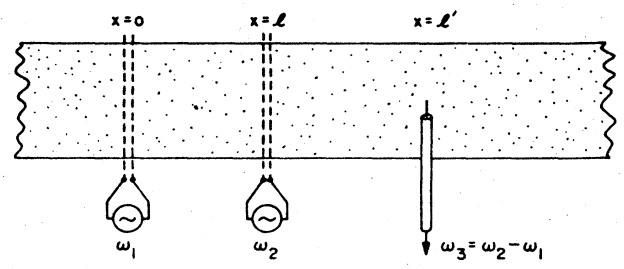

FIG. 15. Schematic drawing of transmitter-receiver arrangement for spatial echoes. (After O'Neil and Gould, 1968.)

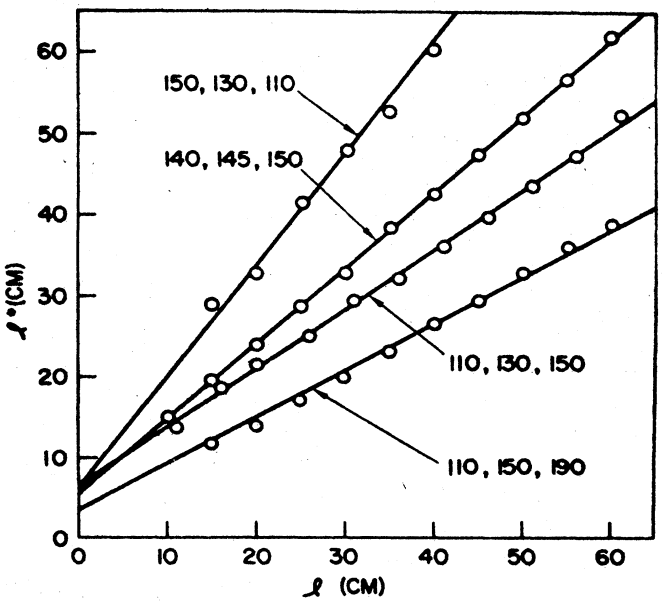

FIG. 17. Echo position vs transmitter separation. The slope of the curves is theory. The numbers on the curves are f_1, f_2, and f_3 in MHz. (After Malmberg *et al.*, 1968.)

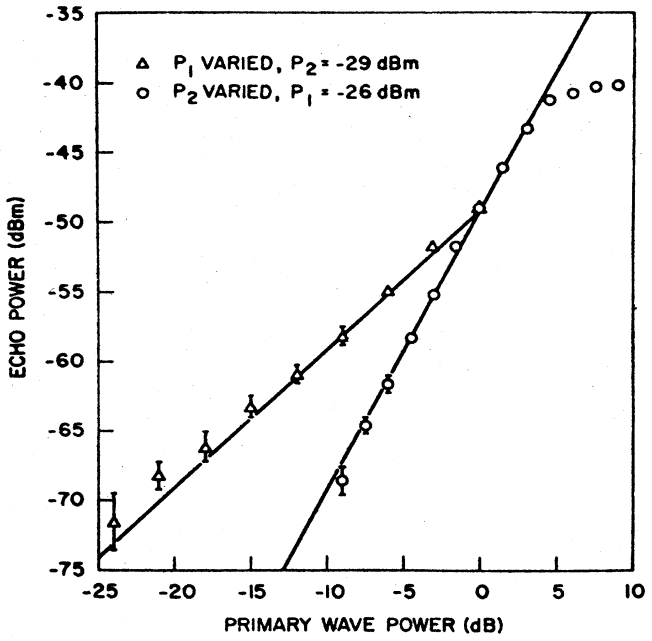

FIG. 18. Echo power vs primary wave amplitudes. Absolute power levels are approximate. (After Malmberg *et al.*, 1968.)

More detailed studies of echo shapes were performed by Goforth and Gentle (1971, 1972). These authors carried out a perturbation calculation of the Vlasov equation to third order, and found satisfactory agreement with the echo shape. For large incident wave amplitudes saturation sets in, and the power law dependence given in the foregoing paragraph breaks down. This is a consequence of the fact that perturbation theory itself breaks down. This saturation phenomenon was studied theoretically by Coste and Peyraud (1969) and experimentally by Guillemot *et al.* (1971). These authors found that ballistic echoes may also occur, even when self-consistent fields do not correspond to one of the frequencies used in the experiment. We may call this nonresonant echo formation. Further studies of such echoes were also carried out by Ripin *et al.* (1970, 1972, 1973), who studied echo phenomena in a drifting plasma.

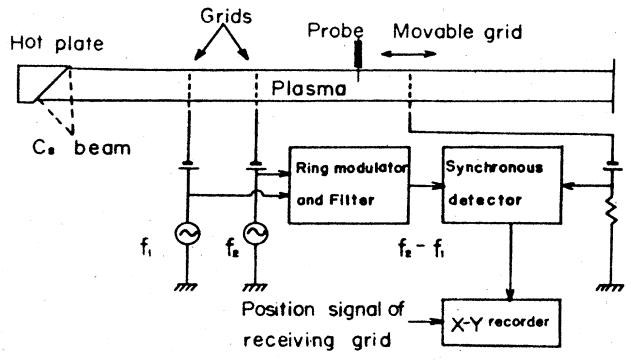

FIG. 19. Experimental setup of Ikezi and Takahashi (1968) for ion wave echo generation.

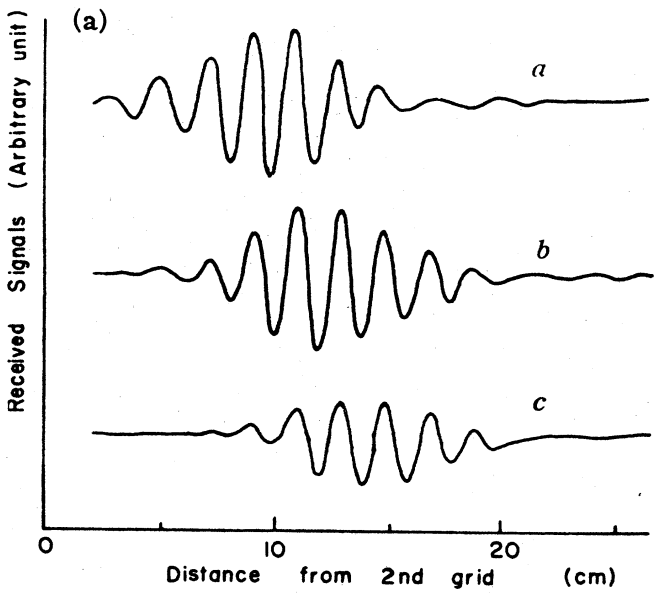

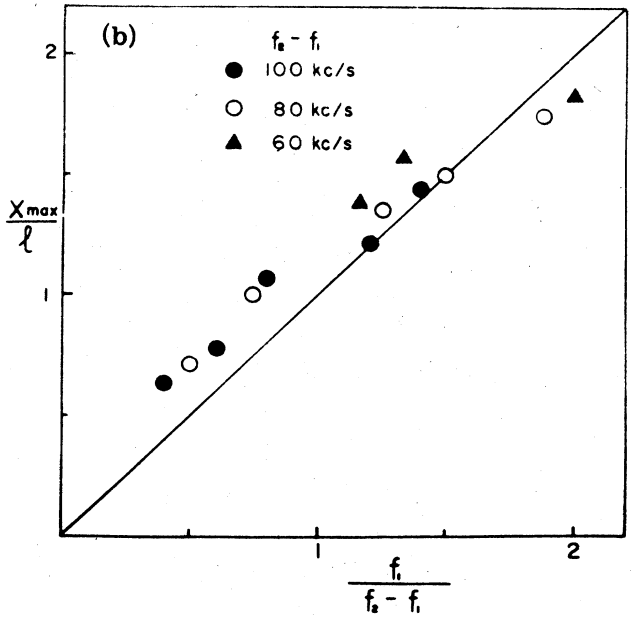

FIG. 20. (a) Recorder output demonstrating the excitation of the echo (amplitude and phase) for three typical sets of frequencies f_1 and f_2. The frequency of the echo ($f_2 - f_1$) is 100 kc/sec. Curves a, b, and c are for exciting frequency f_1 of 80, 120, and 140 kc/sec, respectively. The curves for different sets of frequencies are displaced for display purposes. (b) Relation between the position where the amplitude of the echo is maximum, and the frequencies f_1 and f_2. The solid line indicates the relation $x_{max} = 1f_1/(f_2 - f_1)$. The frequencies of the echoes are given in the figure. (After Ikezi and Takahashi, 1968.)

Ion wave echoes have been observed experimentally by Ikezi *et al.* (1968, 1969) and Baker *et al.* (1968). These experiments were done in Q-machine plasmas, where $T_e \simeq T_i$. The experimental setup of Ikezi *et al.* (1968) is shown in Fig. 19. Two grids are used to launch the pri-

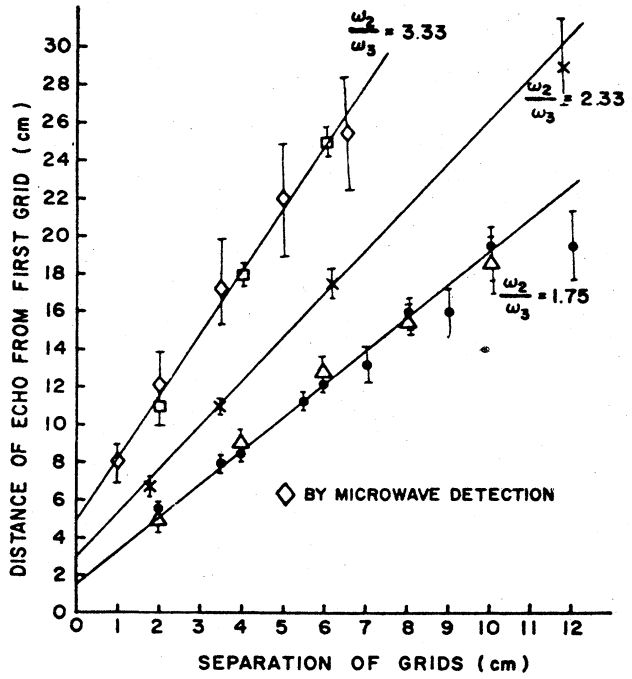

FIG. 21. A plot of the distance of the echo maximum from the first grid for different values of ω_2/ω_3. The slope of the solid line is given by ω_2/ω_3. The points indicated by diamonds were obtained from the X-band microwave system. All other points were obtained with the biased grid. $N=2\times10^{10}$ cm^{-3}; $T_i=T_e$ = 0.2 eV. Squares, $\omega_1/2\pi=35$ kHz; $\omega_2/2\pi=50$ kHz. Diamonds, $\omega_1/2\pi=70$ kHz; $\omega_2/2\pi=100$ kHz. Crosses, $\omega_1/2\pi=40$ kHz; $\omega_2/2\pi=70$ kHz. Circles, $\omega_1/2\pi=40$ kHz; $\omega_2/2\pi=95$ kHz. Triangles, $\omega_1/2\pi=70$ kHz; $\omega_2/2\pi=160$ kHz. (After Baker *et al.*, 1968.)

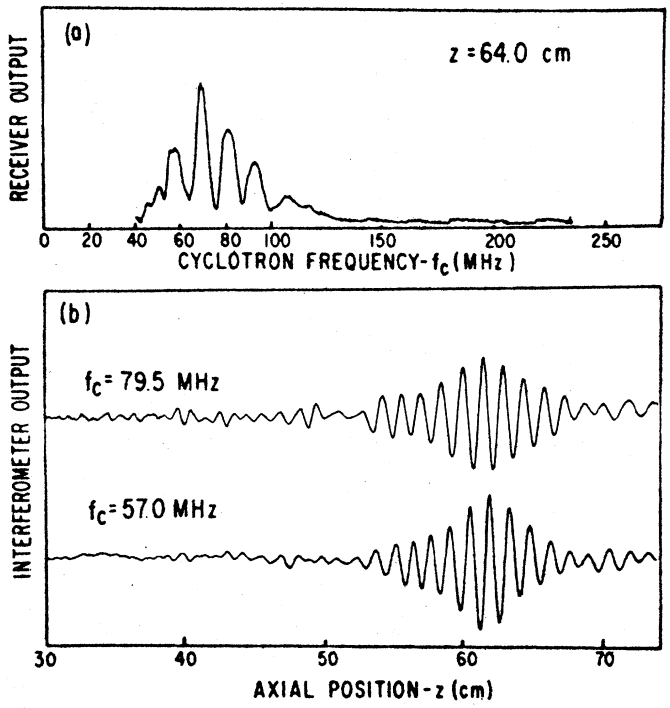

FIG. 22. (a) Echo power as a function of cyclotron frequency f_c. (b) Interferometer output of echo power as a function of receiver position. For both (a) and (b), $(f_1,f_2,f_3)=(391,700,309)$ MHz; transmitters at $z_{1,2}=0$, 30 cm. (After Porkolab and Sinnis, 1968.)

mary waves, and a third, movable grid is used to detect the echoes. In Fig. 20 we present their experimental results, showing echoes associated with various primary wave frequencies. The variation of echo position with transmitting grid separation is also shown in the same figure. We see that an approximately straight-line relationship is obtained as predicted by Eq. (3.3).

Similar results have been obtained by Baker *et al.* (1968); their experimental results are shown in Fig. 21. These results are similar to those of Ikezi *et al.* except that a more pronounced intercept at the origin is visible.

Echoes modified by electron cyclotron harmonic phenomena were studied by Porkolab and Sinnis (1968). The geometry was similar, except that T-shaped transmitting probes were used to launch the primary waves. Such problems allow perturbation with finite $k_\perp$ to be excited; in addition, in these experiments typically $\omega_{pe}>\Omega_e$. In Fig. 22 we show the echo wave amplitude as a function of magnetic field, as well as interferometer outputs of echo shapes. Note the strong dependence of the echo amplitude upon the magnetic field (i.e,, cyclotron frequency). In Fig. 23 we show the variation of echo position (z^*) as a function of transmitter separation (d) for several frequencies. The n and p integers in the figures are those corresponding to Eq. (3.4), and the indicated values give the best fit to the experimental results. Note that had we assumed $n=p=0$, no agreement would be possible. These results clearly indicate the importance of cyclotron harmonic phenomena in the present experiments.

The effect of turbulence and/or Coulomb collisions upon echo formation was studied experimentally by Jensen *et al.*(1969), Wong and Baker (1969), Moeller (1975), and Guillemot (1971). In Fig. 24 we show the results of Jensen *et al.*, who studied the variation of echo amplitude as a function of transmitter separation l. We recall that theory predicts $\phi_e\propto l^2\exp(-xl^3)$, which seems to be in reasonable agreement with the present results. These authors attribute the damping to the presence of background turbulence in the plasma. It should be noted, however, that due to the limited range of the experimental parameters (i.e., the variation with l) the $l^2\exp(-l^3)$ dependence cannot be proven conclusively (i.e., another power law may also fit the present data). These authors also estimated the magnitude of the diffusion coefficient from the background turbulence, and again, within experimental error, reasonable agreement was found with quasilinear theory. A more detailed study by Moeller (1975) on the damping of echoes by Coulomb collisions shows that the experimental data can be fitted with an exponential power of $n=2$ to 4. Similar discrepancies were also found by Porkolab and Sinnis (1969).

In the case of ion wave echoes, Wong and Baker (1969) studied the effects of ion–ion Coulomb collisions upon the echo amplitude. The theory was also treated by these authors, and predicts a variation of echo ampli-

tudes as follows:

$$\frac{n_e}{n_0}=\frac{l}{\lambda_1}\exp\left[-\alpha\left(\frac{\lambda_1\lambda_3}{\lambda_2\lambda_{mfp}}\right)^{1/5}\left(\frac{l}{\lambda_1}\right)^{3/5}\right], \tag{3.14}$$

where λ_1, λ_2, and λ_3 are the wavelengths of the primary waves (1, 2) and the echo (3), λ_{mfp} is the mean free path for collisions, and l is the transmitter separation. In Fig. 25 we present their results, which show relatively good agreement between experiment and theory. Again we should emphasize that since the range of parameters on the horizontal axis varies only within a factor of three, some other power law dependence cannot be excluded. Nevertheless, we must conclude that these experiments give strong support to the idea that the Fokker–Planck collision term is operative in damping echoes.

Trapped particle echoes in the anharmonic potential well of a probe were first studied by Wong and Taylor (1968) in a small-scale laboratory experiment. As an application of similar concepts, we should mention the experiments of Chatelier *et al.* (1974), who also used echoes to study trapped particle phenomena. In particular, these authors applied compressional magnetic pulses with frequencies near the ion bounce frequency in

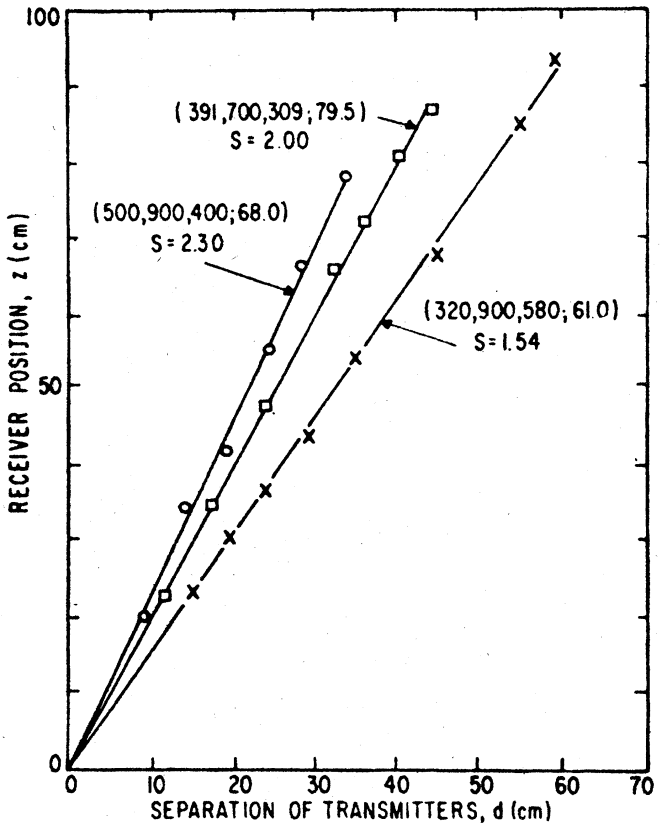

FIG. 23. z^* vs d. The numbers in braces are (f_1,f_2,f_3,f_c). Solid lines show best fit to experimental data, giving $z^*/d=s$. Theoretical lines, according to Eq. (4), show agreement to within 1% or better by assuming that $(n,p)=(2,1)$, $(3,1)$, $(3,2)$ for the lines with $s=2.30$, 2.00, 1.54, respectively. (After Porkolab and Sinnis, 1968.)

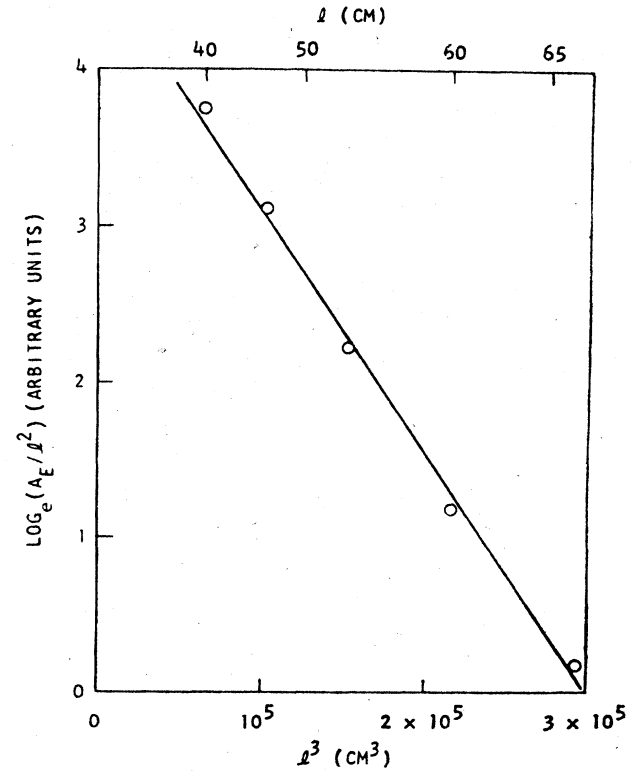

FIG. 24. Logarithm of $A_E/1^2$ vs 1^3; A_E is the amplitude of the echo and 1 the distance between transmitter and receiver. (After Jensen *et al.*, 1969.)

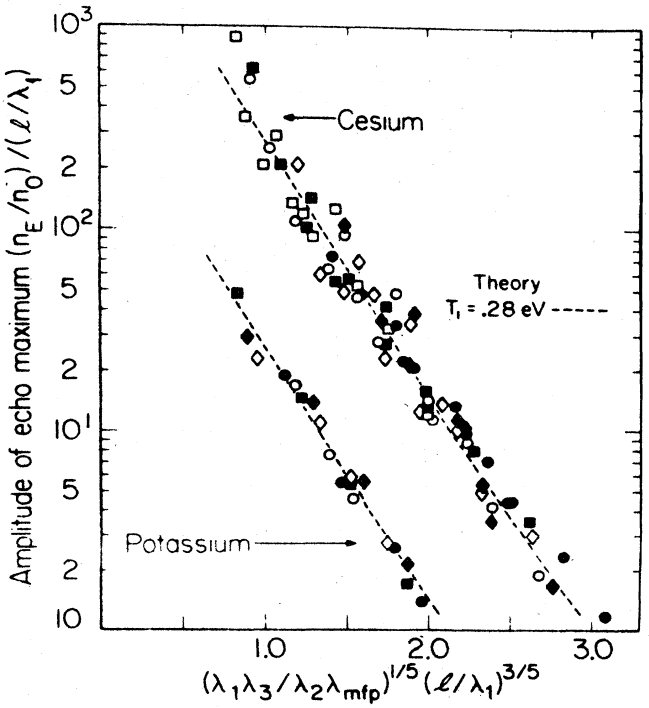

FIG. 25. Echo maximum $\ln[(n_E/n_0)(\lambda_1/1)]$ vs the collisional parameter $(\lambda_1\lambda_3/\lambda_2\lambda_{mfp})^{1/5}(1/\lambda_1)^{3/5}$ for ion wave echoes in cesium and potassium plasmas. The solid line is the theoretical curve. (After Wong and Baker, 1969.)

a mirror machine. The two pulses induced a variation of the parallel energy, and a temporal echo appeared. By varying the pulse separation, Chatelier *et al.* were able to observe the amplitude variation of the echo, and from these measurements to deduce an estimate of the diffusion rate of the magnetic moment of the particles. These measurements were found to be consistent with the Coulomb collision rate. Such experiments prove the feasibility of using echoes to study trapped particle phenomena and diffusion in controlled thermonuclear fusion devices.

In conclusion, we should mention a class of echoes that have to do with collisional effects and weak nonlinearities, which were studied extensively before the collisionless plasma wave echoes. These echoes depend on the cyclotron motion of charged particles, and have been reviewed by Gould (1969). An extensive list of references can also be found in his paper, and thus we shall not discuss them here.

IV. STRONG ELECTRIC FIELDS: PARAMETRIC INSTABILITIES AND SOLITONS

A. Parametric instabilities

Under the influence of high-frequency long-wavelength electromagnetic fields various modes of oscillation in the plasma may become coupled, and may grow exponentially in time or space before saturating at large amplitudes. For example, in the absence of a magnetic field, electron plasma waves and ion acoustic waves may couple in such a manner (DuBois *et al.* 1965; Silin, 1965; Jackson, 1967; Nishikawa, 1968).

If the incident electromagnetic wave ("pump wave") has a relatively long wavelength as compared with the wavelengths of the decay waves, then it is possible that energy is transferred to the particles via collective effects; namely, the energy transferred to the short-wavelength decay waves from the pump wave is absorbed by particles more efficiently than the energy transferred to particles directly from the weakly damped pump wave. Thus the net effect of this process is an "anomalous" absorption of the incident electromagnetic wave. This process is somewhat similar to turbulent heating, and it is expected to be of importance in hot plasmas where collisional absorption of electromagnetic energy is rather inefficient (Kaw and Dawson, 1969). Thus parametric instabilities (which, however, require a finite threshold of pump power for excitation) may form a channel for efficient transfer of electromagnetic energy into hot plasmas. Because of its practical importance to both laser fusion and rf heating of magnetically confined plasmas, this phenomenon has been the subject of extensive investigation both theoretically and experimentally. In this section we shall outline the fundamental aspects of this problem and give a number of illustrations.

We note that in Sec. II we studied coupling among different electrostatic waves of comparable wave numbers. These processes, which form the foundations of weak-turbulence theory, may be called more appropriately mode–mode (or wave–wave) coupling. Instabilities due to these processes, which have been called decay instabilities, are akin to parametric instabilities as long as one of the waves is coherent in phase and large in amplitude as compared with other waves (Galeev and Sagdeev, 1973). In fact, decay instabilities were studied prior to the so-called "parametric" instabilities (Galeev and Sagdeev, 1973). Thus the naming of these processes is somewhat arbitrary, and indeed they have often been used interchangeably in the literature. However, in mode–mode coupling we often discuss scattering of waves of the same type; hence coupling is due to the nonlinearity of the Vlasov equation, and is associated with the presence of finite k_0. Other parametric instabilities exist even if $k_0 = 0$, especially when high-frequency electron modes and low-frequency ion modes are coupled. In this case the instability is driven by the relative electron-ion motion under the influence of the external electric field. Furthermore, instabilities may be driven by the relative ion–ion motion in a multi-ion species plasma, especially if $\omega \simeq \Omega_{i1}, \Omega_{i2}$. In the present paper we shall use the term "parametric instabilities" mainly to describe wave coupling phenomena in which the pump wave number can be ignored as compared with the wave number of the decay waves. Thus the pump can be either an electromagnetic wave or a long-wavelength electrostatic wave. An exception to this terminology is the case of the various electromagnetic decay instabilities in which at least two electromagnetic waves are involved in the decay process. We shall mention these only briefly in the theoretical section, and only one experimental example will be given.

B. Physical mechanisms of parametric instabilities

In the presence of an rf electric field different species of particles (i.e., ions, electrons) are displaced relative to each other due to their different masses, thus causing momentary charge separation (Kruer and Dawson, 1972; Nishikawa, 1968). For example, in the absence of a magnetic field in a singly charged electron–ion plasma for rf pump frequencies $\omega_0 \simeq \omega_{pe}$ (where ω_{pe} is the electron plasma frequency) the electrons make relatively large excursions in the electric field $E_0 \cos\omega_0 t$, i.e.,

$$\Delta x \simeq (eE_0/m\omega_0^2)\cos\omega_0 t\,, \tag{4.1}$$

whereas the ions remain nearly stationary due to their large mass. If there are low-frequency ion fluctuations in the background with frequency $\omega_1 \lesssim \omega_{pi}$ (where ω_{pi} is the ion plasma frequency), these may beat with the oscillating electrons to form additional oscillations in the charge at the frequency $(\omega_0 \pm \omega_1)$, i.e.,

$$\delta n_e \simeq \frac{\partial n_i}{\partial x}\Delta x = ikn_i \frac{eE_0}{m\omega_0^2}\cos\omega_0 t. \tag{4.2}$$

The selection rules associated with this process are (see Fig. 26)

$$\omega_0(\mathbf{k}_0) = \omega_1(\mathbf{k}_1) + \omega_2(\mathbf{k}_2), \mathbf{k}_0 = \mathbf{k}_1 + \mathbf{k}_2 \tag{4.3}$$

which is the usual resonant mode–mode coupling process, demonstrating energy and momentum conservation (Davidson, 1972). For parametric instabilities we

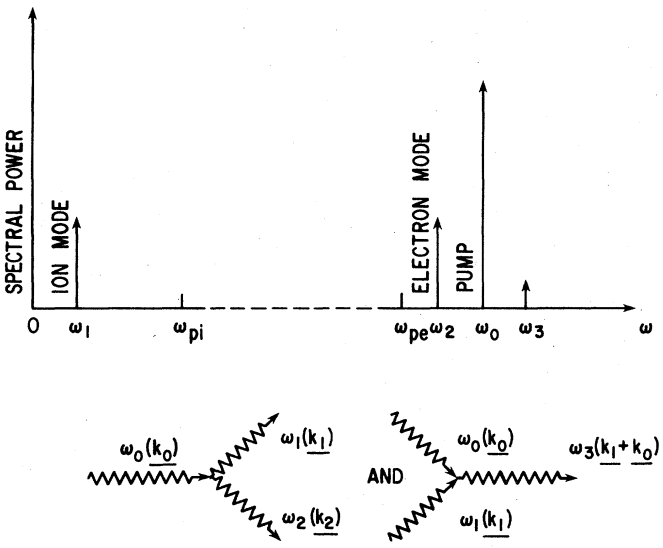

FIG. 26. Typical frequency spectrum for the parametric decay instability. Also shown are the corresponding scattering diagrams.

take $k_0 \simeq 0$, and thus $\mathbf{k}_1 \simeq -\mathbf{k}_2$ (so that $|k_1| = |k_2| \equiv k$). Combining Eq. (4.2) with a simple harmonic oscillator equation which describes electron plasma waves, we obtain

$$\frac{\partial^2 n_e}{\partial t^2} + \nu_e \frac{\partial n_e}{\partial t} + \omega_{ek}^2 n_e = \frac{\partial^2 (\delta n_e)}{\partial t^2} = \frac{ikn_i eE_0}{m} \cos\omega_0 t, \tag{4.4}$$

where $\omega_2 = \omega_{ek}$ is the resonance frequency of electron plasma waves in the absence of the pump field, and $\gamma_c \simeq \nu_e/2$ is their linear damping rate. In the absence of a magnetic field

$$\omega_{ek}^2 = \omega_{pe}^2 + 3k^2 v_{te}^2$$

is the Bohm–Gross dispersion relation [where $\omega_{pe} = (4\pi ne^2/m)^{1/2}$ is the electron plasma frequency, $v_{te} = (T_e/m)^{1/2}$ is the electron thermal speed, and T_e is measured in units of energy]. We also assume that the displacement given by Eq. (4.1) is small as compared with a typical wavelength (i.e., k_1^{-1}). This, plus the fact that only ω_2 is near a resonant frequency, justifies ignoring coupling to other harmonics (the case of strong coupling has been discussed by Silin, 1965).

Consider now the reverse of this process, namely the beating of the electron plasma wave with the rf pump field. This beat produces a ponderomotive force which exerts additional pressure on electrons at low frequencies:

$$\nabla \delta p = \nabla\left(\frac{E^2}{8\pi}\right) = \frac{E_0}{4\pi} \frac{\partial E}{\partial x} \cos\omega_0 t = -eE_0 \delta n_e \cos\omega_0 t. \tag{4.5}$$

Here we have made use of Poisson's equation. Note that the ponderomotive force is equivalent to the $v \cdot \nabla_x v$ term, since

$$v_x \frac{\partial v_x}{\partial x} = \frac{1}{2} \frac{\partial}{\partial x}(v_x^2) = \frac{1}{2} \frac{\partial}{\partial x} \frac{e^2 E^2}{m^2 \omega_0^2},$$

and using $\omega_0^2 \simeq \omega_{pe}^2 = 4\pi ne^2/m$ we obtain

$$nmv_x \frac{\partial v_x}{\partial x} = n\nabla_x\left(\frac{E^2}{8\pi n}\right).$$

Thus, considering that ion acoustic waves are driven by electron pressure, namely $\omega_1 \simeq \omega_s$ where

$$\omega_s^2 n_i = \frac{k_1^2 T n_i}{m_i} = \frac{k^2(p+\delta p)}{m_i}, \tag{4.6}$$

and where m_i is the ion mass, the simple harmonic oscillator equation for ions becomes

$$\frac{\partial^2 n_i}{\partial t^2} + v_s \frac{\partial n_i}{\partial t} + \omega_s^2 n_i = -\frac{ikn_e E_0}{m_i} \cos\omega_0 t, \tag{4.7}$$

where we included Eq. (4.5) for δp, and where $\nu_s/2 = \gamma_s$ is the linear damping rate of ion acoustic waves. Thus we see that Eqs. (4.4) and (4.7) represent the coupled oscillator equations for short-wavelength ion and electron waves in the presence of the long-wavelength rf pump wave. Solving Eqs. (4.4) and (4.7) by Fourier transformation, we find that if the selection rules [Eq. (4.3)] are obeyed, then both electron and ion waves grow exponentially in time above the threshold field

$$\frac{\gamma_e \gamma_s}{\omega_{ek}\omega_s} < \frac{E_0^2}{64\pi n_0 T_e}, \tag{4.8}$$

and that well above threshold the growth rate γ is obtained from Eq. (4.8) by replacing $\gamma_e\gamma_s = \gamma^2$. We note the following: (a) A minimum threshold exists, since there are linear losses present initially which the pump wave has to overcome; (b) In order to obtain Eq. (4.8) we assumed $\omega_s > \gamma_e$ so we could ignore the upper sideband $(\omega_0 + \omega_s)$ (or anti-Stokes line).

C. The purely growing mode

Nishikawa (1972) showed that in the limit $\omega_1 \to 0$, at $k \neq 0$ another instability may also occur, which is called the "purely growing mode" or the "oscillating two-stream" instability. In particular, by Fourier-analyzing Eqs. (4.4) and (4.7), and retaining both sidebands $\omega_{ek} \simeq (\omega_0 \pm \omega_1)$, for $\mathrm{Re}\,\omega_1 = 0$ we obtain the following threshold:

$$\frac{\gamma_e}{\omega_0} < \frac{E_0^2}{32\pi n_0 T_e}. \tag{4.9}$$

For weakly dampled modes $(T_e \gg T_i)$, $\gamma_s/\omega_s \ll 1$, and the threshold for the purely growing mode is higher than that of the decay instability. We note that if we include a finite k_0, the purely growing mode assumes finite real frequencies. An alternate way to derive the purely growing mode will be indicated in the next section, where we show that it is the linearized limit of the so-called nonlinear Schrödinger equation which predicts solitons.

D. Parametric decay in a magnetized plasma

In the presence of a magnetic field the situation becomes much more complicated than that shown above. For example, if we assume a dc magnetic field in the

$\hat{z}$ direction, and an external electric field of the form

$$E_0(x,t) = (E_{0x}\hat{x} + E_{0z}\hat{z})\cos\omega_0 t, \tag{4.10}$$

electrons are displaced relative to ions according to the relations.

$$\Delta x = \frac{e}{m}\frac{E_{0x}\cos\omega_0 t}{\omega_0^2 - \Omega^2}, \tag{4.11a}$$

$$\Delta y = \frac{\Omega}{\omega_0}\frac{e}{m}\frac{E_{0x}\sin\omega_0 t}{\omega_0^2 - \Omega^2}, \tag{4.11b}$$

$$\Delta z = \frac{e}{m}\frac{E_{0z}\cos\omega_0 t}{\omega_0^2}, \tag{4.11c}$$

where $\Omega = eB/mc$ is the electron cyclotron frequency. Since the oscillating particles may couple with waves with wave vectors k (so that the driving term of the instability is $\mathbf{k}\cdot\Delta\mathbf{x}$), we see that waves which propagate parallel to the magnetic field are driven by the $k\Delta z$ term, whereas waves propagating mainly perpendicularly to the magnetic field are driven by the term $\mathbf{k}_\perp\cdot\Delta\mathbf{x}$. A unified treatment of the problem of parametric coupling of waves in a magnetic field has been undertaken by Aliev *et al.* (1966), Amano and Okamoto (1969), and Porkolab (1972, 1974). These authors used the Vlasov equation, which can be solved after transformation to the oscillating frame of reference. The resulting dispersion relation is rather complicated. However, in the weak coupling limit it can be written in the following form:

$$\epsilon(\omega) + \frac{\mu^2}{4}\chi_i(\omega)[\chi_e(\omega)]\left[\frac{1}{\epsilon(\omega-\omega_0)} + \frac{1}{\epsilon(\omega+\omega_0)}\right] = 0, \tag{4.12}$$

where we assumed $\epsilon(\omega - \omega_0) \ll 1$, $\mu^2 \ll 1$. Here

$$\epsilon(\omega \pm j\omega_0) = 1 + \chi_1(\omega \pm j\omega_0) + \chi_e(\omega \pm j\omega_0)$$

is the linear dielectric function, $j = 0, \pm 1$, and $\chi_i(\chi_e)$ is the linear ion (electron) susceptibility. These susceptibilities can be written quite generally in terms of the complete hot plasma dielectric tensor in a magnetic field, including collisions. The coupling coefficient μ is given by the expression

$$\mu = \frac{e}{m}\left[\left(\frac{E_{0\parallel}k_z}{\omega_0^2} + \frac{E_{0x}k_x + E_{0y}k_y}{\omega_0^2 - \Omega^2}\right)^2 + \frac{(E_{0x}k_y - E_{0y}k_x)^2\Omega^2}{(\omega_0^2 - \Omega^2)^2\omega_0^2}\right], \tag{4.13}$$

which shows the effects of parallel drift, perpendicular polarization drift, and E$\times$B drift. Equation (4.12) predicts three types of instabilities: (i) the resonant decay instability, (ii) the oscillating two-stream instability, (iii) decay into quasimodes.

The resonant decay instability is characterized by resonant modes at both the low-frequency response and at the lower sideband. Assuming weakly damped waves, Eq. (4.12) can be expanded about the low- and high-frequency normal modes ω_1 and ω_2, respectively, and we obtain for the growth rate γ,

$$(\gamma+\gamma_1)(\gamma+\gamma_2) = \frac{\mu^2\chi_i(\omega_1)\chi_e(\omega_1)}{4}\left.\frac{\partial\epsilon_1}{\partial\omega}\right|_{\omega_1}\left.\frac{\partial\epsilon_2}{\partial\omega}\right|_{\omega_2}, \tag{4.14}$$

where we neglected the upper sideband. Here γ_1, γ_2 are the linear damping rates, and

$$\mathrm{Re}\epsilon_j(\omega_j, k_j) \simeq 0$$

defines the normal modes $\omega_j(k_j), j = 1, 2$. We note that these normal modes satisfy the selection rules [Eq. (4.3)]. The threshold is obtained from Eq. (4.14) by setting $\gamma = 0$.

The purely growing mode is obtained by assuming $\omega_1 = 0$, $\epsilon_R(\omega_2, k) \simeq 0$, in which case the growth rate near threshold is (Porkolab, 1974)

$$\gamma = -\gamma_2 + \frac{\mu^2}{4k^2\lambda_D^2\,|\partial\epsilon_R(\omega_2)/\partial\omega_2|\,(1 + T_i/T_e)} \tag{4.15}$$

so that $\gamma \propto E_0^2$ (since $\mu \propto E_0$). For large electric fields (i.e., for $\gamma \gg k_\parallel v_{ti}, \gamma \gg kc_s$), we obtain

$$\gamma = \frac{\mu^{2/3}\omega_{pi}^{2/3}}{(4|\partial\epsilon_R(\omega_2, k)/\partial\omega_0|)^{1/3}(1 + T_i/Te)^{1/3}} \tag{4.16}$$

so that $\gamma \propto E_0^{2/3}$, where $\omega_2 \approx \omega_0$.

Decay into quasimodes is obtained by assuming a resonant mode at the lower sideband [so that $\epsilon_R(\omega - \omega_0) = \epsilon_R(\omega_2) = 0$] and a nonresonant mode at the low-frequency response so that $\epsilon_R(\omega) \neq 0$]. The growth rate is (Porkolab, 1974, 1977)

$$\gamma = -\gamma_2 + \frac{\mu^2}{4}\frac{[(|\chi_i(\omega)|^2 + \chi_{iR}(\omega))\chi_{eI}(\omega) + (|\chi_e(\omega)|^2 + \chi_{eR}(\omega))\chi_{iI}(\omega)]}{|\partial\epsilon/\partial\omega_2||\epsilon(\omega)|^2} \tag{4.17}$$

where $|\epsilon(\omega)|^2 = \epsilon_R^2(\omega) + \epsilon_I^2(\omega)$, etc. Depending upon which term is the largest, the growth rate is $\gamma \propto E_0^2\chi_{(e,i)I}$ or $\gamma \propto E_0^2/\chi_{(e,i)I}$. A simplified form of Eq. (4.17) is obtained by noting that typically $|\chi_{iR}| \gg 1$, $|\chi_{eR}| \gg 1$. We note that Eq. (4.17) predicts particularly strong instabilities when the wave-particle resonance conditions

$$(\omega_0 - \omega_2)/k_\parallel \simeq v_{te},$$

$$(\omega_0 - \omega_2)/k_\parallel \simeq n\Omega/k_\parallel \simeq v_{ti},$$

are satisfied. These are similar conditions to nonlinear Landau damping, which we discussed earlier. Since k_0

=0 in the present treatment, the growth rates are obtained more easily than in the nonlinear Landau damping calculations.

There are also processes in which two electromagnetic waves couple. For example, the decay of a whistler wave into another whistler wave and an ion acoustic wave is an example of so-called Brillouin scattering, in which an incident electromagnetic wave decays into another electromagnetic wave and an ion acoustic wave (Forslund *et al.*, 1972; Porkolab *et al.*, 1972). In this case the coupling mechanism is the $\mathbf{j}\times\mathbf{B}$ force, i.e., particles oscillating in the electric field of one of the waves produce a current $\mathbf{j}$, which then couples with the magnetic field component B of the second electromagnetic wave. The $\mathbf{j}\times\mathbf{B}$ force then gives a contribution to electron pressure which may drive electrostatic ion waves unstable. This process is of the backscattered type, namely,

$$\mathbf{k}_0 = -\mathbf{k}_1, \mathbf{k}_2 = 2\mathbf{k}_0 , \tag{4.18}$$

where $\mathbf{k}_2$ is the wave vector of the ion wave. This type of instability may also occur in the absence of a magnetic field, and in laser fusion schemes it could be dangerous and undesirable. In particular, if a large fraction of the incident power were reflected from the outer layers of the expanding plasma, it would reduce efficiency and/or damage optics (Forslund *et al.*, 1973; Eidman and Sigel, 1974).

There are other types of decay processes which may be of importance in laser fusion. A schematic of some processes of interest is shown in Fig. 27. In particular, noteworthy processes include Raman scattering (EM → EM + E.P.), decay into two electron plasma waves (EM → E.P. + E.P.), Compton (induced) scattering (EM

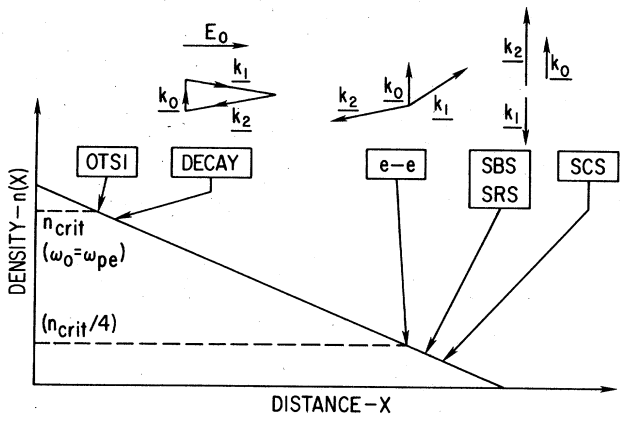

FIG. 27. "Theoretician's model" of inhomogeneous plasma with linearly varying density gradient. Also shown are locations of instabilities of possible importance in laser fusion schemes, including some momentum diagrams. OTSI designates the purely growing mode, (*ee*) designates the $\omega_0 \simeq 2\omega_{pe}$ instability, and (SBS), (SRS), and (SCS) designate stimulated Brillouin, Raman, and Compton scatter, respectively.

TABLE I. Typical thresholds in magnetized plasma.

Pump wave	Decay wave	Threshold
Extraordinary mode (if ignore tunneling) $(E_\perp B_0)$; $\omega_0 \simeq \omega_{UH}$ $(\omega_{pe} \ll \Omega_e)$	Lower-hybrid Upper-hybrid	$\frac{\omega_{pe}}{(2\Omega_e\omega_1)^{1/2}}\left(\frac{\gamma_1\gamma_2}{\omega_1\omega_2}\right)^{1/2} \leqslant \frac{E_0}{8(\pi n_0 T_e)^{1/2}}$
Extraordinary mode (if ignore tunneling) $(E_\perp B_0)$; $\omega_0 \simeq \omega_{UH}$ $(\omega_{pe} \ll \Omega_e)$	Ion acoustic Upper-hybrid	$\frac{\omega_2}{\omega_{pe}}\left(\frac{\gamma_1\gamma_2}{\omega_1\omega_2}\right)^{1/2} \leqslant \frac{E_0}{8(\pi n_0 T_e)^{1/2}}$
Ordinary mode $(\omega_0 \gtrsim \omega_{pe})$	Ion acoustic Electron plasma	$\left(\frac{\gamma_1\gamma_2}{\omega_1\omega_2}\right)^{1/2} \leqslant \frac{E_0}{8(\pi n_0 T_e)^{1/2}}$
Electron plasma wave (Trivelpiece–Gould)	Ion acoustic (ion cyclotron) Electron plasma	$\frac{\omega_0\Omega_e}{\omega_{pe}^2}\left[\frac{\gamma_1\gamma_2}{\omega_1\omega_2}\left(1+\frac{\omega_{pe}^2}{\Omega_e^2}\right)\right]^{1/2} \leqslant \frac{E_0}{8(\pi n_0 T_e)^{1/2}}$
Whistler wave $\omega_0 < \Omega_e < \omega_{pe}$	Ion acoustic Electron plasma	$\frac{\omega_0(\Omega_e-\omega_0)}{\omega_{pe}^2}\left[\frac{2\gamma_1\gamma_2}{\omega_1\omega_2}\left(1+\frac{\sin^2\theta\,\omega_{pe}^2\Omega_{pe}^2}{(\omega_2^2-\Omega_e^2)^2}\right)\right]^{1/2} \leqslant \frac{E_0}{8(\pi n_0 T_e)^{1/2}}$
Lower-hybrid wave (resonance cone, whistler wave) $k_\parallel/k \gtrsim 3(m_e/m_i)^{1/2}$	Lower-hybrid Ion quasimode	$\frac{\Omega_e\omega_0}{2\omega_{pe}^2}\left[\frac{2.6\gamma_2}{\omega_2}\left(1+\frac{\omega_{pe}^2}{\Omega_e^2}\right)\right]^{1/2} \leqslant \frac{E_0}{8(\pi n_0 T_e)^{1/2}}$
	Lower-hybrid Purely growing mode	$\frac{\Omega_e\omega_0}{2\omega_{pe}^2}\left[\frac{2\gamma_2}{\omega_2}\left(1+\frac{\omega_{pe}^2}{\Omega_e^2}\right)\right]^{1/2} \leqslant \frac{E_0}{8(\pi n_0 T_e)^{1/2}}$
Magnetosonic wave $(\omega_0 \simeq \Omega_i)$	Ion cyclotron Drift wave	$2(\omega^*\Omega_i)^{1/2} \leqslant \frac{kcE_0}{B}$

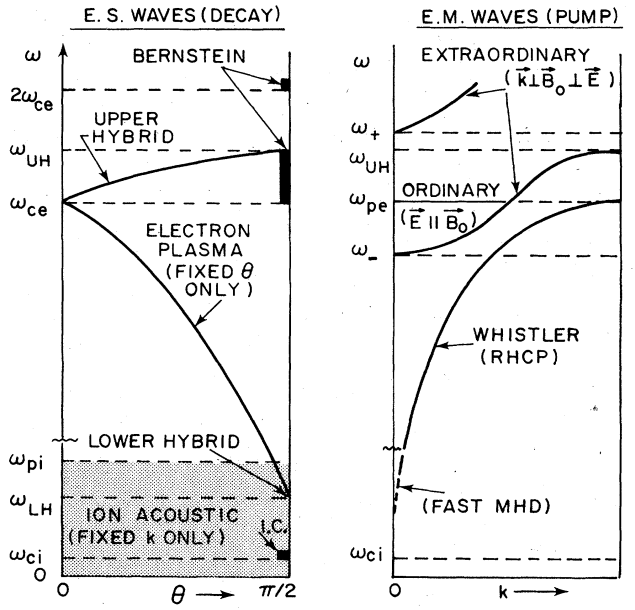

FIG. 28. A schematic of possible choices for pump waves and decay waves in a magnetized plasma. 0 designates the angle of propagation with the magnetic field.

→ EM + particles), and filamentational and modulational instabilities (where EM designates the electromagnetic wave, and E.P. designates longitudinal electron plasma waves). Thresholds and growth rates for these processes have been given in the literature (see, for example, DuBois, 1974; Drake *et al.*, 1974; Manheimer and Ott, 1974). These instabilities have been reviewed recently (DuBois, 1974; Liu *et al.*, 1976).

In Fig. 28 we show schematically different modes in a magnetized plasma which may be used as pump waves and/or decay waves. For example, the extraordinary mode may decay into Bernstein waves and ion cyclotron waves or electron quasimodes. The ordinary wave and the whistler wave may decay into electron plasma waves and ion acoustic waves. Lower-hybrid waves may decay into other lower-hybrid waves and quasimodes. Ion cyclotron waves may decay into other ion cyclotron waves and drift waves. Alfvén waves may decay into kinetic Alfvén waves and ion quasimodes (Hasegawa and Chen, 1975). In Table I we present various combinations of these modes which may form triplets of decay waves which have been considered and/or observed in past experiments. Several of these decay processes are expected to be of importance in rf heating of fusion plasmas (Porkolab, 1977).

E. Convective effects due to inhomogeneities

In recent years considerable effort has been spent on taking into account the inhomogeneities of density, temperature, finite interaction region, and nonuniform pumps, i.e., finite extent (Kroll, 1965; Porkolab and Chang, 1970; Harker and Crawford, 1970; Perkins and Flick, 1970; Rosenbluth *et al.*, 1972; Pesme *et al.*, 1973; Liu *et al.*, 1974; DuBois *et al.*, 1974; Forslund *et al.*, 1975). All of these processes may introduce new, possibly higher thresholds of instability than in a uniform plasma. The essential feature of these effects is that often the instabilities become convective (forward scattering) and the matching of the selection rules [Eq. (4.3)] is destroyed in a distance short compared with effective growth lengths. Alternatively, finite lengths or nonuniform pumps limit the region of spatial growth. However, for backward scattering ($\mathbf{v}_1 \cdot \mathbf{v}_2 < 0$) absolute instability may occur if

$$\gamma_0^2 > \frac{|v_1 v_2|}{4}\left[\left(\frac{\gamma_1}{v_1}-\frac{\gamma_2}{v_2}\right)^2+\frac{\pi^2}{L^2}\right], \tag{4.19}$$

where L is the length of the system, v_1, v_2 are the group velocities of the two decay waves, γ_1, γ_2 are their damping rates, and γ is the homogeneous, uniform plasma growth rate (see, for example, Pesme *et al.*, 1973).

The effects of density gradients can be obtained following the procedure outlined by Rosenbluth 1972. Assuming a WKB-type phase variation and defining

$$K(X) = \Delta K = k_0 - k_1 - k_2$$

(where we assumed a one-dimensional propagation so that all k's depend on x only), the equations describing the spatial variation of the two coupled modes can be written in the following form (Rosenbluth, 1972).

$$\frac{dE_1}{dx}+\frac{\gamma_1}{v_{1x}}E_1=\frac{\gamma E_2^*}{v_{1x}}\exp\left(i\int_0^x K(x)dx\right), \tag{4.20a}$$

$$\frac{dE_2}{dx}+\frac{\gamma_2}{v_{2x}}E_2=\frac{\gamma E_1^*}{v_{2x}}\exp\left(-i\int_0^x K(x)dx\right), \tag{4.20b}$$

where E_1, E_2 are the electric field amplitudes of the decay waves, and the other quantities have been defined earlier. Assuming a linear variation of the mismatch with distance, namely $K(x) \simeq K'x$, Eqs. (4.20a) and (4.20b) can be combined in the following form

$$\frac{d^2\psi}{dx^2}-\left[\frac{\zeta^2}{4}+\frac{1}{2}\frac{d\zeta}{dx}+\frac{\gamma_0^2}{v_1 v_2}\right]\psi=0, \tag{4.20c}$$

where $\zeta = \gamma_2/v_{2x} - \gamma_1/v_{1x} - iK(x)$, and $\psi \propto E_1$. Integrating Eq. (4.20) by WKB techniques, the total spatial amplification of wave intensity obtained between the turning points $x_t = 2\gamma_0/K'(v_{1x}v_{2x})^{1/2}$ is given by

$$I = I_0 \exp(2\pi\gamma_0^2/|K'|v_{1x}v_{2x}), \tag{4.21}$$

where linear damping has been ignored. Thus the effective threshold may be defined as the pump power for which the initial background noise is amplified by a factor of 2π, namely,

$$1 < \gamma_0^2/|K'|v_{1x}v_{2x}. \tag{4.22}$$

For example, for decay into weakly damped ion acoustic waves an electron plasma waves one finds for the threshold

$$\frac{v_0^2}{v_t^2} > \frac{16}{(k^2\lambda_D^2)}\left(\frac{\lambda_D}{H}\right)^{4/3}, \tag{4.23}$$

where $v_0 = eE_0/(m\omega_0)$ is the "quiver" velocity, and $H = (\nabla_x n/n)^{-1}$. The minimum value is obtained for the largest value of k just before strong Landau damping sets in at the sideband, namely $k\lambda_D = 1/4$. For strongly damped ion waves ($T_e \simeq T_i$) Perkins and Flick (1971) obtained the threshold

$$\frac{v_0^2}{v_t^2} > \frac{16}{Hk}\left(\frac{\gamma_1}{\omega_1}\right)^{1/2}. \tag{4.24}$$

Again the minimum threshold obtains at $k\lambda_D \simeq \frac{1}{4}$.

If the group velocities of the decay waves are in the opposite direction, and if $K' = 0$ but $K'' \neq 0$, then absolute instability may result (Rosenbluth, 1973). On the other hand, if finite size effects are included, for $\mathbf{v}_1 \cdot \mathbf{v}_2 < 0$, the convective instability may become an absolute instability at the threshold given by Eq. (4.22) even if $K' \neq 0$ (DuBois *et al.*, 1974). According to Nicholson and Kaufman (1974) and Spatchek *et al.*, (1975), if background turbulence is present absolute instability may result even in an inhomogeneous plasma. Finally, we note that the effect of a broad rf pump may reduce the growth rates considerably (Valeo and Oberman, 1973; Thomson 1975; Obenschain *et al.*, 1976).

F. Nonlinear saturation

So far we have considered only linearized perturbation-type solutions. An important question is the nonlinear limit of these instabilities. There have been several attempts to describe the nonlinear saturated state as being due to induced scattering and cascading of the sideband into further lower-frequency waves (Pustovalov *et al.* 1970, 1971; DuBois and Goldman, 1972; Valeo *et al.*, 1972; Fejer and Kuo, 1972; DuBois *et al.*, 1973; Chen and Hasegawa, 1975:, Rogister, 1975; Berger *et al.*, 1976) or as due to other mechanisms including broadening (Dupree, 1966; Bezzerides and Weinstock, 1972), pump depletion, and quasilinear effects (i.e., heating).

One may define a nonlinear conductivity associated with the decay instabilities as follows (DuBois, 1974)

$$\sigma_{NL} E_0^2 \equiv \frac{\nu_{\text{eff}}}{4\pi} E_0^2$$

$$= \frac{d^3k}{(2\pi)^3}[\gamma(E_0, k) - \gamma(0, k)]\frac{|E_k|^2}{4\pi}, \tag{4.25}$$

where the left-hand side is the effective pump energy depletion rate, and the right-hand side is the rate of growth of the energy of the excited electrostatic wave (the negative contribution due to damping is subtracted). Note that by the above equation one could also define an effective "nonlinear resistivity," "ν_{eff}". In order to calculate the nonlinear conductivity, one has to have a theory for the saturated spectrum. This has been done in only a few special cases as mentioned above. For example, in the case of $T_e = T_i$, the nonlinear conductivity just above threshold was calculated by DuBois *et al.* (1974) as

$$\sigma_{NL}(E_0) = \eta \frac{\omega_{pe} E_0^2}{16\pi n T_e}, \tag{4.26}$$

where η is a numerical coefficient of the order of unity. However, for large values of E_0 the total energy goes as E_0^2 (instead of E_0^4) so that σ_{NL} approaches a constant value, independent of E_0.

While the linear theory of parametric instabilities is now well understood (except in strongly inhomogeneous plasmas), with a few possible exceptions the nonlinear state is still not well understood. In addition, there are very few experimental results to verify the theories. Here computer simulation has been of considerable help and guidance (Kruer *et al.*, 1972; DeGroot *et al.*, 1973; Thomson *et al.*, 1974; Forslund *et al.*, 1975). However, how realistic these computer "experiments" are is still not known.

There have also been extensions of these nonlinear theories to some uses in magnetized plasmas. For example, the saturation of the lower-hybrid decay instability by cascading has been proposed (Hasegawa and Chen, 1975; Berger *et al.*, 1976). These theories predict further cascading of the sideband into either longer-wavelength modes or shorter-wavelength modes, depending upon the pump field structure. When cascading produces sideband modes sufficiently close to the lower-hybrid frequency, strong damping and hence saturation of the whole spectrum results.

An alternate saturation mechanism may be orbit diffusion (Porkolab, 1977). In this case when $\nu_{\text{eff}} \gtrsim \Omega_i$, straight-line ion orbit motion results, and perpendicular ion Landau damping sets in. For example, for lower-hybrid waves the condition of strong orbit diffusion is given by (Porkolab, 1977)

$$\frac{\epsilon}{\epsilon_{\text{th}}} = \frac{\sum_k E_k^2}{4\pi n_0 T} = \left(\frac{\Omega_i}{\omega_{\text{pi}}}\right)^2 \frac{\omega_2}{k_\perp V_i} \quad \text{if } \omega_2 \gg k_\perp V_i;$$

$$= \left(\frac{\Omega_i}{\omega_{\text{pi}}}\right)^2 \frac{\Omega_i}{k_\perp V_i} \quad \text{if } \omega_2 \ll k_\perp V_i,$$

where $V_i^2 = T_i/m_i$, ω_2 is the sideband frequency, Ω_i is the ion cyclotron frequency, and ω_{pi} is the ion plasma frequency. This level should be compared with that predicted by cascading (Rogister, 1975)

$$\frac{\sum_k E_k^2}{4\pi n_0 T} = \frac{\omega_0}{\Delta\omega}\left(\frac{U}{c_s}\right)^2\left(\frac{\Omega_i}{\omega_{\text{pi}}}\right)^2,$$

where $U = cE/B$ is the $\mathbf{E}\times\mathbf{B}$ drift velocity and $c_s = (T_e/m_i)^{1/2}$ is the acoustic speed. Since typically $(\omega_0/\Delta\omega) \simeq 4$, $U/c_s \simeq 1$, short-wavelength decay waves ($k\lambda_D \gtrsim 0.2$) may saturate by orbit diffusion and convective damping due to finite pump widths, whereas long-wavelength decay modes would stabilize by cascading.

In general, much more work remains to be done concerning the saturation of parametric instabilities. Similarly, quasilinear theories predicting the type of heating produced by the instabilities is also lacking in most cases. In the steady state this can only be done once a saturated spectrum is calculated.

G. Soliton formation and density cavities

Let us now consider another type of nonlinear solution, namely soliton formation. This may be relevant to the nonlinear state of the purely growing mode (Zakharov, 1972; Karpman, 1971; Morales *et al.*, 1974; Valeo *et*

al., 1974; Hasegawa, 1975). In particular, due to the ponderomotive force, strong local electric fields may deplete the density, hence trapping the electric field. As the field grows, more density is removed and a cavity is produced which then traps the fields further, etc., until a collapse of the field may occur in two- and three-dimensional cases. Since locally strong fields may be produced, we may expect strong particle acceleration and energetic particle tail formation.

As shown by the above authors, the equation describing this nonlinear state is the nonlinear Schrödinger equation. It can be obtained as follows: Ignoring the magnetic field, and assuming $\omega_0 \simeq \omega_{pe}$, the low-frequency ($\omega \approx 0$) time-averaged response of electrons in the presence of the external electric field is described by Eq. (4.5). That is, we balance the pressure by the ponderomotive force,

$$\nabla_x p_e + \nabla_x(|E|^2/8\pi) = ne\nabla_x\phi\,, \tag{4.27}$$

ignoring electron inertia and including an ambipolar potential ϕ. Although only electrons respond to the ponderomotive force, ions respond to the ampipolar potential (trying to achieve charge neutrality)

$$\nabla_x p_i = -ne\nabla_x\phi\,, \tag{4.28}$$

where we ignore ion inertia. Requiring quasineutrality, i.e., requiring that $n_e \simeq n_i$, and since $p_e = n_e T_e$, $p_i = n_i T_i$, we may eliminate ϕ from Eqs. (4.27) and (4.28) and obtain

$$n(x) \simeq n_0\left\{\exp -\left[\frac{|\bar{E}| - \langle|\bar{E}|^2\rangle}{16\pi n(T_e+T_i)}\right]\right\}, \tag{4.29}$$

where the bar represents the time average, and $\langle\ \rangle$ represents the spatial average. Equation (4.29) describes modifications in the equilibrium density due to the high-frequency field.

Let us now consider the high-frequency response at the electron plasma frequency ($\omega_0 \simeq \omega_{pe}$), which is described by the simple harmonic oscillator motion

$$\frac{\partial^2 E}{\partial t^2} + \omega_{ek}^2 E + \nu_e\frac{\partial E}{\partial t} = 0\,, \tag{4.30}$$

where we use the left-hand side of Eq. (4.4) and Poisson's equation, namely $E \propto n_e$ at high frequencies. Then, recognizing that $\omega_{ek}^2 \simeq \omega_{pe}^2(1+3k^2\lambda_D^2)$ and that $\omega_{pe}^2 \propto n(x)$, we may perform a WKB-type expansion of E, that is, assume $E = E_H(t,x)\exp(-i\omega_0 t)$ (where E_H is a slowly varying function of x and t). From Eqs. (4.29) and (4.30) and from the resonance condition $\omega_0^2 = \omega_{ek}^2(x=0)$ we obtain

$$i\frac{\partial E_H}{\partial t} + \frac{3v_t^2}{2\omega_0}\frac{\partial^2 E_H}{\partial x^2} + \frac{\omega_{po}^2}{2\omega_0}\frac{|\bar{E}_H|^2}{16\pi nT_e}E_H = 0\,, \tag{4.31}$$

where $v_{te}^2 = T_e/m_e$, and where the last term of Eq. (4.31) contains the cubic nonlinearity. This is the so-called nonlinear Schrödinger equation. It is easy to show that in the linearized limit Eq. (4.31) predicts the purely growing mode. The computer solution of this equation in the nonlinear limit has been discussed recently in some detail (Morales, 1974). If we include ion inertia, a similar equation is obtained in the moving frame of reference, except that the nonlinear term [the last term in Eq. (4.31)] is divided by the term $(1 - v_g^2/c_s^2)$, where c_s is the speed of sound and v_g is the group velocity of the high-frequency wave (this is valid only as long as $v_g \neq c_s$). The solution of this equation in higher dimensions is still under investigation. In particular, this equation may be unstable to transverse perturbations (Schmidt, 1975).

More recently work on solitons has been concentrating on modes occurring in magnetized plasmas. For example, Kaufman and Stenflo (1975) and Porkolab and Goldman (1976) tested the regime of the upper-hybrid frequency; Morales and Lee (1975), Schmidt (1975), Kaw *et al.* (1976), and Sen (1977) treated the lower-hybrid frequency; Petviashvili (1976) treated the second harmonic of the electron cyclotron frequency; and Mikhailovskii *et al.* (1976) treated the Alfvén wave regime. In these cases density depletion may take place due either to particle motion along the magnetic field or to drift motion across the magnetic field from Larmor orbit effects. Thus steepening of the electric fields could occur under suitable conditions.

H. Experimental observations

1. Early experiments

Early experimental research concerning parametric instabilities includes the work of Stern and Tzoar (1966), Hiroe and Ikegami (1967), Chang and Porkolab (1970, 1972), Stenzel and Wong (1973), and Franklin *et al.* (1971). In some of these experiments the decay spectrum as well as wave number selection rules (Chang and Porkolab, 1970, 1972) were measured and compared with the theoretically predicted threshold fields. In Fig. 29 we show the experimental results of Chang *et al.* (1972), which demonstrate the selection rules [Eq. (4.3)]. At approximately the same time, Gekker and Sizukhin (1969), and Batanov *et al.* (1971) attempted to demonstrate anomalous absorption due to parametric instabilities by injecting plasma into a waveguide from one end and measuring the transmission (or reflection) coefficient of microwave power sent from the other end. The measurements indicated strong reduction in the reflection coefficient above some threshold. Although energetic particles were also detected in some of these experiments, no measurements were made to detect the presence of parametric instabilities. Eubank (1971) attempted to improve on this situation by shining microwave power onto a plasma column in both the ordinary and the extraordinary modes of propagation. He had a probe in the plasma which detected ion acoustic oscillations up to the ion plasma frequency, as well as grided probes (energy analyzers) which showed plasma heating. However, the threshold measurements and/or anomalous absorption measurements remained less than clear, since, due to the low rise time of the microwave pulses (milliseconds), strong ionization occurred near the open-ended waveguide.

There was also a series of experiments performed in Q (quiescent) machines by Dreicer *et al.* (1971), and Chu and Hendel (1972). In these experiments the plasma was placed in a high-Q rf cavity, and by measuring the Q of the cavity it was possible to observe an increase in the dissipation above some critical threshold input power level. In Fig. 30 we exhibit the results of Chu and Hen-

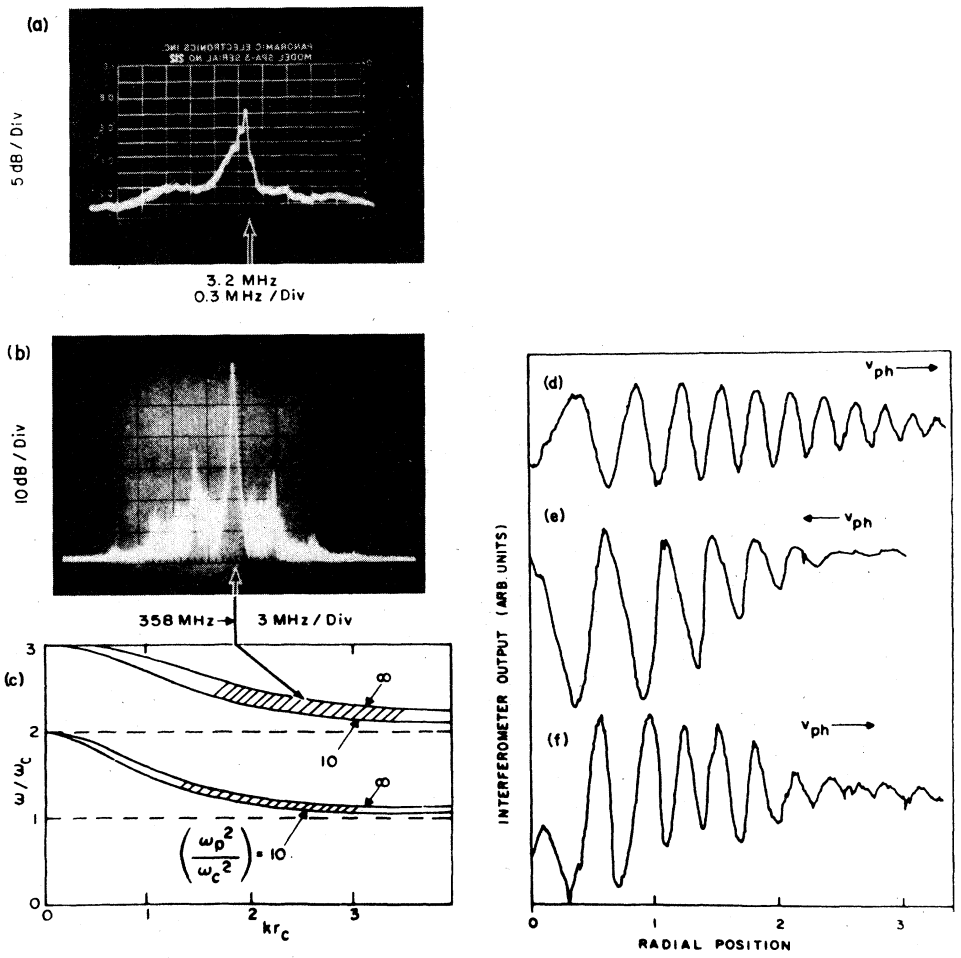

FIG. 29. Decay spectrum showing energy (frequency) conservation of: (a) low-frequency ion acoustic wave; (b) high-frequency cyclotron harmonic (Bernstein) waves, when pumped by $E_0 \perp B$ in the shaded regions of the dispersion curves of cyclotron harmonic waves. (c) The dispersion relation for the Bernstein waves. The momentum conservation is verified from the interferometer traces of the waves: (d) ion acoustic wave; (e) lower sideband (Bernstein wave); (f) upper sideband (Bernstein wave). (After Chang, Porkolab, and Grek, 1972.)

del (1972), which show the increase of plasma rf resistivity ($1/Q$), increase of effective plasma heating (T/T_0 determined from conductivity measurements), and growth of the noise spectrum (picked up by a probe from within the cavity). Figure 31 indicates in the same experiments a break in the absorption curve when the input power was above threshold for parametric instability. In particular, it appeared that in the unstable regime $P_{abs} \propto E^4$, and hence it was concluded that $v_{eff} \propto E_0^2$, in agreement with the nonlinear theories of Valeo *et al.* (1972) and DuBois *et al.* (1974). However, in the more recent experiments of Flick (1975), the input power was extended to higher levels, and the $P_{abs} \propto E^4$ law was not observed. In particular, even near threshold, Flick found a faster variation of P_{abs} with E than the fourth power, and a slower variation well above threshold. In addition, the cascading process assumed in the theories of DuBois *et al.* (1974) and Valeo *et al.* (1972), was not observed in the experiment. Flick (1975) proposed that pump depletion and random-phase effects may be the relevant processes to explain his experiments.

We must also include here the results of high-power radar modification experiments in the ionosphere (Utlaut and Cohen, 1971; Wong and Taylor, 1971; Carlson *et al.*, 1972.) These experiments also showed that parametric instabilities are operative and are responsible for some of the observed plasma heating in the ionosphere.

Let us now consider some of the more recent experiments in which parametric instabilities and the resulting plasma heating were studied in more detail than previously. We shall discuss these experiments in order of decreasing frequencies.

2. Upper-hybrid frequency

In the regime of the upper-hybrid frequency recent measurements on parametric decay have been performed in both linear geometry (Grek and Porkolab, 1973; Porkolab *et al.*, 1976) and toroidal devices (Okabayashi *et al.*, 1973). These experiments include the regimes $\lambda_0 \ll d$ and $\lambda_0 \gg d$ (where λ_0 is the free-space wavelength of the electromagnetic wave, and d is the characteristic plasma size). Wavelength measurements of the decay waves have shown decay into upper-hybrid waves (Bernstein waves) and lower-hybrid and/or ion acoustic waves. Measurements of thresholds, growth rates, pump depletion, and anomalous resistivity have been performed (Grek and Porkolab, 1973), in which significant electron heating was associated with the presence of the decay in-

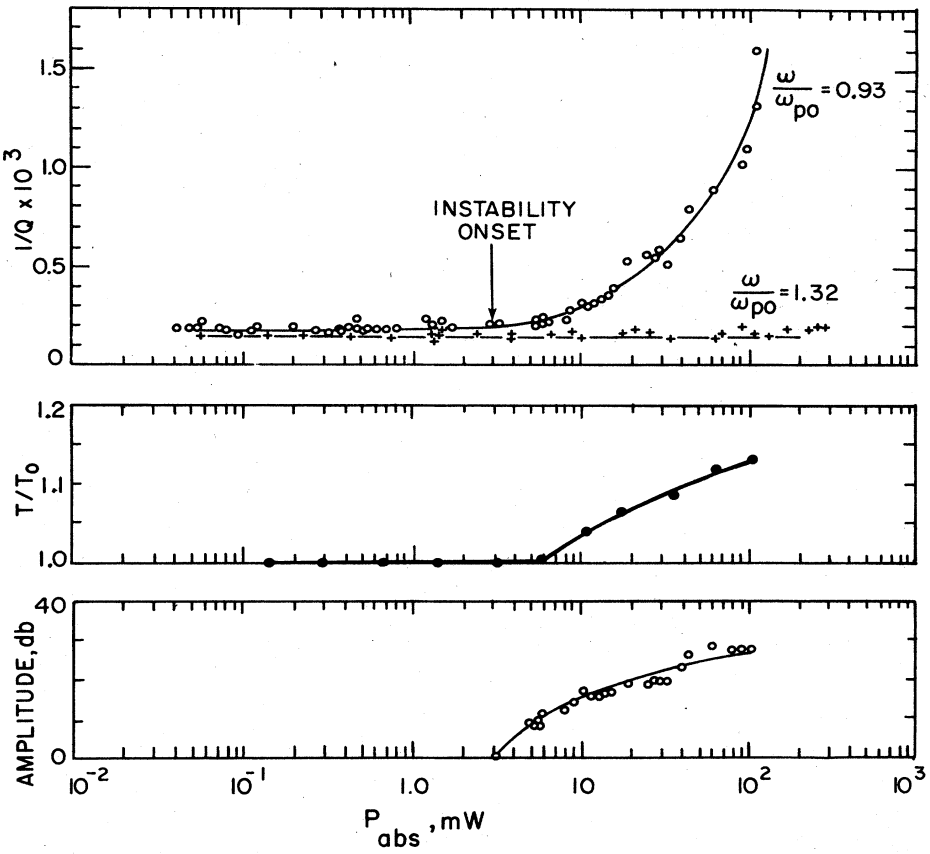

FIG. 30. Measurements of the cavity Q, temperature, and fluctuation amplitude in the experiments of Chu and Hendel (1972).

stability. An effective anomalous resistivity of a factor of ten to twenty times larger than classical resistivity has been measured (Grek, 1973). In Figs. 32 and 33 we show some of these experimental results on plasma heating. Significant heating was observed only above threshold for decay instability. A similar phenomenon has been observed in the Princeton L-3 device (Porkolab *et al.*, 1976) and the Princeton FM-1 toroidal device (Oka-

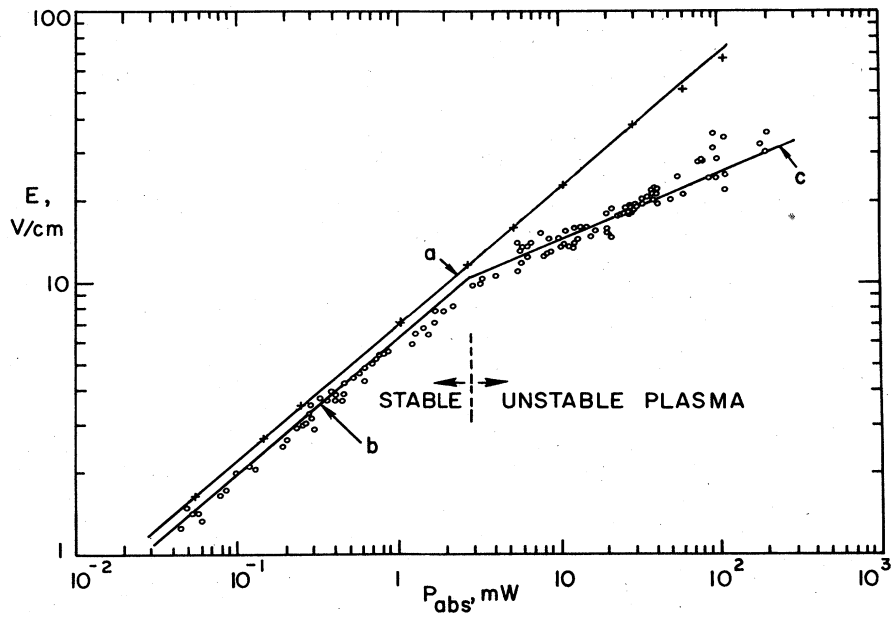

FIG. 31. Results of the power absorption measurements in the experiments of Chu and Hendel (1972).

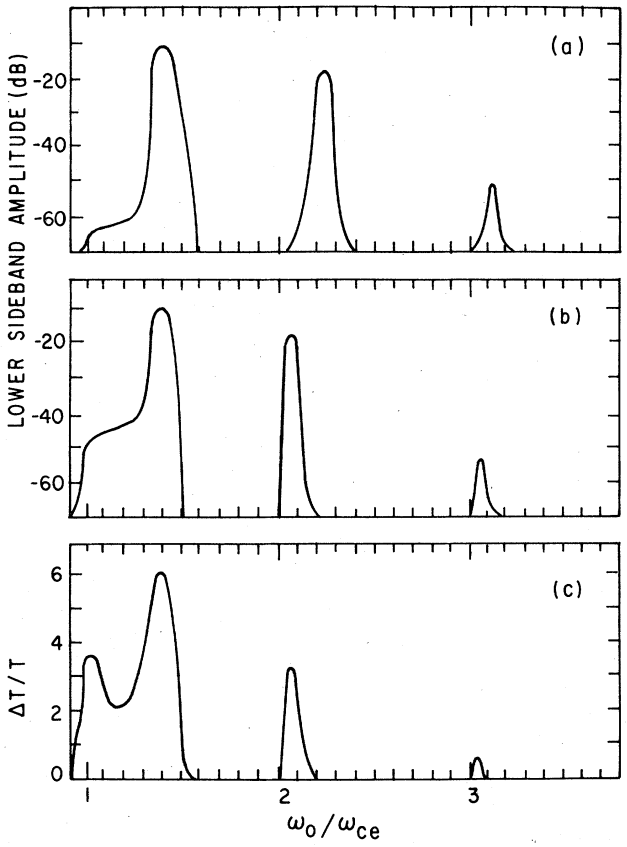

FIG. 32. (a) Amplitudes of Bernstein waves which couple with lower-hybrid waves: $\omega_{ce}=\omega_{pe}$; ω_0 (the pump frequency) is varied. (b) Amplitudes of Bernstein waves which couple with ion acoustic waves. (c) Fractional increase of the main-body electron temperature as obtained from a swept Langmuir probe; $P_0 \simeq 30$ W. (After Grek and Porkolab, 1973.)

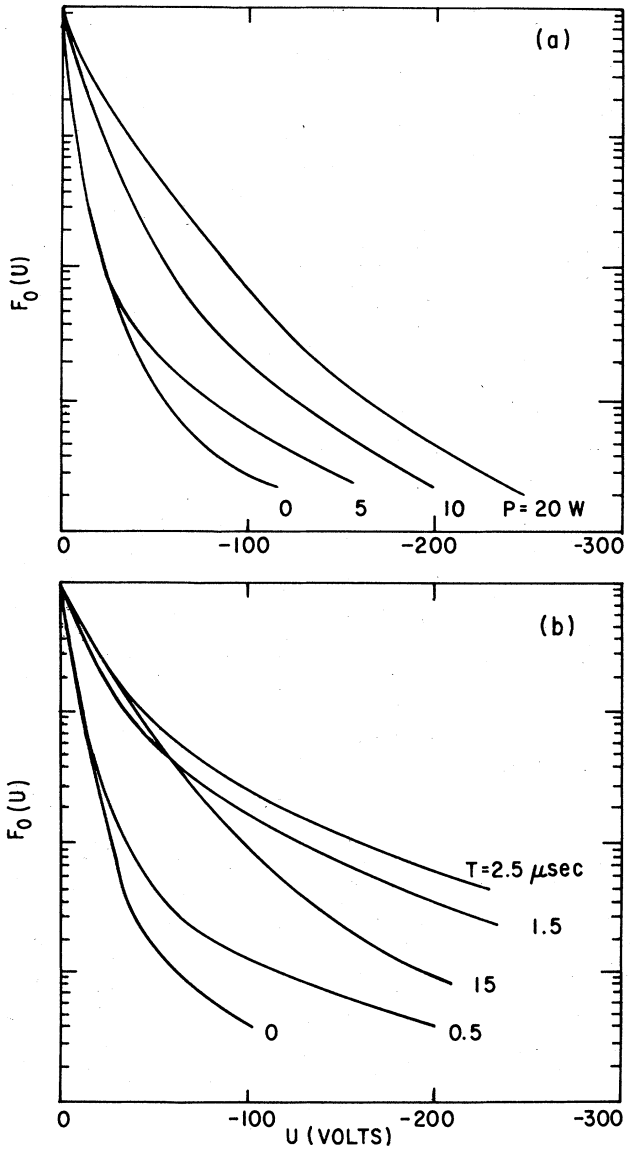

FIG. 33. (a) Electron energy distribution [$F_0(\mu)$] for different powers (P) 5μs after the start of the heating pulse. $\omega_{pe}/\omega_{ce}=1$, $\omega_0/\omega_{ce}\simeq 1.5$. (b) Energy distribution for different times (t) after the start of the heating pulse; $P_0=25$ W. (After Grek and Porkolab, 1973.)

bayashi *et al.*, 1973). The results from the latter are shown in Figs. 34 and 35, again demonstrating that significant ion and electron heating occurs only above threshold for parametric instabilities. In this toroidal experiment, in the presence of parametric instabilities, no significant deterioration of confinement was observed. In particular, because of the short wavelengths excited ($k_\perp r_{ce} \simeq 1$) and decay well within the body of the plasma column, we do not expect much enhanced loss due to this instability.

3. Electron plasma frequency

Experiments showing parametric instabilities and plasma heating just above the electron plasma frequency have been performed recently by Dreicer *et al.* (1973), Mizuno and DeGroot (1975), and Porkolab *et al.* (1976). Dreicer's experiments were performed in a cavity geometry as discussed previously. Mizuno and DeGroot (1975) made their measurements in a waveguide using an externally made plasma. In both of these experiments the resulting hot electron tail (suprathermal electrons) was measured. It was found that 1% to 10% of the particles ended up in the tail, depending on power and geometry (with Dreicer's experiments measuring the lower percentage). Maximum electron energies of up to two orders of magnitude above thermal energy were detected for input powers up to three orders of magnitude above threshold.

In the experiments of Porkolab *et al.* (1976) a geometry was employed similar to that of Eubank (see Fig. 36), but the pulse rise time was decreased to 50 nsec, and the pulse duration was reduced to at most 10 μsec so that ionization problems could be avoided. An attempt was made to verify the inhomogeneous threshold theory discussed earlier. However, it was found that while for

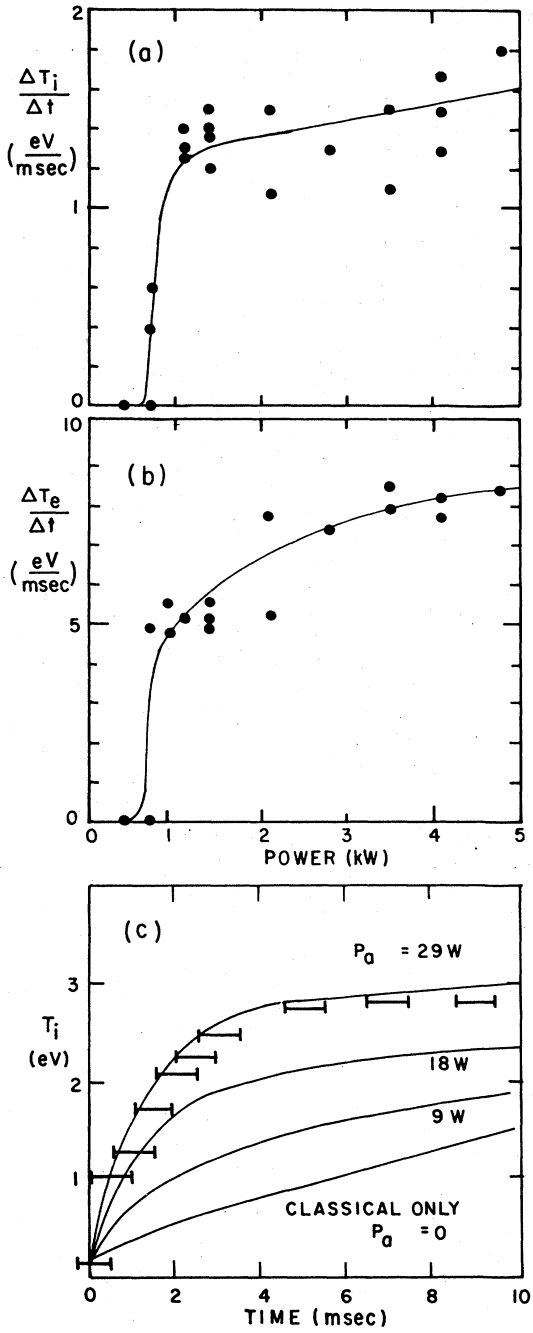

FIG. 34. (a) Heating rate of ion temperature vs input power. (b) Heating rate of electron temperature vs input power. (c) Comparison of time dependence of T_i with numerical calculations. (After Okabayashi, Chen, and Porkolab, 1973.)

some density profiles the spectrum behaved roughly in agreement with Eq. (4.23) or (4.24), in many cases no such agreement was observed. In addition, the incident electric field was strongly nonuniform $[(\nabla n/n)^{-1} \sim (\nabla E/E)^{-1}]$, so that the validity of the previous theories was in question. Also, strong refraction of the pump field around the plasma column was observed. In spite of the large

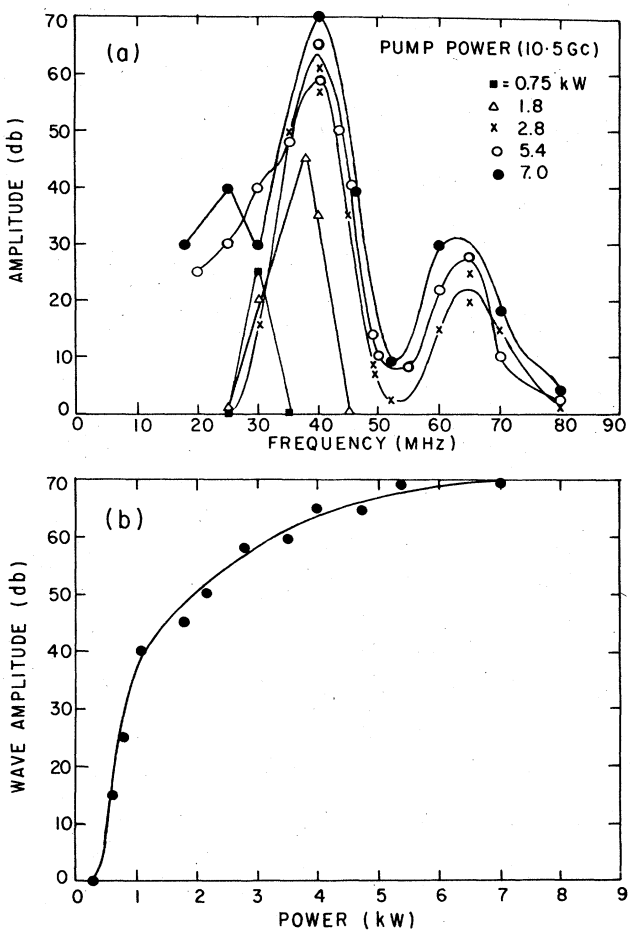

FIG. 35. (a) Frequency spectrum for different input rf powers. (b) Decay wave amplitude vs input power. (After Okabayashi, Chen, and Porkolab, 1973.)

gradients, strong parametric instabilities were observed near the critical layer ($\omega_0 \simeq \omega_{pe}$) and plasma heating of the main body was observed above threshold. Although the incident power at threshold was higher than uniform theory predicted, because of the radially decreasing

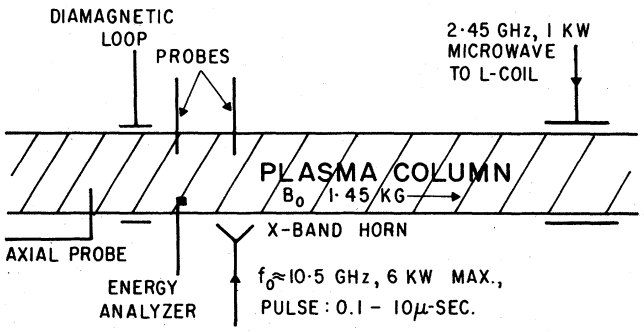

FIG. 36. Experimental setup to measure parametric instabilities in an inhomogeneous plasma. (After Porkolab *et al.*, 1975.)

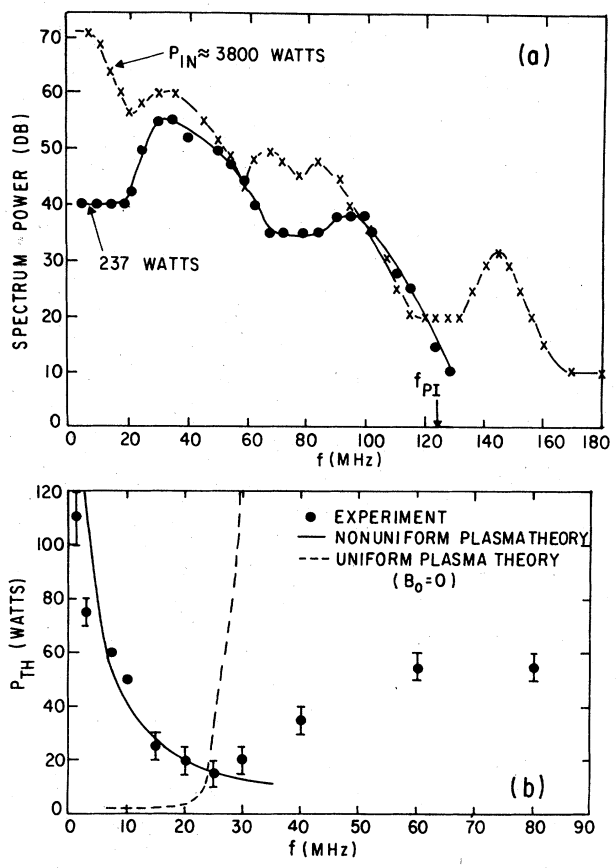

FIG. 37. (a) Low-frequency decay spectrum. 0-mode (b) Experimentally measured thresholds at $A = 1$ (dots), uniform plasma theory (dashed line), and nonuniform plasma theory (solid line), the latter only estimated from the incident power levels; 0-mode. (After Porkolab *et al.*, 1975.)

electric fields due to refraction, the local electric field was estimated to be near the uniform threshold theory (within an order of magnitude). In Fig. 37 we show a typical low-frequency decay spectrum (which was identified by interferometry as ion acoustic waves) and in Fig. 38 measurements of the heating rates of the main-body electron temperature are shown. The heating results of Fig. 38 indicate an anomalous heating of a factor of twenty faster than classical collisional absorption. The production of energetic tails was also observed, with a few percent of the particles occupying the tail, and with maximum energies up to a factor of fifty above the mean bulk energy. In Fig. 39 we show a distribution function for input powers two orders of magnitude above threshold. In addition, production of energetic ions was also observed (a few percent with maximum energies up to 70 eV).

4. Trivelpiece-Gould modes

Because of possible applications to heat-controlled fusion devices, a large number of experiments have been performed in this regime, i.e., $\omega_{pi} \ll \omega_0 < \omega_{pe}$, Ω_e (Porkolab *et al.*, 1973, 1974; Hendel and Flick, 1973; Flick, 1975; Chu *et al.*, 1973; Bernabei *et al.*, 1973, 1974; and Edgley *et al.*, 1975). In this regime decay into other Trivelpiece–Gould modes [magnetized electron plasma waves (Trivelpiece and Gould, 1959)] and low-frequency ion acoustic waves, or ion cyclotron waves, or ion quasimodes occurs. We should also include here experiments using whistler waves (Porkolab *et al.*, 1972). In these experiments both energetic electron and ion tails have been observed at high input powers and short pulse durations (Porkolab *et al.*, 1975) as well as main-body ion heating at longer times (Hendel *et al.*, 1973; Chu *et al.*, 1973; Bernabei *et al.*, 1973, 1974). It is believed that the energetic ion tails are due to acceleration by the

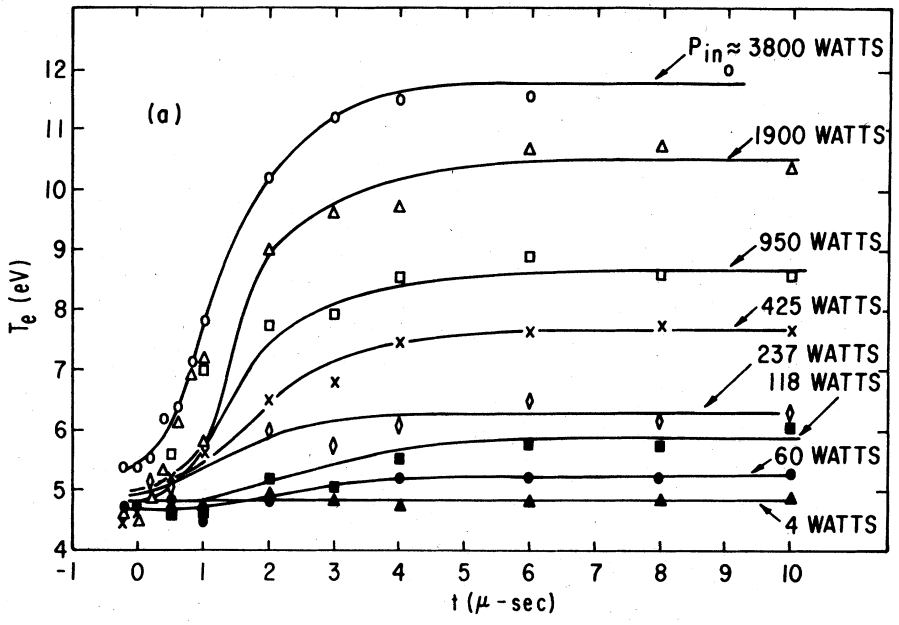

FIG. 38. (a) Temperature obtained from a Langmuir probe as a function of time and input power; 0-mode. (b) Initial heating rates in the first few microseconds as a function of power; 0-mode. (After Porkolab *et al.*, 1975.)

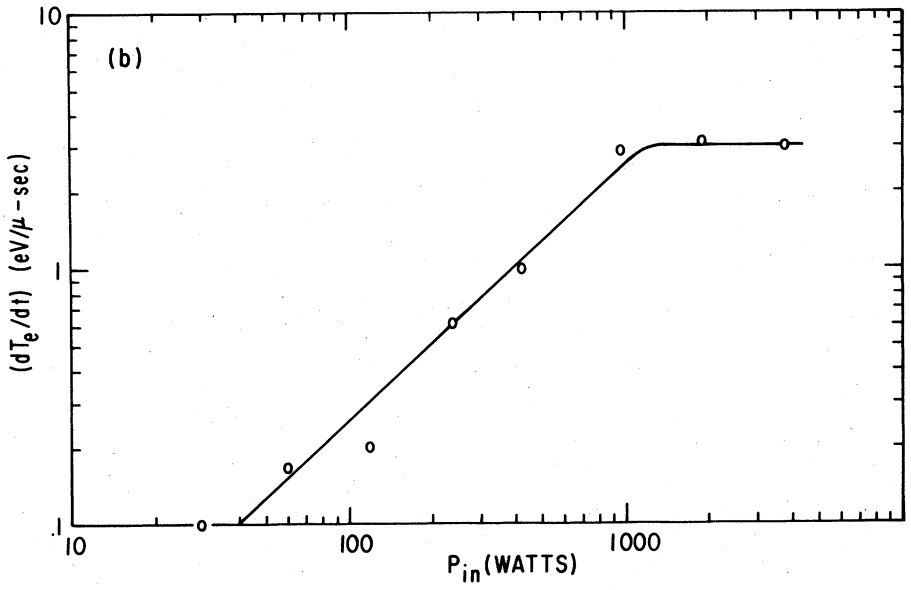

FIG. 38. (*Continued*)

expanding parametrically heated energetic electrons, as well as due to the turbulent ion acoustic fields. In the work of Bernabei *et al.*, (1973, 1974), main-body ion heating was also observed for pump frequencies $\omega_0 \simeq 3\omega_{pi} \ll \omega_{pe}$, even though initially $T_{e0} \gg T_{i0}$. Simultaneously a strong parametric decay spectrum in the ion cyclotron regime was observed. Chu *et al.* (1973) in a Q machine operated in the regime $\omega_{pi} \ll \omega_0 \ll \omega_{pe}$, $T_e \simeq T_i$, observed parametric decay in the ion cyclotron regime and detected concomitant main-body ion heating. In all of these cases significant heating was observed only above threshold for parametric excitation.

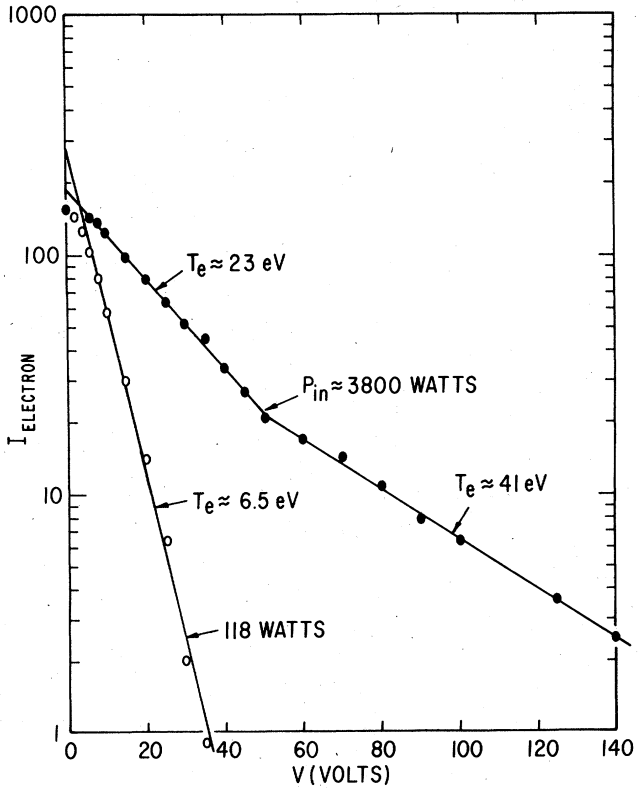

FIG. 39. Energy analyzer measurements of the parallel electron energies; 0-mode. (After Porkolab *et al.*, 1975.)

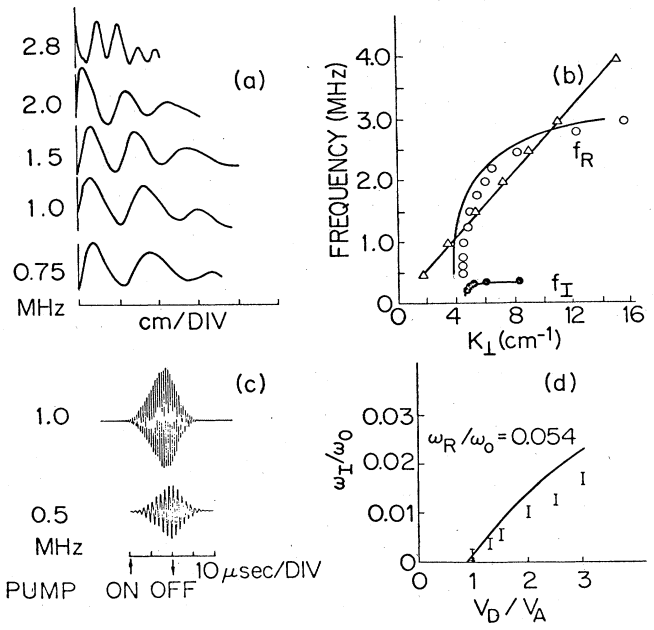

FIG. 40. (a) Interferometer traces of ion quasimodes propagated at different frequencies. (b) Dispersion curve of the ion quasimode (circles and dots) and the ion acoustic mode (triangles); solid curves, theory. (c) Typical ion quasimode oscillation amplitudes after switching on the rf pump field. (d) Growth rates as a function of the $E \times B$ drift velocity V_D, vs the acoustic speed V_A. Solid curve, theory. (After Chang and Porkolab, 1974.)

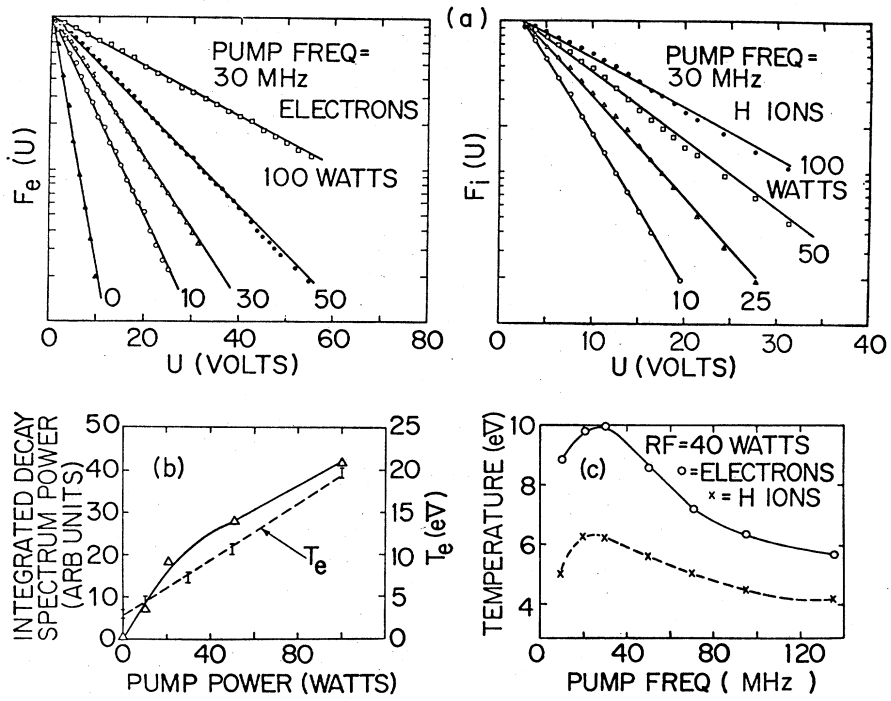

FIG. 41. (a) Electron and ion energy distributions for different rf pump powers. $\omega_0/\omega_{LH} \simeq 1.5$. (b) Integrated decay wave power (triangles) and electron temperature as a function of the pump power. (c) T vs ω_0 for fixed pump power; $f_{LH} \simeq 20$ MHz. (After Chang and Porkolab, 1974.)

5. Lower-hybrid waves

There are several small-scale experiments in this regime ($1 < \omega_0/\omega_L < 3$) which show parametric decay and strong heating (Farenik *et al.*, 1973; Chang and Porkolab, 1974; Brusati *et al.*, 1974). More recently, evidence of parametric heating in tokamaks has also been obtained (Porkolab *et al.*, 1977). In this regime decay into lower-hybrid waves and ion acoustic waves, ion cyclotron waves, ion quasimodes, or drift waves may occur (Porkolab 1973, 1974; Kindel *et al.*, 1972; Berger *et al.*, 1975; Karney *et al.*, 1973; Rogister, 1975; Ott, 1975.) The purely growing mode has been demonstrated recently by Doppler-shifting the frequency by a radial dc electric field so as to produce a real part of the frequency ($\omega_k = kV_D$) in the laboratory frame of reference (Chang and Porkolab, 1974). In Fig. 40 we demonstrate verification of the excitation of ion quasimodes (after Chang and Porkolab, 1974). In this experiment both parallel and perpendicular wavelengths of the decay waves were measured. In the same experiment strong plasma heating was observed above threshold for parametric instabilities (both ions and electrons). This is shown in Fig. 41. Note the increase of plasma heating as the lower-hybrid frequency is approached (between 20 and 30 MHz). Brusati *et al.* (1974) observed similar effects. In Fig. 42 we show from the recent experiments of Porkolab *et al.* (1977) the correlation between parametric decay and plasma heating.

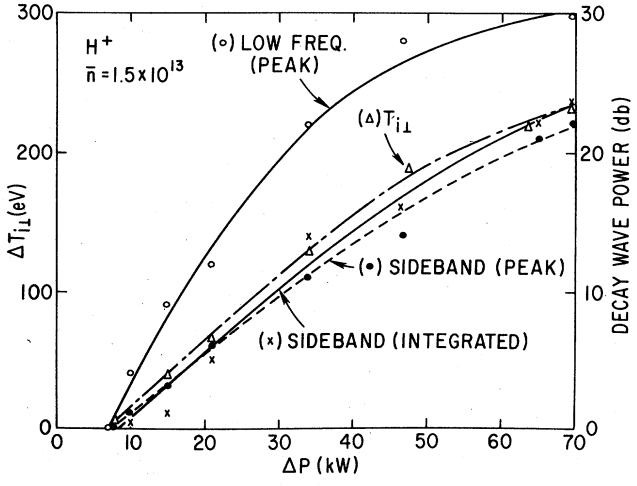

FIG. 42. $\Delta T_{i\perp}$ and decay wave amplitude vs input rf power; H_2 gas; $\bar{n} = 1.5 \times 10^{13}$ cm^{-3}. (After Porkolab *et al.*, 1977.)

6. Magnetosonic waves

These waves represent a contribution of the whistler wave branch in the regime $\omega_{ci} < \omega_0 < \omega_{pi}$. A number of theoretical papers have considered parametric decay instabilities in this regime (Ivanov and Parail, 1972; Sperling and Perkins, 1974; Kitsenko and Stepanov, 1973; Harms *et al.*, 1974; Martinov and Samain, 1974. In addition, a number of experiments have been performed both in linear devices and in toroidal devices (Voloshko *et al.*, 1972; Voitsenya *et al.*, 1972; Ivanov *et al.*, 1972; Vdovin *et al.*, 1971). In these interesting experiments evidence of strong anomalous ion heating was found. For input powers of the order of 100 kW, pulse duration of less than one msec, the ion temperature was doubled from 50 to 100 eV. In addition, in some cases the plasma confinement was actually doubled due to the

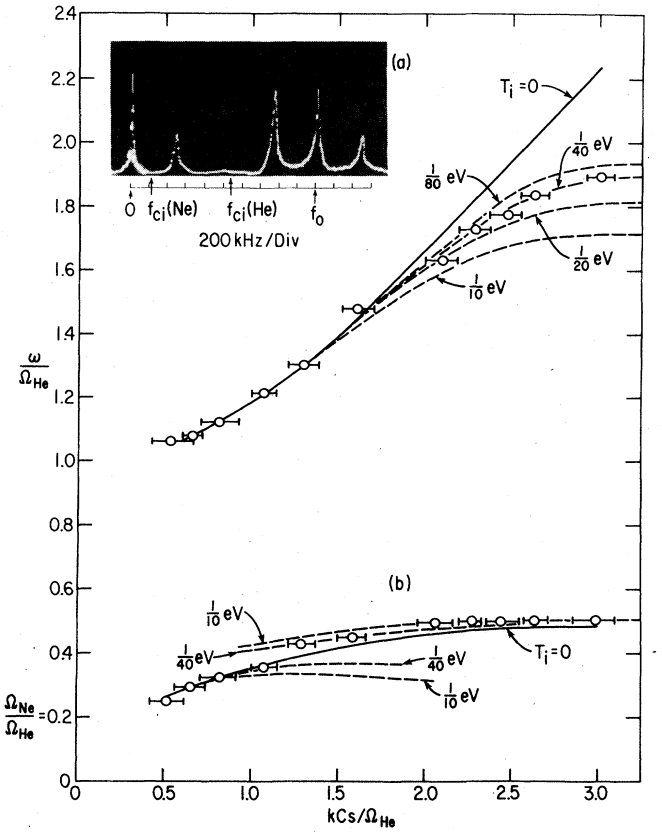

FIG. 43. (a) Parametric decay spectrum. f_{ci}(He) and f_{ci}(Ne) are the helium and neon ion cyclotron frequencies. (B_0=2.9 kG, f_0=2 MHz, He:Ne=4:6). (b) Dispersion curve of kinetic ion–ion hybrid mode. Solid and dashed curves, theory. (He:Ne=4:6, Cs is the helium acoustic speed.) Circles are experimentally measured values. (After Ono *et al.*, 1977.)

application of the rf power (Vdovin *et al.*, 1971). The anomalous ion heating was attributed to parametric decay into ion cyclotron waves and short-wavelength drift waves, and the increased confinement time was attributed to stabilization of long-wavelength drift waves. As shown in the above mentioned theoretical papers, additional instabilities may be expected to occur in multi-ion species plasmas. In Fig. 43 we show results from the recent work of Ono *et al.* (1977), who observed parametric decay in a laboratory multi-ion species plasma. In this case the instability was driven by the relative drift between the two ion species. Similar effects may be expected in a deuterium–tritium fusion plasma mixture.

I. Soliton formation and density depletion

In much of this paper we have concentrated on parametric mode coupling effects and ignored the nonlinear modification of the density. However, as discussed in the theoretical section, when the incident fields are sufficiently strong, the equilibrium density may be strongly modified by the ponderomotive force and the electric fields can be trapped in the density cavities. Such effects are particularly important in unmagnetized plasmas near the $\omega_0 \simeq \omega_{pe}$ critical layer, where strong electric fields can build up (Freidberg *et al.*, 1972). These nonuniform localized electric fields could produce energetic tails on the distribution function by accelerating particles to high energies (Freidberg *et al.*, 1972; Bezzerides *et al.*, 1975; Wong *et al.*, 1975). In addition, the modified density profiles could strongly alter the thresholds for parametric instabilities. Some of these effects have been observed in recent experiments by Kim *et al.* (1974), Ikezi *et al.* (1974), and Wong and Stenzel (1975). In Figs. 44 and 45 we reproduce some of the results from the work of Ikezi *et al.* (1974) and Wong and Stenzel (1975). In particular, these figures show that the density perturbations move away from the critical layer, and

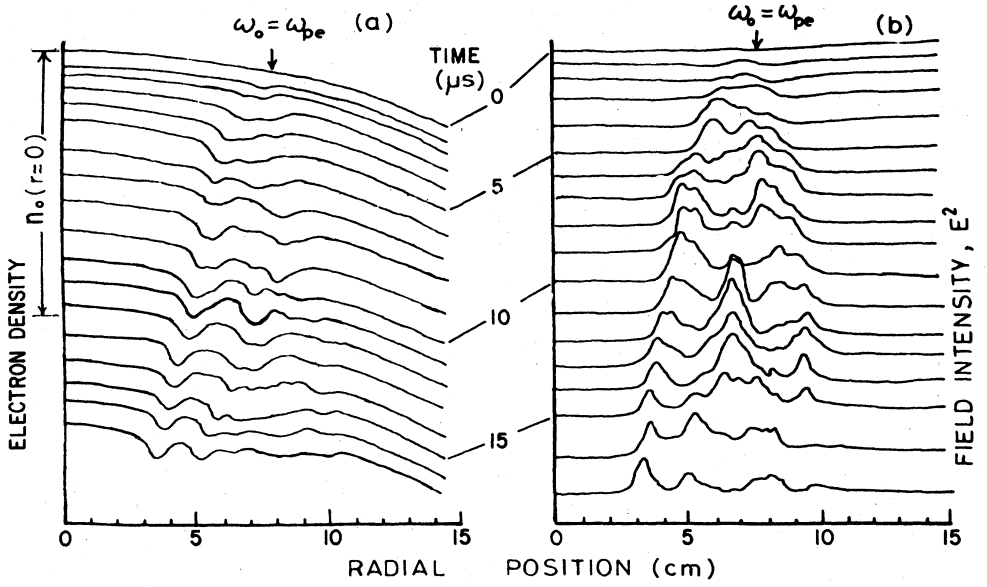

FIG. 44. Profile of the density perturbation (a) and the high-frequency field intensity (b). A stepwise pump starts at $t=0$. Pump power=20 W. (After Ikezi *et al.*, 1974.)

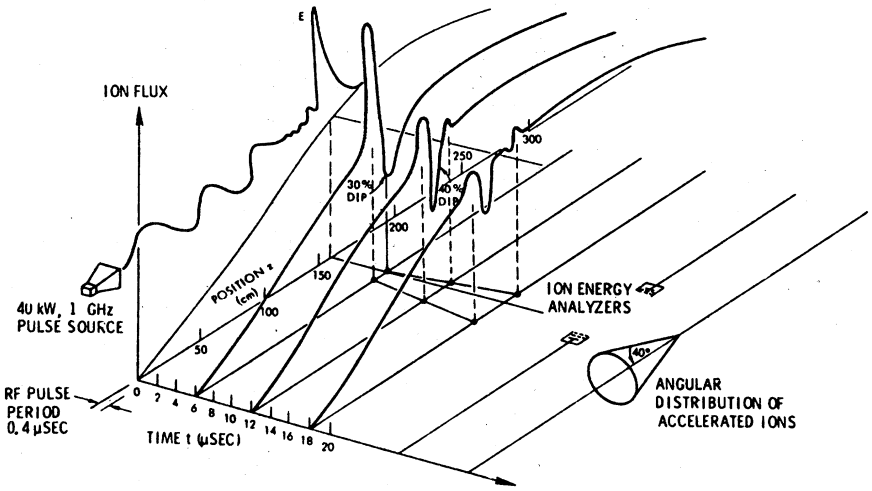

FIG. 45. Space-time representation of ion bursts (shaded) driven by the ponderomotive force. Density cavities are created as a result of ion expulsion. The polarization of ion trajectories is represented by the cone with a half-width of 40° with respect to the z axis. (After Wong and Stenzel, 1975.)

that trapped electric fields are localized in the density cavities. Furthermore, in the experiments of Ikezi *et al.* it was observed that the coupled nonlinear electron plasma wave and the nonlinear ion acoustic wave propagated in the form of periodic wave trains with approximately the ion acoustic velocity. Nishikawa *et al.* (1974) have developed a theory to deal with this special case. These processes may be of importance in situations where very strong rf fields are generated in the plasma. More recent work along these lines has been done near the lower-hybrid frequency and for whistler waves by Stenzel (1975, 1976), but these results were questioned recently by Sugai *et al.* (1977).

J. Summary and conclusions

In the presence of sufficiently strong high-frequency electric fields the plasma is subject to parametric instabilities. In this section we have attempted to summarize the important developments in the theory of parametric instabilities, and to give a considerable amount of experimental evidence for their existence. Although the first theoretical predictions of such instabilities in plasmas were made ten years ago, much of our present day understanding of this phenomenon has been obtained in the past five years. The explosive growth of this field has to do with possible applications to laser-pellet fusion and rf heating of magnetically confined fusion plasmas (and, for a brief period, ionospheric modification experiments). While there is now good theoretical and experimental understanding of linear theory in uniform or weakly inhomogeneous plasmas, our understanding of this phenomenon in strongly inhomogeneous plasmas is rather poor. Also, while there has been much progress in developing nonlinear theories, only a narrow regime ($T_e = T_i$, $B = 0$, E_0 close to threshold) are such theories capable of predicting the saturated state and the associated anomalous absorption. Even in this case, detailed experimental verification is lacking or agreement between theory and experiment is not satisfactory. The distribution of absorbed energy between the main body and/or a suprathermal tail is not well known. To the present date, most of the experimental information available has been obtained in small-scale microwave experiments, or in computer simulations. Whether such experimental and/or theoretical results can be extrapolated to the highly complex geometries of laser-pellet interaction and/or hot, magnetically confined fusion plasmas, remains to be seen.

In the case of magnetically confined plasmas, to date there have been only a few relevant experiments in fusion (toroidal) plasmas. In these experiments the crucial questions are the heating efficiency and the effects of the excited turbulence upon plasma confinement. Further experimental results are expected in the coming years, which will hopefully answer some of these questions.

V. STRONG-TURBULENCE THEORIES

A. Resonance broadening

The first attempts to improve weak-turbulence theory were proposed by Dupree (1966, 1967): he suggested resumming some of the terms left out of weak-turbulence theories in order to obtain a more accurate theory. Both Dupree and Weinstock (1968, 1969) showed that the net result of such an approach was an improved Green's function which took into account orbit perturbation due to the waves. Later these results were criticized by Rudokov and Tsytovich (1970) and Galeev (1969), who asserted that Dupree's results were not self-consistent since the particle distribution function also had to be modified by the turbulent fluctuations; in particular, Dupree's theory did not reproduce the results of weak-turbulence theories in the appropriate limits. Further attempts to improve these theories were made by Benford and Thomson (1972) and Choi and Horton (1974, 1975), who attempted to re-sum all the singular terms in the perturbation expansion, thus obtaining a "renormalized" turbulence theory. However, they could not solve the general equations either. Nevertheless, in principle an improved theory was set up. More recently Fisch and Bers (1975) obtained similar results.

In essence the problem arises from the fact that when wave-particle resonances of the form

$$\omega_1 - \omega_2 - \omega_3 \ldots - (\mathbf{k}_1 - \mathbf{k}_2 - \mathbf{k}_3 \ldots) \cdot \mathbf{v} = 0 \tag{5.1}$$

coincide to all orders, the perturbation expansion used in weak-turbulance theories breaks down. Thus, in any improved theory, these singularities must be removed; hence the name "renormalization" analogy with quantum field theory.

Let us briefly outline the approach taken by some of these authors. First, linear theory is represented by a linear dielectric function which can be written in a one-dimensional form as follows:

$$\epsilon(k, \omega) = 1 - \frac{\omega_p^2}{k^2} \int_{-\infty}^{\infty} dv \int_{-\infty}^{\infty} dv' \int_0^{\infty} dt' e^{i\omega\tau} G_0(k, t, v; t', v') \frac{\partial g}{\partial v}, \tag{5.2}$$

where $\tau = t - t'$, and the Green's function is given by

$$g_0(z, t, v; z', t', v') = \delta(v - v')\delta(z - z' - v\tau); \tag{5.3a}$$

$$g_0(k, t, v; t', v') = \delta(v - v')\exp(-ikv\tau); \tag{5.3b}$$

$$g_0(k, \omega, v; v') = \delta(v - v')i/(\omega - kv). \tag{5.3c}$$

[Equation (5.3c) is a Fourier–Laplace transform of (5.3a). This Green's function introduced the numerous resonant denominators we saw earlier in our section on weak-turbulence theory. It is clear that the unperturbed particle orbits used in Eq. (5.3a) are not satisfactory. Therefore, let us assume that we use a more accurate orbit, i.e., replace g_0 with G, where

$$G = \langle G \rangle + \delta G,$$

and replace G_0 by $\langle G \rangle$, assuming $\delta G \ll \langle G \rangle$. Then let us write the perturbation series in a schematic form, omitting constants such as (q/m), etc. (Drummond and Ross, 1973)

$$f_k = G_0(k)E_k \frac{\partial g}{\partial v} + G_0(k) \sum_{k' \neq k} E_{k-k'} \frac{\partial f_{k'}}{\partial v}. \tag{5.4}$$

Let us now operate upon Eq. (5.4) with $G_0^{-1}(k)$, and then iterate once

$$G_0^{-1}(k) f_k = E_k \frac{\partial g}{\partial v} + \sum_{k' \neq k} E_{k-k'} \frac{\partial}{\partial v} G_0(k') E_{k'} \frac{\partial g}{\partial v} + \sum_{\substack{k \neq k' \\ k' \neq k''}} E_{k-k'} \frac{\partial}{\partial v} G_0(k') E_{k'-k''} \frac{\partial f_{k''}}{\partial v}. \tag{5.5}$$

The second term gives resonant mode–mode coupling, which we shall ignore here (since it does not have singular terms). In the third term we had two contributions in the previous section to nonlinear wave-particle resonance

$$k'' = k' - k \text{ or } k'' = k.$$

Let us now transfer the $k'' = k$ term to the left-hand side, so we have

$$\left[G_0^{-1}(k) - \sum_{k' \neq k} E_{k-k'} \frac{\partial}{\partial v} G_0(k') E_{k'-k} \frac{\partial}{\partial v}\right] f_k = E_k \frac{\partial g}{\partial v} + \sum_{k' \neq k} E_{k-k'} \frac{\partial}{\partial v} G_0(k') E_{k'} \frac{\partial g}{\partial v} + \sum_{k' \neq k} E_{k-k'} \frac{\partial}{\partial v} G_0(k') E_{k'-k''} \frac{\partial f_{k''}}{\partial v}. \tag{5.6}$$

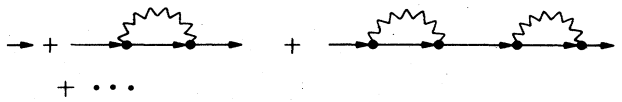

FIG. 46. Feynman diagrams for the propagator $\langle G_k \rangle^{-1}$.

The iteration may now be continued by substituting Eq. (5.4) into the last term of Eq. (5.6), transferring selected terms containing f_k to the left-hand side, and so on, to all orders. Now we take the ensemble average and call the left-hand side $\langle G_k \rangle^{-1} f_k$. Using diagrams, we can represent $\langle G_k \rangle^{-1}$ by the propagator diagram Fig. 46, where the wavy lines represent waves, the solid lines are the particle propagators $G(k)$, and the dots represent the velocity operator $(\partial/\partial v)$. This sum is the solution to the integro-differential equation

$$\langle G(k) \rangle = G_0(k) + G_0(k) \sum_{k' \neq k} |E_{k'-k}|^2 \frac{\partial}{\partial v} \langle G(k' - k) \rangle \frac{\partial}{\partial v} \langle G(k) \rangle \tag{5.7}$$

which is known as Dyson's equation in quantum field theory. An approximation to Eq. (5.7) is

$$\langle G(k) \rangle \simeq G_0(k) + G_0(k) \sum_{k' \neq k} |E_{k'-k}|^2 \frac{\partial}{\partial v} G_0(k) \frac{\partial}{\partial v} \langle G(k) \rangle. \tag{5.8}$$

So far only Eq. (5.8) has been solved with the assumption that the spectrum of unstable waves is flat over a range of phase velocities $\Delta(\omega/k)$. The result is a diffusion equation for f_k, with a resulting Green's function which predicts "resonance broadening," namely

$$\langle G(k) \rangle \simeq \delta(v - v')\exp\left[-ikv\tau - \frac{1}{3}k^2 D\tau^3\right] \tag{5.9}$$

where for resonant particles

$$D \simeq \frac{e^2}{m^2} \frac{1}{k\Delta(\omega/k)} \sum_k |E_k|^2 \simeq \tau_{ac} \sum_k \left(\frac{e}{m}\right)^2 |E_k|^2. \tag{5.10}$$

Here $\tau_{ac} = [k\Delta(\omega/k)]^{-1}$ is the autocorrelation time discussed in the introduction. From Eq. (5.9) it is clear that wave-particle resonances such as Eq. (5.1) will be washed out within the diffusion time

$$k^2 D\tau_D^3 \simeq 1, \text{ or } \tau_D \simeq (k^2 D)^{-1/3},$$

which we discussed briefly in the introduction. Note that since we have removed some of the terms from the previous kinetic equations, no longer do we have the symmetry of the matrix elements obtained in the previous chapter. Also, the conservation laws do not hold any more. Thus a fully consistent, mass-conserving operator perturbation theory will require simultaneous renormalization of both plasmon and particle propagators.

The foregoing theories have been applied to the ion acoustic instability by Capone and Davidson (1973, 1974), Sleeper *et al.* (1973), and Choi and Horton (1974, 1975). The theories have also been extended to include waves which propagate nearly perpendicularly to a magnetic field (such as the modified two-stream instability and Bernstein waves) by Galeev (1969), Lominadze (1972), Dum and Sudan (1969), and Dum and Dupree (1970). We should also mention here the work of Okuda *et al.* (1973,

1974), who attempted to observe the effects of diffusion by computer simulation experiments. Indeed, Okuda *et al.* (1973, 1974) found some discrepancies with some of these theories, pointing to the importance of a completely renormalized theory. In addition, the recent work of Dum (1975) shows that the most important effect of turbulence is not necessarily resonance broadening. Rather, the difficult problem of integration of the velocity-dependent diffusion coefficient must be faced in each specific case under consideration, and the final result may well be different from an automatic application of resonance broadening results [e.e., Eq. (5.9)].

B. Clumps and two-dimensional vortices

The most recent theories attempt to open new ways to treat plasma turbulence, and thus improve upon resonance broadening theories. The pioneering work along these lines was carried out by Dupree (1970, 1972, 1975), who proposed that in the turbulent phase ballistic "clumps" of plasma may be formed which may then scatter each other like dressed test particles. For example, for the particular case of excitation of the ion acoustic instability by an electron drift, saturation may occur due to the friction force exerted by the clumps (or macroparticles).

Following Dupree (1972), let us briefly outline the fundamental ideas behind clump formation. The distribution function can be written as a sum of four parts

$$f = f_0 + f^{(c)} + \tilde{f} + f_m , \tag{5.11}$$

where f_0 is the average distribution function, $f^{(c)}$ is the phase-coherent response to the electric field, $\tilde{f}$ describes the clumps, and f_m contains other effects which will be ignored here. The main question concerns the clump self-correlation function $\langle \tilde{f}(1)\tilde{f}(2)\rangle$. The brackets $\langle\rangle$ denote an ensemble average, and 1 stands for x_1, v_1. If the phase-space volume of a clump is sufficiently small, then all the particles which consititute the clump will tend to move together. Such clumps will behave like a single large discrete particle (macroparticle). It is expected that many plasma processes which depend upon particle discreteness, such as radiation, absorption, conductivity, diffusion, etc. can be greatly enhanced by the presence of clumps. In the collisional case, the self-correlation function for discrete particles is

$$\langle \tilde{f}\tilde{f}\rangle = n^{-1}\delta(v_-)\delta(x_-)f_0(v_1) , \tag{5.12}$$

where n is the average density, and $x_- = x_1 - x_2$, $v_- = v_1 - v_2$. Here the delta functions tell us that the particles have zero spatial extent and that all parts move at the same speed. Let us now estimate $\langle \tilde{f}\tilde{f}\rangle$ as follows. Let us assume that the turbulent spectrum has an average wave number k and a spectral width $\Delta k \simeq k$, and $\tau_c = (k\Delta v_p)^{-1} \ll \tau_t$, where the trapping width is given by Dupree (1966) as $\Delta v_t \simeq (D/3k)^{1/3}$ and $\tau_t \simeq (k\Delta v_t)^{-1}$ (D is the velocity diffusion coefficient discussed earlier). Now $\langle \tilde{f}(1)\tilde{f}(2)\rangle$ will be zero unless $x_- \lesssim k^{-1}$, since scattering will tear a clump of size $x_- \simeq k^{-1}$ apart in a time $(k^2D/3)^{-1/3}$; smaller clumps will last longer. Therefore the clump lifetime τ_{cl} is of order τ_t. Similarly, $v_- \lesssim (k\tau_t)^{-1} \simeq \Delta v_t$, or velocity dispersion will destroy the clump.

In steady-state turbulence clumps will be continuously created as long as $(\partial f_0/\partial v) \neq 0$ in the resonant velocity region. Clump formation occurs because the average gradients in velocity space are converted into spatial fluctuations (or clumps) by the phase-space mixing produced by the turbulent electric field. During a clump lifetime f_0 is mixed over a distance $(D\tau_{cl})^{1/2} \simeq \Delta v_t$, and thus the amplitude of a fluctuation of f about the mean is $\tilde{f} \simeq \Delta v_t(\partial f_0/\partial v)$. Combining this result with the limits on x_- and v_-, we obtain the clump function

$$\langle \tilde{f}(1)\tilde{f}(2)\rangle = 6\pi^{-2}\delta(x_-)\delta(v_-)D(\partial f_0/\partial v)^2 , \tag{5.13}$$

where the constant in front was obtained by Dupree (1972). Comparing Eqs. (5.12) and (5.13), the ratio of clump to particle mass (i.e., the number of particles in a clump) is

$$3n\lambda f_0^{-1}\frac{D}{k}\left(\frac{\partial f_0}{\partial v}\right)^2 \simeq 3n\lambda\left(\frac{\Delta v_t}{v_{te}}\right)^3 . \tag{5.14}$$

Clumps may move along ballistic orbits and interact with each other and the turbulent fields. If the clump produces a potential without shielding

$$\langle \phi^2\rangle_{k\omega} = \frac{4\pi nq}{k^2}\int_{-\infty}^{\infty} dv_1 \int_{-\infty}^{\infty} dv_2 \langle \tilde{f}\tilde{f}\rangle_{k\omega} , \tag{5.15}$$

then the shielded potential will be

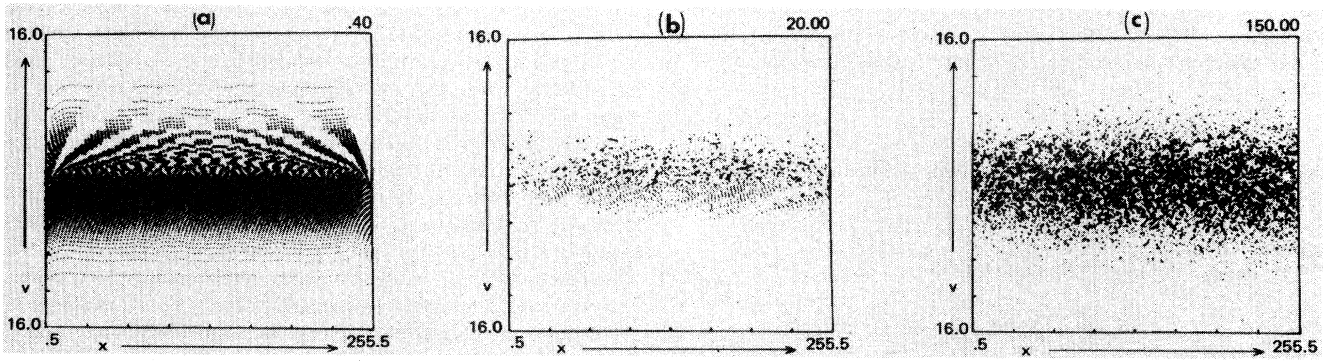

FIG. 47. Computer simulation of clump formation: phase-space density. Velocity is plotted vertically and distance horizontally. Every tenth particle is shown. (a) $\omega_p t = 0.4$, (b) $\omega_p t = 20$, (c) $\omega_p t = 150$.

$$\langle\phi^2\rangle_{k\omega} = \langle\bar{\phi}^2\rangle_{k\omega} / |\epsilon(k,\omega)|^2, \quad (5.16)$$

where $\epsilon(k,\omega)$ is the plasma (nonlinear) dielectric constant. Since $\langle\bar{\phi}^2\rangle_{k,\omega}$ depends on $\langle\phi^2\rangle_{k,\omega}$ through $D(v)$, Eq. (5.16) is the equation for $\langle\phi^2\rangle_{k,\omega}$ for steady-state turbulence. Thus the state described by Eq. (5.16) contains clumps as a major constituent (in addition to waves and particles). In the spectrum clump motion will produce ballistic singularities with $\omega \simeq kv$, which may show up strongly in experimental spectra. So far the only detailed verification of these theories is in a computer experiment by Dupree *et al.*(1975). In Fig. 47 we show the results of the computer simulation. Figure 47(c) shows granulation even at a time $t \simeq 150\ \omega_p^{-1}$ after the initial perturbation is applied; by this time the plasma should have relaxed to the thermal equilibrium. In particular, the authors find $\langle\delta N\rangle^2$ for $v = v_{th}$ to be ten times $\langle N\rangle$ at $\omega_p t = 150$. This is invoked as evidence that particles are not randomly distributed within small cells but tend to occur in clumps.

We should also note the work done by Taylor and McNamara (1971), Dupree (1974), and Joyce *et al.* (1974) along the lines of developing two-dimensional plasma turbulence in a magnetized plasma. In these cases guiding center motion of the plasma is used to obtain correlation functions and vortex motion. Due to lack of experimental data, we shall not discuss these novel ideas here any further.

C. Experimental results

Because of great difficulties in obtaining meaningful experimental data, detailed verification of strong-turbulence theories is naturally lacking. Some information on resonance broadening was deduced from the damping of plasma wave echoes. In particular, the experiments of Jensen *et al.* (1969), which we discussed earlier in connection with echoes, gave evidence of diffusion of particle orbits due to the presence of turbulence. Further evidence of resonance broadening and its saturating effect upon instabilities (or its reduction of their growth rates) was obtained recently by Correll *et al.* (1975), Slusher *et al.* (1976), Benford and Correll (1977), and Hershcovitch (1977). In the experiments of Slusher *et al.* (1976) the saturation of the current-driven ion acoustic instability was studied. It was concluded that saturation was not inconsistent with resonance broadening and Landau damping on the tail of an impurity particle distribution. However, conclusive proof of resonance broadening could not be given in this experiment.

A more recent experiment on resonance broadening is that performed by Benford and Correll (1977). These authors studied stabilization of the electrostatic ion cyclotron instability with frequency $\omega = \Omega_i$, by injecting external noise into the plasma with frequencies $0 \lesssim \Delta\omega \lesssim \Omega_i$. The instability level just above threshold was monitored as the noise level was raised. The noise level was typically large, i.e., $e\bar{\phi}/T_e \gtrsim 1$. The authors found that stabilization occurs for $\gamma_l = k_\perp^2 D_n$, where γ_l is the linear growth rate of the instability, and D_n is the diffusion coefficient due to the noise. This relation implies $(v_D - \omega/k_\parallel)/v_{te} \propto k_\perp^2 D_n \propto \bar{\phi}$, where v_D is the electron drift velocity, and $\bar{\phi}$ is the rms noise level (potential). The

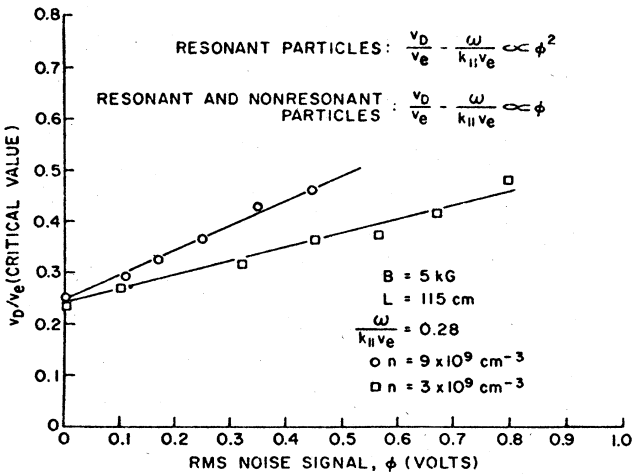

FIG. 48. Dependence of critical electron drift velocity on the amount of external noise potential. (After Benford and Correll, 1977.)

authors found agreement with this law experimentally, and this is shown in Fig. 48. We note that a similar law would also apply in the case of stabilization by mode–mode coupling, which cannot easily be ruled out in this experiment. However, mode coupling theories are not expected to apply at such large fluctuation levels.

In the experiments of Hershocovitch the stabilization of the $(\Omega_e/2)$ instability was studied (Maxim and Trivelpiece, 1965; Murkami and Lidsky, 1970). In these experiments the instability was excited by injecting two counter-streaming electron beams along a magnetic field. Turbulence was injected into the chamber by rf antennae. Probes were used to monitor the level of instability and an energy analyzer was used to measure the time evolution of the energy distribution of the beam. According to theory, as saturation

$$k_\perp^2 D_n + k_\perp^2 D_t = \gamma_L, \quad (5.17)$$

where γ_L is the linear growth rate, D_n and D_t are the diffusion rates due to the externally injected turbulence and to the instability, respectively. Herschcovitch obtained the following expression for Eq. (5.17)

$$\gamma_L = \frac{k_\perp^4}{\Omega^2}\frac{e^2}{m^2}\left[C_1 R^e |\phi_{ext}|^2 + C_2 R^i |\phi_{inst}|^2\right], \quad (5.18)$$

where C_1 and C_2 are the coupling coefficients between the antennae and the plasma, and R^e, R^i are resonance functions, respectively. When $D_n \gg D_t$, the R's become independent of D's, and Eq. (5.18) reduces to

$$\frac{|\phi_{ext}|^2}{a} + \frac{|\phi_{inst}|^2}{b} = \gamma_L \quad (5.19)$$

which is the equation of an ellipse, with γ_L as a varying parameter (since $\gamma \propto I_B^{2/3}$, where I_B is the beam current). Thus, in contrast to the results of Benford and Correll, Hershocovitch found $D_{ext} \propto |\phi|^2$. In Fig. 49 we show the experimental results, demonstrating good agreement with Eq. (5.19). In addition, it was verified that when sufficiently strong turbulence was injected into the chamber so that stabilization with the external noise alone

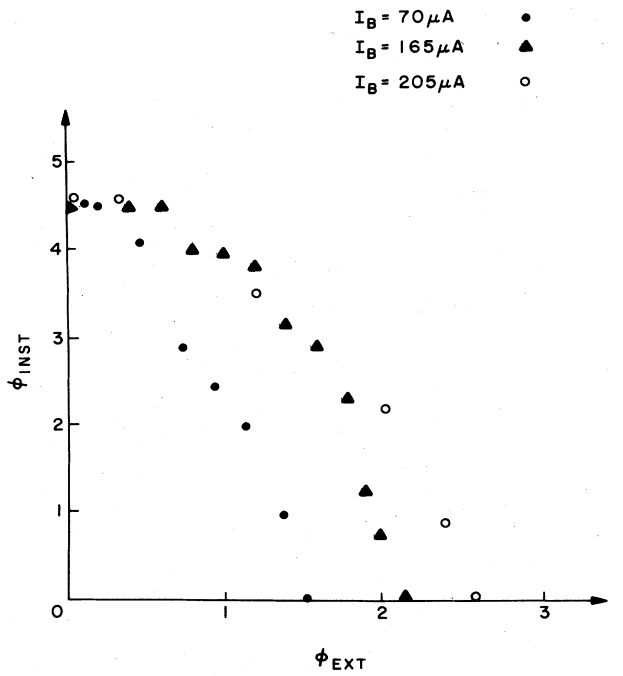

FIG. 49. Saturated instability amplitude vs injected turbulence for three values of the beam current. Scales are relative rms amplitudes of the fluctuating potentials. (After Hershcovitch, 1977.)

could be achieved (i.e., when $k_\perp^2 D_n = \gamma_L$), no changes in the beam distribution occurred (i.e., quasilinear changes could be ignored.) The discrepancy between the results of Benford and Correll, and those of Hershcovitch is not clear. In particular, neither set of results is applicable to the important regime in which D_t due to the instability dominates. Thus we must await further experimental work concerning self-produced resonance broadening.

At this time it is appropriate to mention the early experiments of Porkolab and Kino (1968), who first attempted to study diffusion due to low-frequency noise in a potassium plasma. The diffusion coefficient was obtained by measuring changes in the density profile as the level of turbulence was varied. These authors found $D \propto \overline{\phi}/B$, which is similar to Bohm diffusion (Bohm, 1949) and also similar to the results of Benford and Correll (1977). A typical result is shown in Fig. 50. Again, $e\overline{\phi}/T_e \gg 1$, so that a comparison with the previous theory is not easily justified. Perhaps strong-trubulence theories will be necessary to explain these experiments.

Experimental evidence for "clump" formation is still lacking. We expect that if such objects exist, they should have occurred in some of the foregoing experiments. However, it is not clear how one verifies experimentally the existence of such clusters of particles. Perhaps computer simulation is the only means of obtaining a detailed observation of clumps.

Finally, we should mention some of the large-scale experiments where strong trubulence, generated by strong electric fields, was used to heat the plasma (Mah *et al.*, 1970; Wharton *et al.*, 1971; Hamberger *et al.*, 1971; Zavoisky *et al.*, 1972; Bengston *et al.*, 1975). In

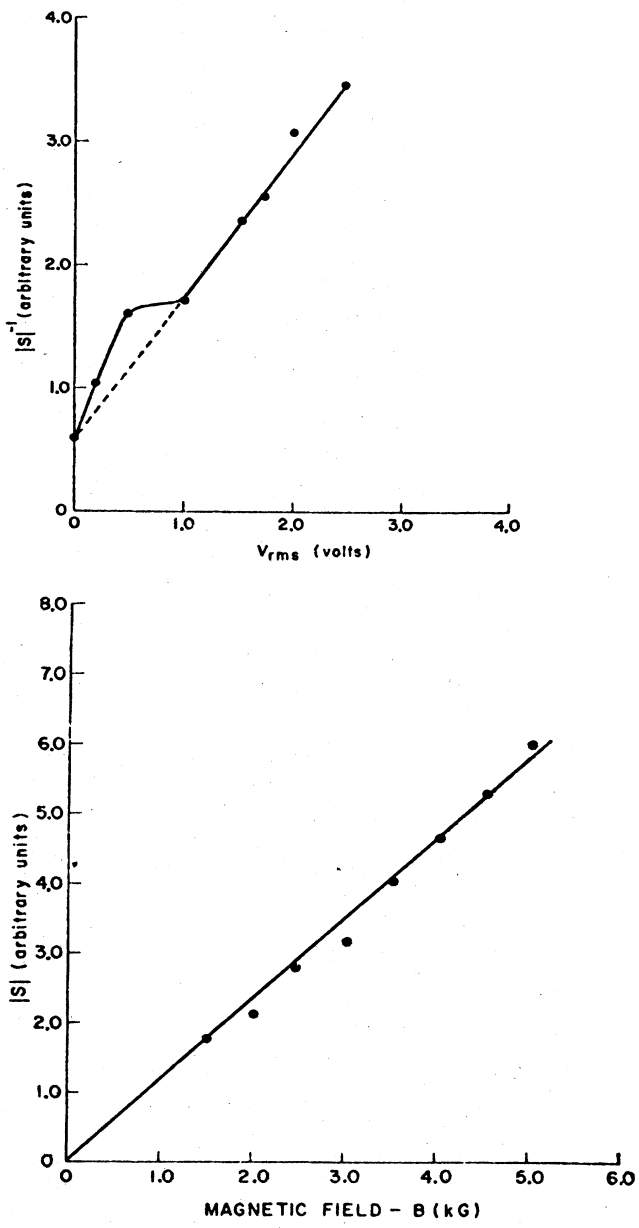

FIG. 50. (a) Diffusion coefficient vs broadband injected noise level. $30 \lesssim f \lesssim 100$ KHz, $B = 3$ KG, $|S|^{-1} \propto D$. (b) Diffusion coefficient vs magnetic field, $V_{rms} = 2$ V and constant.

these experiments $e\phi/T_e \gtrsim 1$ also, so that strong-turbulence theories will be needed to interpret the results. Thus it is clear that much more work is needed to understand the turbulent state in plasma.

VI. LARGE-AMPLITUDE ELECTRON PLASMA WAVES AND SIDEBAND INSTABILITIES

A. Historical background

The study of large-amplitude electron plasma (LAEP) waves and the associated sideband instabilities is a good example of a problem in which plasma theorists and ex-

perimentalists worked closely to unravel the underlying physics. The theories of Al'tshul' and Karpman (1965) and O'Neil (1965) led to the experimental observation by Malmberg and Wharton (1967) of the nonlinear amplitude oscillation of LAEP waves. During the course of their experimental investigation Wharton, Malmberg, and O'Neil (1968) discovered the sideband instability associated with the presence of a LAEP wave. They verified that the frequency separation between the sideband peak and the LAEP wave was proportional to the bounce frequency, $\omega_B = k_0(e\phi_0/m)^{1/2}$, where ϕ_0 and k_0 are the large-amplitude electric potential and wave number, respectively. Subsequent experiments (Franklin *et al.*, 1972) showed that the sideband waves satisfied the linear dispersion relation, and that their frequencies were predicted by the formula $\omega \simeq kv_0 \pm \omega_B$, which is just the bounce frequency Doppler shifted by the main-wave phase velocity $v_0 = \omega_0/k_0$. Furthermore, it was shown that a test wave at the sideband frequency was amplified and that the growth rate was proportional to $\phi_0^{1/2}$. Similar results were also reported for large-amplitude ion acoustic waves (Ikezi *et al.*, 1972). To explain these experimental results, two classes of theories were proposed: (1) the parametric sideband theories and (2) the quasilinear sideband theories. The mechanism for the former theory was originally proposed by Kruer *et al.*, (1969). It involves a parametric interaction between the LAEP wave and the trapped electrons acting as Doppler-shifted harmonic oscillators. This simple model was further pursued formally by using the Vlasov equation (e.g., Goldman, 1970; Mima and Nishikawa, 1971; Goldman and Berk, 1971; Wong, 1972). These theories all predicted the existence of a series of sidebands about the LAEP wave, and also predicted that the growth rate of the instability γ varies as $\phi_0^{1/2}$ or ϕ_0, depending on the shape of the potential well chosen. On the other hand, the quasilinear theories assume that the electron distribution is modified by the LAEP wave, and thus the growth rates of the unstable waves are a function of the slope of the distorted portion of the distribution function. In this section we shall briefly review the theory of O'Neil, the original experiments of Malmberg *et al.*, the parametric instability model of Kruer, Dawson, and Sudan, and the experiments which purport to support the quasilinear theory. We shall also summarize some recent experiments on sideband instabilities which were explained by the detrapping of the electrons in the troughs of the large-amplitude wave.

B. Theoretical model of O'Neil

The collisionless damping of an electron plasma wave was first calculated by Landau (1946) using the linearized Vlasov equation and Poisson's equation. The solution was obtained by solving an initial value problem for the dynamics of the electrons, and the ions were treated as neutralizing background. For an electron plasma, Landau's formula for the damping decrement is

$$\gamma_L = \frac{\pi}{2}\,\omega\,\frac{\omega_p^2}{k^2}\,\frac{\partial f_0}{\partial v}\bigg|_{v=\omega/k} ,$$

where ω/k is the wave phase velocity, and f_0 is the unperturbed equilibrium distribution. This formula tells us that if there are more electrons moving slower than there are moving faster than the wave phase velocity, the wave will be damped. However, this linearization procedure is only valid for a time t, which is short enough that the wave does not have a chance to trap the electrons, i.e., $t \ll \tau \equiv (m/e\phi)^{1/2}/k$, where k is the wave number, and ϕ is the wave amplitude. The question as to what happens to the wave for $t \geq \tau$ was first tackled by Al'tshul' and Karpman (1965), and independently by T. O'Neil (1965). We shall here briefly describe the approach taken by O'Neil (1965); Al'tshul' and Karpman have obtained a similar result by a different method.

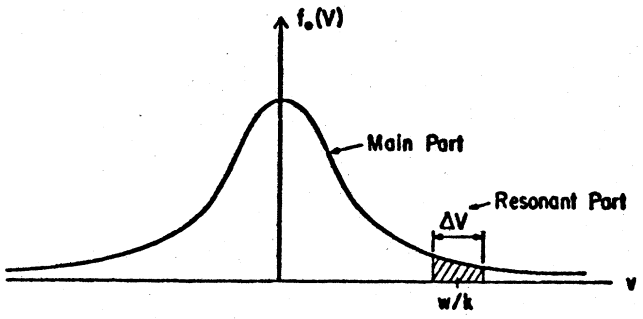

FIG. 51. The division of the electron distribution into a main part and a resonant part. (After O'Neil, 1965.)

Following Dawson's physical model (1961) for describing the linear Landau damping mechanism, O'Neil divided the electron distribution into a main part and a resonant part (see Fig. 51). The main part of the distribution supports the oscillatory motion of the plasma wave and the resonant part of the distribution damps the wave. To get the damping coefficient, O'Neil first calculated the rate of increase of the kinetic energy, T, of the resonant electrons. Then by invoking the conservation of energy, he set the rate of increase of the kinetic energy equal to the rate of decrease of wave energy, $E^2/8\pi$. From this equality the damping coefficient of the wave was obtained immediately. O'Neil considered a plasma wave with a constant amplitude of the form

$$E(x,t) = E\sin(kx - \omega t) .$$

In a coordinate system which moves with the wave, the electric field can be written as $E\sin(kx)$ and the rate of increase of kinetic energy density can be written as

$$\frac{dT}{dt} = \frac{nm}{2}\int_{-\lambda/2}^{\lambda/2}\frac{dx}{\lambda}\int_{\infty}^{\infty} dv\left(v+\frac{\omega}{k}\right)^2\frac{\partial f_w}{\partial t} , \qquad (6.1)$$

where n is the electron density, λ is the wavelength, and f_w is the electron distribution in the wave frame. The x integration just gives the spatial average of f_w. In order for this calculation to be applicable for time greater than $t = \tau$, the exact Vlasov equation in the resonant region was solved. In the wave frame, the solution of the Vlasov equation (which expresses the incompressible flow in phase space) can be written as

$$f_w(x,v,t) = f_w[x_0(x,v,t), v_0(x,v,t), 0] ,$$

where $f(x_0, v_0, 0)$ is the initial distribution, and (x_0, v_0) is the point from which (x, v) evolved. The evolution of this point is governed by the equation of motion

$$m\ddot{x} = -eE\sin(kx), \tag{6.2}$$

with initial conditions $(x,v)=(x_0,v_0)$. This equation can be solved in terms of elliptic functions. The first integral of the equation is just the expression for conversation of energy, i.e.,

$$(mx^2/2) - (eE/k)\cos(kx) = w\,. \tag{6.3}$$

When we use the transformations $kx \equiv 2\xi$ and $\kappa^2 \equiv 2eE/(kw+eE)$, Eq. (6.3) becomes $\xi^2 = (1/\kappa^2\tau_2)[1-\kappa^2\sin^2(\xi)]$. By going through the calculation outlined above, O'Neil obtained a nonlinear growth rate

$$\gamma(t) = \gamma_L \sum_{n=0}^{\infty} \frac{64}{\pi}\int_0^1 d\kappa\, \frac{2n\pi^2 \sin[\pi nt/\kappa F\tau]}{\kappa^5 F^2(1+q^{2n})(1+q^{-2n})} + \frac{(2n+1)\pi^2\kappa \sin[(2n+1)\pi t/2F\tau]}{F^2(1+q^{2n+1})(1+q^{-2n-1})}\,, \tag{6.4}$$

where

$$q \equiv \exp(\pi F'/F), \quad F \equiv F(\kappa, \pi/2),$$

$$F' \equiv F[(1-\kappa^2)^{1/2}, \pi/2],$$

and F is the elliptic integral of the first kind. The first term of this equation represents the untrapped electrons (see Fig. 52), and the second term represents the trapped electrons. On the nonlinear time scale, the trapped electrons make complete cycles with a period of order τ. These electrons carry along the density from their original position and thus cause a cyclic variation in the density at any one point. It is this variation in density that causes the oscillatory behavior of the second term. On the other hand, the untrapped electrons all are going over the hill and valley, producing the oscillatory behavior of the first term. Thus this calculation predicts that in the limit of small damping, $(\gamma_L/\omega_B \ll 1)$ and when the wave electric field is large (and almost constant in time) some electrons oscillate in the trough of the wave. When the trapped electrons oscillate in resonance, their kinetic energy causes an oscillation in wave amplitude on a time scale which is longer than the wave period.

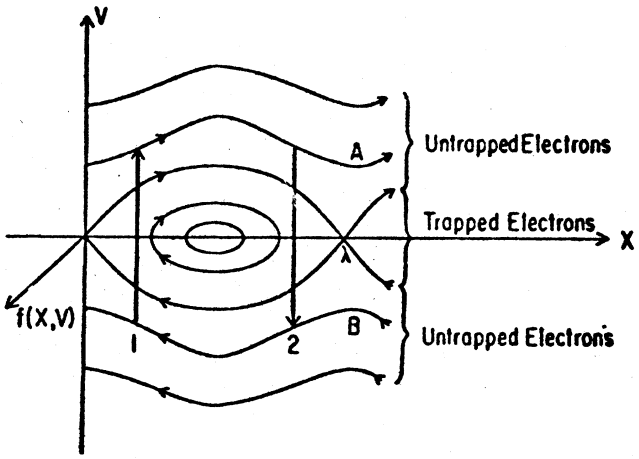

FIG. 52. The phase trajectories of the resonant electrons. (After O'Neil, 1965.)

An extension of O'Neil's theory was carried out by Sugihara and Kamimura (1972). They computed the self-consistent equilibrium solutions to the initial-value problem, which effectively cover the range $0 < q = \gamma_L/\omega_B < \infty$, and in the limit $q \to 0$ the result of O'Neil was recovered. Their solutions show that: (a) for $q \geq 3$ the wave damps at a constant rate γ_L, (b) for $q > 0.77$ the damping rate decreases monotonically with time from its initial value γ_L, and (c) for $q < 0.77$, the wave amplitude, after several oscillations, becomes constant with time, and its actual value depends on the precise value of q.

Related large-amplitude wave theories and computer simulations have also been studied by Knorr (1961), Armstrong (1967), Gary (1967), Dawson and Shanny (1968), Bailey and Denairt (1970), Nürenberg (1971), and Morales and O'Neil (1972).

C. Early experimental observations

The first experimental observation of amplitude oscillations associated with a large-amplitude plasma wave was carried out by Malmberg and Wharton (1967). Their experiment dealt with the spatial damping and oscillation of LAEP waves. From elementary physical arguments one can show that the spatial problem and the temporal problem are related if one scales time τ by the wave phase velocity (i.e., $L = \tau\omega/k$) and the damping rate γ_L by the group velocity (i.e., $= \gamma_L/\partial\omega/\partial k$). [These arguments were later confirmed by Lee and Schmidt (1970) in a detailed calculation.] The experiments were carried out in a magnetically confined hydrogen plasma column, which was 2m long and was bounded by a conductor at a radius of 5.2 cm. The plasma was collisionless in the sense of the theory (i.e., all electron collisional lengths were longer than the machine). When an rf voltage was applied to a probe inserted in the plasma, an electron plasma wave corresponding to the lowest radial eigenmode was excited (waves corresponding to higher eigenmodes were also excited, but they were damped heavily). The excited electron plasma wave was picked up with another probe which moved axially along the machine. Figure 53 shows a plot of the wave amplitude versus position for various transmitter voltages. At low voltages, the usual Landau damping was observed. As the wave amplitude was increased (curve c), the experimenters

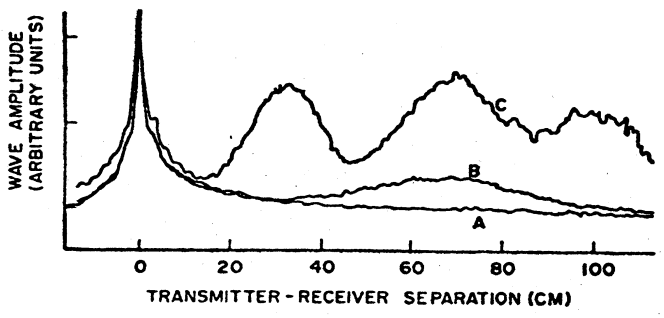

FIG. 53. Wave amplitude vs position. Transmitter voltage 0.9, 2.85, and 9 V, for Curves A, B, and C, respectively. (After Malmberg *et al.*, 1967.)

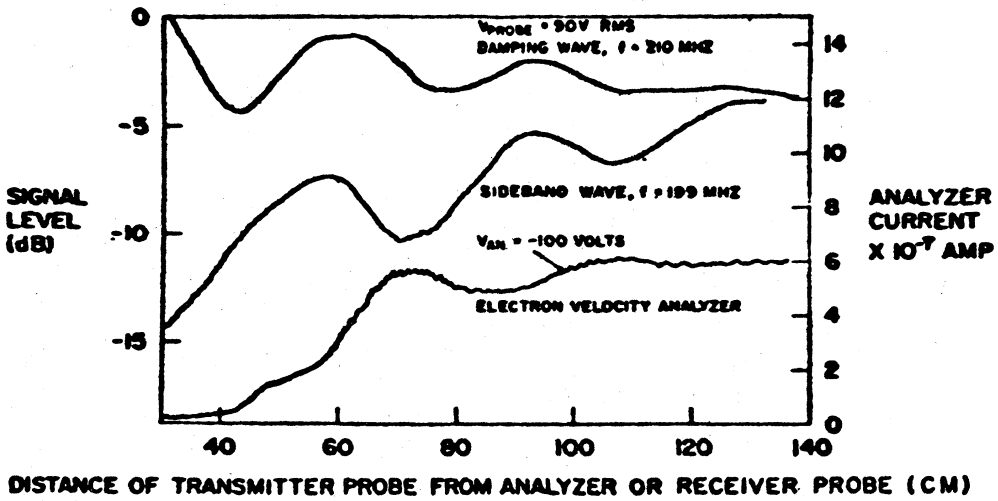

FIG. 54. Large-amplitude wave effects: fluctuating damping, amplitude of a sideband frequency, and enhanced current collected by the biased energy analyzer. (After Wharton *et al.*, 1968.)

observed that the wave no longer damped exponentially; rather the oscillations expected from the large-amplitude theory were observed. Malmberg and Wharton have also determined that the wave number (associated with the amplitude oscillation) increased as the square root of the wave electric field. To show that the spatial oscillations in resonant electron kinetic energy were 180° out of phase with the spatial oscillations of the wave amplitude, Wharton, Malmberg, and O'Neil (1968) used an electrostatic electron energy analyzer to detect the increase in the electron current associated with the presence of a large-amplitude electron plasma wave. Figure 54 shows a plot of the spatial variation of the enhanced current from electrons that have gained energy from the damping of the wave. In the same experiment, they also observed (using frequency analysis of the received probe signal) the broadening of the LAEP wave and its associated sidebands. The amplitude of the lower sideband is plotted versus distance in Fig. 54. Note that the oscillations in sideband amplitude correspond to those of the main wave, and that there is a sharp growth up to 60 cm. The frequency separation ($\Delta\omega$) of the sideband from the main wave was measured to be a linear function of the square root of the wave potential, ϕ_0, i.e., $\Delta\omega \propto \phi_0^{1/2}$. These measurements demonstrated that the frequency separation of the sideband from the main wave was the oscillation frequency of the electrons in the trough of the wave ($\Delta\omega \simeq \omega_B$).

These early experimental results led to considerable theoretical work on the stability of plasma supporting a large-amplitude monochromatic wave, all of which included the effect of resonant trapping of electrons in the potential well of the electrostatic wave. However, theories specifically applied to the sideband instability differ in the physical mechanism assumed responsible for growth. There are two classes of theoretical approaches to the problem, the so-called "parametric" sideband theories and the "quasilinear" sideband theories.

D. Parametric sideband theories

The physical mechanism behind the parametric sideband theories is as follows. The presence of a large-amplitude (traveling) electron plasma wave in a plasma sets up a spatially periodic potential for the electrons (similar to the periodic potential for the case of a solid [see, for example, Kittel (1976)] in the wave frame. The trapping of electrons in the wave trough produces a bounce frequency resonance. The coupling of the LAEP wave with the bounce resonance frequency produces upper and lower sidebands about the traveling wave frequency. The relative amplitudes of the sidebands depend on the details of each theoretical calculation. Since all the sidebands are coupled through the bounce resonance, they have equal temporal growth rates. However, the scaling of the growth rate with wave amplitude differs from one theory to the next. Wong (1972), using a sinusoidal wave potential and a general distribution of trapped electrons, found that the growth rate varies as the square root of the wave potential. On the other hand, Mima and Nishikawa (1971) found linear dependence on the potential, most likely from the assumption of a parabolic potential well which does not allow differential orbital periods for the trapped electrons. These authors also found higher-order resonances which are analogous to the energy levels of a harmonic oscillator, i.e.,

$$\omega - kv_\phi = \pm(2N+1)^{1/2}\omega_B , \tag{6.5}$$

where v_ϕ is the phase velocity and $N = 0, 1, 2, 3, \ldots$.

We shall now briefly outline the early physical model proposed by Kruer, Dawson, and Sudan (1969) to explain the first sideband instability experiment performed by Wharton, Malmberg, and O'Neil (1968). [For a more general and rigorous derivation of the trapped particle instability, we refer the reader to the work of Goldman (1970).] In their model, they assume that a significant number of electrons are trapped in the troughs of the wave due to its large amplitude. These electrons move with the wave at the mean velocity equal to its phase velocity. The oscillation frequencies for a large number of the trapped electrons near or at the bottom of the wave troughs are equal. With these assumptions, the perturbed equation of motion for such a simple oscillator is

$$\ddot{x}_n(t) = -\omega_B^2(x_n - x_{n0} - v_\phi t) - \frac{e}{m}\int dk'd\omega' \frac{E(k',\omega')}{(2\pi)^2} e^{ik'x_n - i\omega' t}, \tag{6.6}$$

where v_ϕ is the phase velocity of the LAEP wave, $x_n - x_{n0} - v_\phi t$ is the position of the oscillator relative to the nth trough, and $E(k,\omega)$ is the Fourier amplitude of the perturbing field. Now Fourier-analyzing in time the displacement of the oscillator $\xi_n(t) = x_n(t) - x_{n0} - v_\phi t$ gives

$$\xi_n(\omega) = \frac{e}{m(\omega^2 - \omega_B^2)} \int dk' \frac{E(k', \omega - k'v_\phi)}{2\pi} e^{ik'x_{n0}}. \tag{6.7}$$

To obtain the dispersion relation, Kruer, Dawson, and Sudan demand that the electric field produced by the perturbed motion of the oscillators be consistent with the field pertubing the oscillators. The perturbed charge density of an oscillator is

$$P_n(x,t) = -\xi_n(t)\frac{\partial}{\partial x}\delta(x - x_{n0} - v_\phi t). \tag{6.8}$$

Fourier-analyzing and summing over all such oscillators, we have

$$\rho_n(k,\omega) = ike\sum_n N_n e^{ikx_{n0}}\xi_n(\omega - kv_\phi), \tag{6.9}$$

where ξ_n is the Fourier-analyzed perturbation position evaluated at $\omega - kv_\phi$, and N_n is the number of trapped particles in the nth wave trough. Treating the background plasma as a continuous medium with dielectric function $\epsilon_L(k,\omega)$, from Poisson's equation we have

$$ik\epsilon_L(k,\omega)E(k,\omega) = 4\pi\rho(k,\omega). \tag{6.10}$$

Now substituting Eqs. (6.7) and (6.9) into Eq. (6.10) we obtain

$$E(k,\omega) = \frac{\omega_T^2}{\Omega^2 - \omega_B^2}\sum_n \frac{E(k + mk_0, \omega + m\omega_0)}{\epsilon_L(k,\omega)}, \tag{6.11}$$

where k_0 is the large-amplitude wave number, ω_T is the plasma frequency of the trapped particles, and $\Omega = \omega - kv_\phi$. Equation (6.11) is a set of coupled equation; the zeroes of the determinant of the coefficients of E give us the stability properties of the system. We can simplify this set of equations by noting that the plasma does not support waves of frequency ω which are greatly different from the plasma frequency ω_p. For $\omega \simeq \omega_p$, the two dominant waves are $E(k,\omega)$ and $E(k - 2k_0, \omega - 2\omega_0)$, which lead to the dispersion relation

$$1 = \frac{\omega_T^2}{\Omega^2 - \omega_B^2}\left[\frac{1}{\epsilon_L(k,\omega)} + \frac{1}{\epsilon_L(k - 2k_0, \omega - 2\omega_0)}\right], \tag{6.12}$$

where

$$\epsilon_L(k,\omega) = 1 - \frac{\omega_p^2}{\omega^2 - 3k^2v_t^2} \tag{6.13}$$

is the dielectric function of the background plasma and v_t is the plasma electron thermal velocity. A numerical analysis (for the experimental parameters used by Wharton *et al.*) of Eq. (6.12) shows that an instability appears near ω_0 and k_0. The growth rate and the corresponding frequency as a function of k is shown in Fig. 55. We note that the growth rate forms a double-humped curve about k_0 suggesting the unstable upper and lower sidebands observed in the experiment. The upper curve of Fig. 56 shows the growth rate as a function of the bounce frequency. These growth rates are in reasonably good agreement with the observation of Wharton *et al.* For example, in the experiment for $\omega_B \simeq 0.07\,\omega_0$ and $v_T \simeq 0.26v_\phi$, the sidebands grew by a factor of 10 in a time of roughly $225\,\omega_p^{-1}$, giving $\gamma \simeq 5\times10^{-3}\,\omega_p$, which compares well with the theoretical value of $\gamma \simeq 8\times10^{-3}\,\omega_p$. The lower curve in Fig. 56 gives the frequency separation of the sidebands from a LAEP wave. This frequency separation is reasonably linear with the square root of the LAEP wave amplitude, in agreement with the experiment. The absolute value of $\Delta\omega$ is off from the experiment by about a factor of 2.

Thus we see that the simple parametric model of Kruer *et al.* explains qualitatively the experiments of Wharton *et al.* Using computer simulations, a further investigation of this instability was carried out by Kruer and Dawson (1970) and Denavit and Kruer (1971). Their results also agreed qualitatively with the experiments and the simple parametric model presented here.

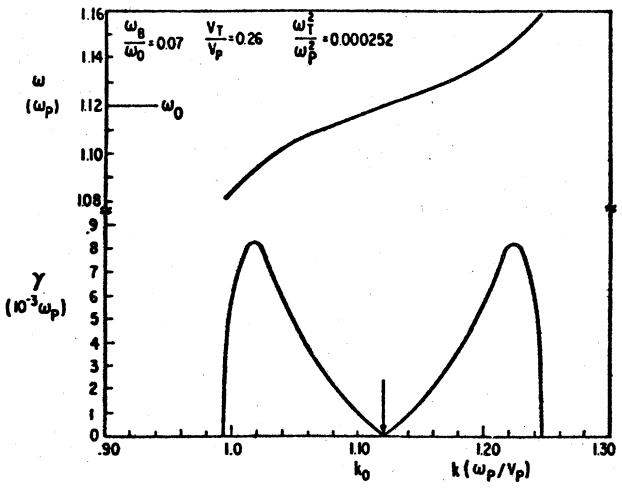

FIG. 55. Growth rate and frequency as functions of wave number. (After Kruer *et al.*, 1969.)

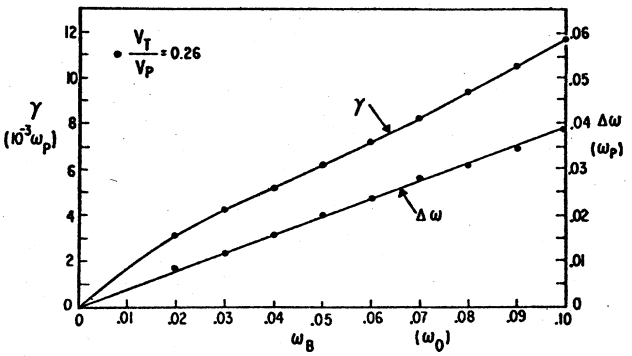

FIG. 56. Growth rate and frequency separation as functions of the bounce frequency. (After Kruer *et al.*, 1969.)

E. Quasilinear sideband theories

In the theories of O'Neil (1965) and Sugihara and Kamimura (1972), the interchange of energy between a single large-amplitude wave and the trapped electrons was considered. However, in the "quasilinear" sideband theories Bud'ko *et al.* (1972) and Brinca (1972) considered the further possibility of particle energy being put into other modes. This was done by considering either the direct relationship between wave and particle energies, or by using the linear Landau formula for the growth (damping) rate in conjunction with the distorted resonant velocity distribution. Using the approximation $f(v) = f(v_0) + \partial f/\partial v\,|_{v_0}(v - v_0)$, Brinca (1972) found that modes at velocities near the edge of the trapping region experienced a large growth in one positive half-cycle of oscillation, after which the sideband would be established. Bud'ko *et al.* extended the Taylor expansion to include the ergodic (stationary) contribution due to $\partial^2 f_0/\partial v^2$ (in addition to the oscillatory effect coming from the second term), which eventually dominates the growth above threshold. Their theory predicts that only a lower sideband $\omega_L \simeq \omega_0 - \omega_B v_g/v_\phi$ (where v_g and v_ϕ are the group and phase velocities of the LAEP wave) will be generated when the condition $\omega_0\omega_B/k_0^2 v_T^2 > \frac{1}{2}$ is satisfied. The growth rate of this sideband scales as $\phi_0^{1/2}$.

F. Recent experimental studies

In the light of these theories, further experiments have been carried out by various authors to check different aspects of the theoretical predictions. We shall briefly discuss some of the important experimental contributions from Franklin *et al.* (1972), Van Hoven and Jahns (1973, 1975), and DeNeff (1974).

In an attempt to study in detail the transition from linear Landau damping to the oscillatory behavior of an electron plasma wave, Franklin *et al.* (1972) carried out in a series of experiments in a collisionless, thermally ionized plasma. Their experimental setup was similar to that of Malmberg *et al.* The results showed qualitatively good agreement with the theory of Sugihara and Kamimura (1972). Figure 57 shows a comparison between the experimental and the theoretical growth curves for various values of $q = \gamma_L/\omega_B$. For $q \lesssim 0.04$ Franklin *et al.* reported the detection of sidebands above the background noise level. In a second series of experiments these authors studied the sideband instability in some detail. They demonstrated that the sideband frequency obeys the relationship $\omega - kv_\phi = \pm\omega_B$. Franklin *et al.* pointed out that for the case of Malmberg's experiment when $\Delta\omega \ll \omega_0$, then $\Delta\omega \approx \omega_B$. These authors also showed that the growth rate γ is proportional to $\phi^{1/2}$. From these results, they concluded that the amplification mechanism is a parametric coupling between the sideband frequencies and the oscillations of electrons trapped in the LAEP wave.

On the contrary, Van Hoven and Jahns (1975) found from their experiments that the sideband growth rate varies linearly as the wave potential (i.e., $\gamma \propto \phi_0^{1.2}$). Using an external signal at the sideband frequency, they launched a small-amplitude test wave in the presence of a LAEP wave to study the behavior of the sideband mode.

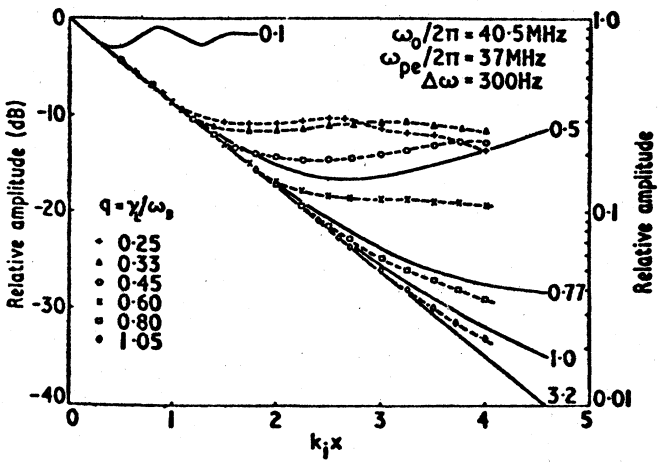

FIG. 57. Experimental data and theoretical curves showing relative spatial amplitude variations for different initial amplitudes. $k_0 = 3.64$ cm^{-1}, $k_i = 0.09$ cm^{-1}. (After Franklin *et al.*, 1972.)

What they observed was the following: (a) the test was damped faster than the linear Landau damping rate, in accord with the quasilinear theory of Brinca (1972). (b) the instability growth of the test wave depended on the initial amplitude of the LAEP wave and could persist after the LAEP wave field had decayed by tens of decibles. This implied that the driving force of the instability resided in the particles. This picture was also supported by measurements of the electron distribution function, which showed the establishment of the unstable distribution required by theory.

To further understand the behavior of the test wave DeNeef (1974) studied its behavior in the presence of a LAEP wave. He regarded the test wave as a modulation of the LAEP wave. This is true only if $\Delta\omega(=\omega - \omega_0)$ is small enough so that each trapped electron "sees" an essentially monochromatic wave during the transit time of the electron through the experiment. Thus, if $\Delta\omega < 2\pi v_\phi/L$ (where L is the length of the experimental region), the wave evolves in time as a sequence of almost monochromatic, large-amplitude waves in space, each of which differs slightly in amplitude and phase from its predecessor. From this point of view, the nonlinear dynamics are implicitly contained in the evolution of a monochromatic, large-amplitude wave, and it is not necessary to solve for the trapped electron orbits in order to determine the behavior of the test wave. Using this approach DeNeff has shown that the amplitude oscillations of the spontaneously unstable lower sideband agree well with the modulational calculation when the sideband frequencies lie within the range $\omega - 4\pi v_p/L < \omega < \omega_0$. Thus his experiments showed that the origin of the oscillating growth rate of the sideband may be explained by a slow modulation of the LAEP wave.

More recently Bussac *et al.* (1974) have proposed yet another mechanism for the sideband instability. According to these authors, the stability is attributed to a beam-type velocity distribution of detrapped electrons which are produced as a consequence of an initial wave

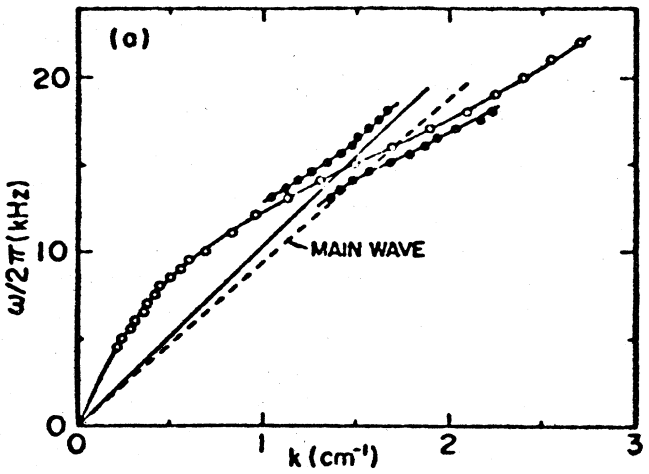

FIG. 58. (a) Linear dispersion relation without the main wave (MW) (open circles), which is split into two branches (closed circles) in the presence of the MW at 16 MHz. The dashed line corresponds to the phase velocity of the MW, v_M. A solid straight line shows a beam expected for the two-branch dispersion relation. (After Sato *et al.*, 1976.)

damping. The physical picture given by them is as follows. Assume an initial Maxwellian plasma where a monochromatic wave is injected at $t=0$. During the first half bounce period, trapped electrons with velocities $v < v_\phi$ are accelerated by the wave electric field, whereas electrons with $v > v_\phi$ are decelerated. If the damping rate is small enough compared to the bounce time, the net energy exchange between wave and particles tends to be zero. However, if these two scales are comparable, many of the accelerated particles are not reflected during the second half bounce period, and they become a beam of detrapped particles. On the other hand, reflected particles lose kinetic energy to the wave, inducing a new rise in the main-wave amplitude. A lower-amplitude oscillatory regime takes place when the slope of the distribution function of the remaining trapped particles is small enough. Then the main effect of the wave damping is to give rise to a beam of detrapped particles which are responsible for instability. This theoretical model has been checked by recent experiments of Starke and Malmberg (1976) and Sato *et al.* (1976). These authors studied the behavior of a continuously launched sinusoidal test wave in the presence of a LAEP wave. A typical dispersion relation is shown in Fig. 58 [after Sato *et al.* (1976)] where we notice the splitting of the dispersion into two branches in the presence of the LAEP wave, indicative of a beam-initiated instability.

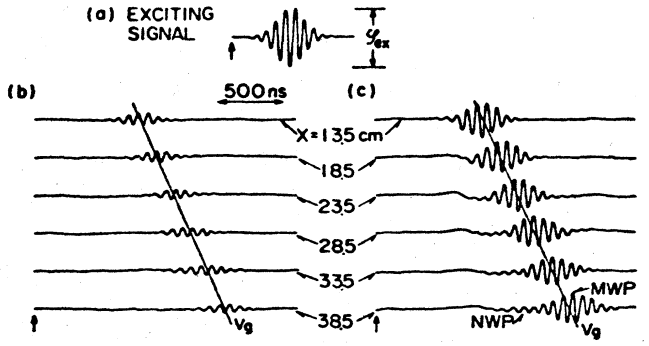

FIG. 59. (a) Excitation signal (carrier frequency $\omega/2\pi=14$ MHz). Corresponding temporal traces of wavepacket propagation for (b) $\phi_{ex}=0.5$ V and (c) $\phi_{ex}=1.5$ V at fixed positions X (distance from excitation position). Solid straight lines yield the group velocity v_g of the main wave packet. The vertical arrows show the starting positions of the traces. (After Sato *et al.*, 1977.)

To observe the temporal development of the detrapping of the electrons, Denavit and Sudan (1972) performed a series of numerical simulations studies. These authors found that particles with speeds equal to the group velocity v_g of the large-amplitude wave packet were trapped in the potential well. However, those which moved with the phase velocity v_ϕ such that $v_\phi > v_g$, passed through the wave packet. The wave amplitude, however, decreased gradually to zero toward its front even if there was no appreciable wave damping. Thus there appeared a group of correlated detrapped particles in front of the wave packet which was explained by the authors as the creation of a new wave packet. This theoretical prediction of Denavit and Sudan has recently been verified by Sato *et al.* (1977) in a series of experiments performed in a Q-machine (Motley, 1975). The electron plasma wave packet was generated by an external potential packet of peak amplitude ϕ_{ex}, which is shown in Fig. 59(a). In order to avoid strong Landau damping the carrier frequency ω was kept in the range $\omega \lesssim \omega_p$. Figure 59(b) shows the spatial evolution of the wave packet in the linear regime. It was found that the wave damps mainly as a result of Landau damping. However, for large values of ϕ_{ex} ($\gtrsim 1.2V$) we observe the generation of a new wave packet (NWP) [see Fig. 59(c) and 60(a)]. The peak amplitudes of the main wave packet (MWP) and the NWP are plotted as a function of ϕ_{ex} in Fig. 60(b). From Fig. 61 we see that for a fixed ϕ_{ex} the amplitude ratio of the NWP to the MWP depends on the frequency. (Landau damping is stronger at a higher frequency.) The speed of the NWP was found to be in the range of $1.1-1.2v_\phi$. The mechanism for generation of the detrapped electrons suggests that, if the MWP damps strongly, detrapped electrons are generated in the region near the excitation position. Since the correlated detrapped electrons constitute a kind of bounced beam the signal produced by them should not damp as strongly as the MWP (see Fig. 58).

To see the relationship between the new wave packet and the sideband instabilities (or test wave amplification), Sato *et al.* noted in their experiments that under the conditions where the NWP appears, they have also observed amplitude oscillation of the continuously launched wave. This amplitude oscillation was shown to be accompanied by a clear generation of the beam due to the detrapped electrons. The beam speed was nearly equal to the speed of the NWP. Thus these authors concluded that the NWP is due to the detrapped electrons. They also noted that the NWP appeared to originate near the position where the continuously launched wave had the first amplitude minimum.

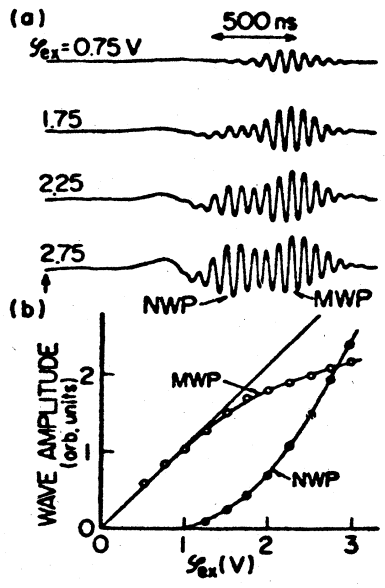

FIG. 60. Dependence of wave packet ($\omega/2\pi$=14 MHz) on ϕ_{ex} at X=40.5 cm. (a) Temporal shapes of wave packet and (b) peak amplitudes of the main wave packet (MWP) and the new wave packet (NWP) as a function of ϕ_{ex}. The normalized wave amplitude $e\phi/\kappa T_e$ is roughly estimated to be 0.1 for ϕ_{ex}=1.0 V by measuring a test wave dispersion relation in the presence of a large-amplitude continuously launched wave. (After Sato *et al.*, 1977.)

In conclusion it appears that at present no single theory can explain all aspects of the experimentally observed behavior of the sideband instability. This may be due to the different assumptions and models used in the various theories. Since the physics of the nonlinear evolution of a beam-generated large-amplitude wave is quite similar to that of the probe-launched LAEP wave, in this section we have not discussed experiments on the beam-excited waves. As the amplitude of the beam-generated waves grows, it tends to trap the beam particles, causing the instability to saturate. Some recent experiments on large-amplitude waves generated by beams have been carried out by Gentle and Roberson (1971), Van Wakeren and Hopman (1972), Gentle and Lohr (1973), and Seidl *et al.* (1976). We refer interested readers to these papers.

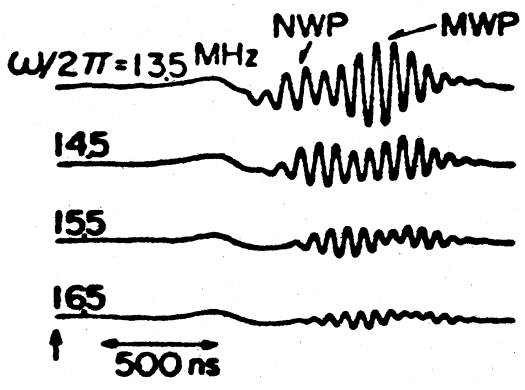

FIG. 61. Dependence of wave packet (temporal trace) on $\omega/2\pi$ for ϕ_{ex}=2.25 V at X=40.5 cm. (After Sato *et al.*, 1977.)

VII. ION ACOUSTIC SHOCKS AND SOLITONS

In this section we shall briefly review the physics of ion acoustic shocks and solitons, and the laboratory experimental observations of these phenomena. For a more extensive study of plasma shocks in general we refer the readers to the review papers and texts by Sagdeev (1966), Chu and Gross (1969), and Tidman and Krall (1971).

One of the most important results of nonlinear effects in plasma oscillations is to cause steepening of the leading edge of the wave. Unlike the case of ordinary gas dynamics, where dissipative effects are important for short-wavelength waves, in plasma dynamics it is often found that dispersion effects arising as a consequence of the departure from charge neutrality become significant as the steepness of the wave front increases. The difference between these two mechanisms is reflected in the mathematical structure of the original equations. Dissipative effects (viscosity, thermal conductivity, etc.) introduce irreversibility and increase the order of the derivatives in the dynamic equations by an odd number. Dispersion effects, on the other hand, do not affect reversibility and increase the order of the derivatives in the equations by an even number. Let us now consider a specific simple example of one-dimensional ion acoustic wave propagation for the case of $T_e \gg T_i$. The dynamic equations are

$$M\left(\frac{\partial v}{\partial t}+v\frac{\partial v}{\partial x}\right)=-e\frac{\partial \phi}{\partial x},$$

$$\frac{\partial n_i}{\partial t}+\frac{\partial (n_i v)}{\partial x}=0,$$

$$-\frac{\partial^2 \phi}{\partial x^2}=4\pi e(n_i-n_0\exp(e\phi/T_e)), \tag{7.1}$$

where M, v, n_i, and n_e are the ion mass, velocity, and ion and electron densities, respectively. Now if we assume quasineutrality [i.e., $n_i=n_e=n_0\exp(e\phi/T_e)$] for motions with a characteristic length much greater than the Debye length, then Eq. (7.1) can be reduced to

$$M\left(\frac{\partial v}{\partial t}+\frac{\partial v}{\partial x}\right)=-\frac{T}{n}\frac{\partial n}{\partial x}$$

$$\frac{\partial n}{\partial t}+\frac{\partial}{\partial x}(nv)=0. \tag{7.2}$$

Equation (7.2) is identical in form to the equations for isothermal motion (γ=1) in ordinary gas dynamics. It has been shown (Landau and Lifshitz, 1959) that the development of a finite-amplitude wave governed by Eq. (7.2) (which results in a steepening of the wave into a shock, i.e., a discontinuity in the wave form) is given by a Riemann solution. Thus, on the basis of the mathematical analogy, one would expect the presence of shock waves in collisionless plasmas. A set of equations anal-

ogous to Eq. (7.2), governing the nonlinear behavior of surface waves which propagate in a heavy fluid in a shallow channel, have been studied extensively. It was shown (using appropriate approximation) that in such a case the steepening of the wave was balanced by dispersion effects (as would be the case in collisionless plasmas). Not only were periodic waves found which were characterized by wavelengths of the order of the channel depth, it was also shown that "solitary" waves (propagation of isolated humps) could exist in the fluid channel. From these analogies, one would expect to observe both collisionless shock waves and solitons in a collisionless plasma.

To see how this comes about we follow the analysis of Sagdeev (1966). If we assume in Eq. (7.1) that all the quantities depend on x and t only in the form of $(x-ut)$, then Eq. (7.1) can be reduced to a single second-order differential equation for the potential

$$\phi'' = 4\pi n_0 e\left\{\frac{u}{\sqrt{u^2(2e\phi/M)}} - \exp\left(\frac{e\phi}{T_e}\right)\right\}. \tag{7.3}$$

Integrating Eq. (7.3) once, we have

$$-\frac{1}{2}(\phi')^2 = 4\pi n_0 e\left[-\frac{uM}{e}\sqrt{u^2-\frac{2e\phi}{m}} - \frac{T_e}{e}\exp\left(\frac{e\phi}{T_e}\right)\right] + C. \tag{7.4}$$

Depending on the choice of the integration constant C, various periodic waves can now be found. A special case is represented by the value of C given by the condition $\phi' \to 0$ when $\phi \to 0$, i.e.,

$$C = 4\pi n_0(Mu^2 + T_e).$$

This case corresponds to a solitary wave (see Fig. 62) which is a symmetric potential hill. The velocity of propagation u of this wave as a function $\phi_{\max}$ is given by

$$u^2 = \frac{T_e}{2M}\frac{[\exp(e\phi_{\max}/T_e)-1]^2}{\exp[e\phi_{\max}/T_e]-1-(e\phi_{\max}/T_e)}. \tag{7.5}$$

In the limit of $e\phi_{\max} \ll T_e$, n approaches the speed of sound $\sqrt{T_e}/M$. An upper bound on the amplitude for the ion waves (beyond which propagation is impossible) is given by $e\phi_{\max} = Mu^2/2$ or $e\phi_{\max} \simeq 1.3T_e$ which corresponds to a Mach number $M = u/(T_e/M)^{1/2} \simeq 1.6$.

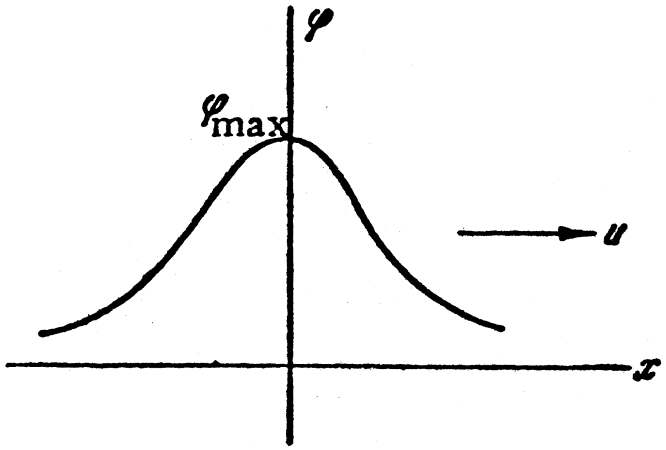

FIG. 62. A solitary wave propagating with speed u.

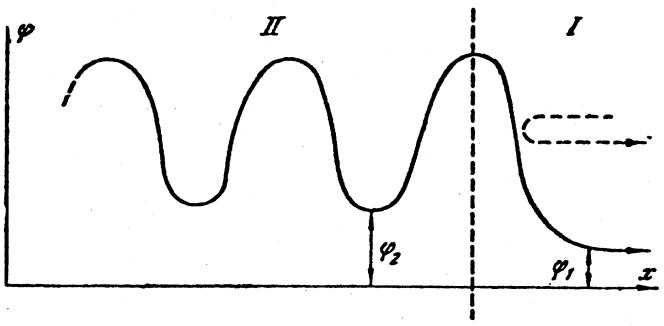

FIG. 63. A shock structure produced as a result of ion reflection. (Dashed arrow implies reflection of ions).

Thus far we see that in the absence of any dissipation we have a solitary wave, which is represented by a symmetric potential barrier. However, there are always ions which get reflected from a moving potential barrier, causing an asymmetry to arise, and beyond the barrier there are periodic oscillations. The net result is a peculiar kind of shock wave which connects two different plasma states: the unperturbed state (in front of the shock) and a state with intense ordered oscillations (behind the front). Figure 63 shows a schematic of the potential profile for the two regions. To take the

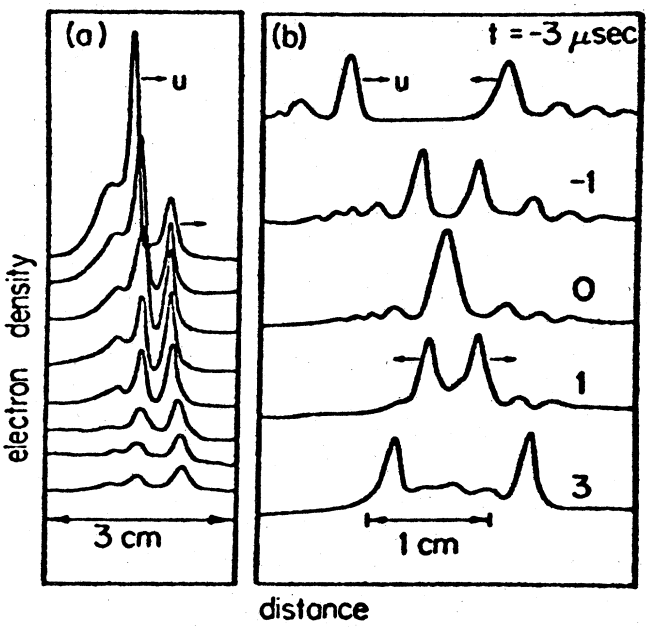

FIG. 64. Interactions of two solitons. (a) Two solitons propagate in the same direction in the laboratory frame. The figure is depicted in the wave frame such that the smaller soliton is initially stationary. Time differences between each adjacent two curves are 10μsec. (b) Two solitons propagating in opposite directions to each other, depicted in the laboratory frame. $\lambda_D \approx 2\times10^{-2}$ cm. (After Ikezi *et al.*, 1970.)

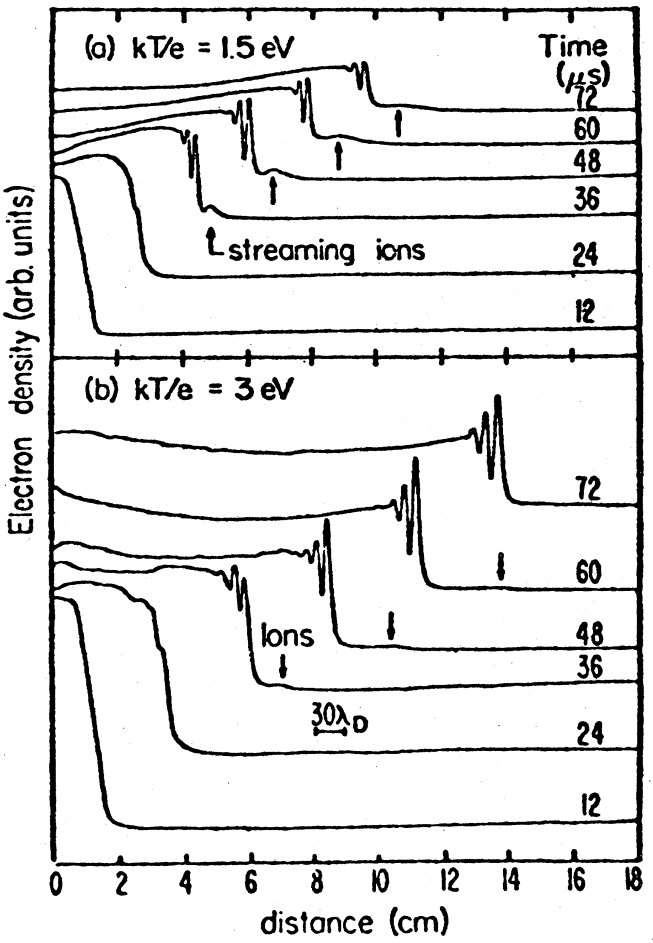

FIG. 65. Spatial plot of the shock propagation at (a) lower and (b) higher electron temperatures, showing variation in the amount of streaming ions, $T_j = 0.2$ eV; $n_0 = 10^9$ cm^{-3}; initial $\delta n_0 = 25\%$; excitation (a) 1 V, (b) 2 V. (After Taylor *et al.*, 1970.)

ion reflection into account, the equation for the potential for region (I) is modified from that of Eq. (7.4) by the presence of two additional terms on the right-hand side (Sagdeev, 1966)

$$-4\pi n_0 e f(\phi_1)\,\frac{u}{\sqrt{u^2-(2e\phi/T_e}} + 8\pi n_0 e f(\phi).$$

The first corresponds to the subtraction of the reflected ions from the total number of ions n_i; the second term represents the contribution of the reflected ions, where $n_0 f(\phi)$ is the total density of the reflected ions at a point characterized by the potential ϕ. The potential jump ϕ_1 is associated with ions that are reflected from the potential barrier and escape to infinity. The plasma state in region (II) is characterized by the quantities ϕ_{max} and ϕ_2 which determine the amplitude of the oscillations and their wavelength λ. Equation (7.4) still holds in this region.

Experimental observations of ion acoustic solitons were first made by Alikhanov *et al.* (1968) and later by Ikezi *et al.* (1970) in a double plasma device (Taylor *et al.*, 1969). In particular Ikezi *et al.* have shown (see Fig. 64) the stability of the interaction of two solitons: (a) different-amplitude solitons propagating in the same direction, with one overtaking the other, and (b) two solitons propagating in opposite directions to each other. The observations of collisionless electrostatic ion acoustic shocks were made by Alikhanov *et al.* (1968) and by Taylor *et al.* (1970). In Fig. 65 we show the shcok propagation (after Taylor *et al.*) for two different electron temperatures. We also notice the presence of streaming ions as predicted by the theory. More recently, studies on ion acoustic shocks and solitons have been carried out by Stern *et al.* (1971) and Ikezi *et al.* (1973).

In conclusion, we have reviewed very briefly in this section the propagation of collisionless ion acoustic solitons and shocks. In particular, we have shown that the presence of solitons is a consequence of the dispersive nature of the plasma and that if one takes into account ion reflection off the moving potential then a shock structure will develop.

ACKNOWLEDGMENTS

This research for one of us (MP) was supported in part by U. S. ERDA contract No. EX-76-A-01-2295.

REFERENCES

Aamodt, R. E., 1965, Phys. Rev. **138**, 45A.
Aamodt, R. E., and W. E. Drummond, 1966, in *Plasma Physics and Controlled Nuclear Fusion Research* (IAEA, Vienna), Vol. 1, p. 435.
Aamodt, R. E., and M. L. Sloan, 1967, Phys. Rev. Lett. **19**, 1227.
Aliev, Y. M., V. P. Silin, and C. Watson, 1966, Zh. Eksp. Teor. Fiz. **50**, 943 [Sov. Phys.-JETP **23**, 626 (1966)].
Alikhanov, S. G., V. G. Belan, and R. Z. Sagdeev, 1968, Zh. Eksp. Teor. Fiz. Pis'ma Red. **7**, 405.
Al'tshul', L. M., and V. I. Karpman, 1965, Zh. Eksp. Teor. Fiz. **49**, 515 [Sov. Phys.-JETP **22**, 361 (1966)].
Amano, T., and M. Okamoto, 1969 J. Phys. Soc. Jpn. **26**, 391.
Armstrong, T. P., 1967, Phys. Fluids **10**, 1269.
Arunasalam, V., M. A. Heald, and J. Sinnis, 1971, Phys. Fluids **14**, 1194.
Bailey, V. L., and J. Denavit, 1970, Phys. Fluids **13**, 451.
Baker, D. R., N. R. Ahern, and A. Y. Wong, 1968, Phys. Rev. Lett. **20**, 318.
Batanov, G. M., and K. A. Sarksyan, 1971, Zh. Eksp. Teor. Fiz. Pis'ma Red. **13**, 539 [JETP Lett. **13**, 384 (1971)].
Batanov, G. M., K. A. Sarksyan, and V. A. Silin, 1969, in the *Proceedings of the 9th International Conference on Phenomena in Ionized Gases*, Bucharest, p. 541.
Benford, G., and D. L. Correll, 1977, Phys. Fluids **20**, 811.
Benford, G., and J. J. Thomson, 1972, Phys. Fluids **15**, 1496.
Bengston, R. D., K. W. Gentle, J. Jancarik, S. S. Medley, P. Nielsen, and P. Phillips, 1975, Phys. Fluids **18**, 710.
Berger, R. L., L. Chen, and F. W. Perkins, 1976, Princeton Plasma Physics Laboratory Report PPL–1307 (to be published).
Berger, R. L., and R. W. Perkins, 1976, Phys. Fluids **19**, 406.
Bernabei, S., T. K. Chu, W. M. Hooke, and R. W. Motley, 1973, Bull. Am. Phys. Soc. **18**, 1314.
Bernabei, S., T. K. Chu, W. M. Hooke, and R. W. Motley, 1974, Second Topical Conference on R. F. Plasma Heating (Texas

Technical University, Lubbock, Texas). p. C5.
Bernstein, I. B., J. M. Greene, and M. D. Kruskal, 1957, Phys. Rev. **108**, 3.
Bezzerides, B., and D. F. DuBois, 1975, Phys. Rev. Lett. **34**, 1381.
Bezzerides, B., and J. Weinstock, 1972, Phys. Rev. Lett. **28**, 481.
Bobroff, D. L., 1965, J. Appl. Phys. **36**, 1760.
Bodner, S. E., G. F. Chapline, and J. DeGroot, 1973, J. Plasma Phys. **15**, 21.
Bohm, D., 1949, in *Characteristics of Electrical Discharges in Magnetic Fields*, edited by A. Guthrie and R. K. Wakerling (McGraw-Hill, New York), p. 65.
Brinca, A. L., 1972, J. Plasma Phys. **7**, 385.
Brusati, M., G. Cima, M. Fontanesi, and E. Sindoni, 1974, Nuovo Cimento Lett. **10**, 67.
Bud'ko, N. I., V. I. Karpman, and D. R. Shklyar, 1972, Sov. Phys.-JETP **34**, 778.
Bussac, M. N., I. Mendonca, R. Pellat, and A. Roux, 1974, Phys. Rev. Lett. **33**, 349.
Cano, R., C. Etiavan, I. Fidone, J. Olivain, M. Mattioli, and M. Perulli, 1967, Phys. Fluids **10**, 2260.
Carlson, H. C., W. Gordon, and R. L. Showen, 1972, J. Geophys. Res. **77**, 1242.
Chang, R. P. H., and M. Porkolab, 1970a, Phys. Fluids **13**, 2766.
Chang, R. P. H., and M. Porkolab, 1970b, Phys. Rev. Lett. **25**, 1262.
Chang, R. P. H., and M. Porkolab, 1972, Phys. Fluids **15**, 297.
Chang, R. P. H., and M. Porkolab, 1973, Phys. Rev. Lett. **31**, 1241.
Chang, R. P. H., and M. Porkolab, 1974, Phys. Rev. Lett. **32**, 1227.
Chang, R. P. H., M. Porkolab, and B. Grek, 1972, Phys. Lett. **29**, 206.
Chatelier, M., P. Lecoustey, and A. Samain, 1974, Phys. Rev. Lett. **32**, 366.
Choi, D., and W. Horton, 1974, Phys. Fluids **17**, 2048.
Choi, D., and W. Horton, 1975, Phys. Fluids **18**, 858.
Chu, C. K.. and R. A. Gross, 1969, in *Advances in Plasma Physics* (Wiley, New York), Vol. 2, p. 139.
Chu, T. K., S. Bernabei, and R. W. Motley, 1973, Phys. Rev. Lett. **31**, 211.
Chu, T. K., and H. Hendel, 1972, Phys. Rev. Lett. **29**, 634.
Coponi, M. Z., and R. C. Davidson, 1973, Phys. Rev. Lett. **31**, 86.
Coponi, M. Z., and R. C. Davidson, 1974, Phys. Fluids **17**, 1394.
Coppi, B., M. Rosenbluth, and R. N. Sudan, 1969, Ann. Phys. (N.Y.) **55**, 248.
Correll, D. L., N. Rynn, and H. Bohmer, 1975, Phys. Fluids **18**, 1800.
Coste, J., and J. Peyraud, 1969, J. Plasma Phys. **3**, 603.
Davidson, R. C., 1968, Phys. Rev. **176**, 344.
Davidson, R. C., 1969, Phys. Fluids **12**, 149.
Davidson, R. C., 1972, *Methods in Nonlinear Plasma Theory* (Academic, New York).
Davidson, R. C., and M. V. Goldman, 1968, Phys. Rev. Lett. **21**, 1671.
Dawson, J. M., 1961, Phys. Fluids **4**, 869.
Dawson, J. M., and R. Shanny, 1968, Phys. Fluids **11**, 1506.
DeGroot, J., and J. Katz, 1973, Phys. Fluids **16**, 401.
Denavit, J., and W. L. Kruer, 1971, Phys. Fluids **14**, 1782.
Denavit, J., and R. N. Sudan, 1972, Phys. Rev. Lett. **28**, 404.
DeNeff, P., 1974, Phys. Fluids **17**, 981.
Dikasov, V. M., L. I. Rudakov, and D. D. Ryutov, 1965, Zh. Eksp. Teor. Fiz. **48**, 913 [Sov. Phys.-JETP **21**, 608 (1965)].
Drake, J. F., P. K. Yaw, Y. C. Lee, G. Schmidt, C. S. Liu, and M. N. Rosenbluth, 1974, Phys. Fluids **17**, 778.
Dreicer, H., R. F. Ellis, and J. C. Ingraham, 1973, Phys. Rev. Lett. **31**, 426.
Dreicer, H., C. Ingraham, and D. Henderson, 1971, Phys. Rev. Lett. **26**, 1616.
Dreicer, H., C. Ingraham, and D. Henderson, 1972, Fifth European Conference on Controlled Fusion and Plasma Physics, Grenoble, France.
Drummond, W. E., and D. Ross, 1973, in *Proceedings of the Culham Symposium on Turbulence and Nonlinear Effects in Plasmas*, edited by B. E. Keen and E. W. Laing.
Drummond, W. E., and M. L. Sloan, 1971, Phys. Fluids **14**, 1431.
DuBois, D. F., 1974, in *Laser Interaction and Related Plasma Phenomena*, (Plenum, New York), Vol. 3A, p. 267.
DuBois, D. F., D. W. Forslund, and E. A. Williams, 1974, Phys. Rev. Lett. **33**, 1013.
DuBois, D. F., and M. V. Goldman, 1965a, Phys. Rev. Lett. **14**, 544.
DuBois, D. F., and M. V. Goldman, 1965b, Phys. Rev. **164**, 2–7.
DuBois, D. F., and M. V. Goldman, 1972, Phys. Fluids **15**, 919.
DuBois, D. F., M. V. Goldman, and D. McKinnis, 1973, Phys. Fluids **16**, 2257.
Dud'ko, N. I., V. I. Karpman, and D. R. Shklyar, 1972, Sov. Phys.-JETP **34**, 778.
Dum, C. T., 1975, Phys. Rev. Lett. **35**, 947.
Dum, C. T., and T. H. Dupree, 1970, Phys. Fluids **13**, 2308.
Dum, C. T., and E. Ott, 1971, Plasma Phys. **13**, 177.
Dum, C. T., and R. N. Sudan, 1969, Phys. Rev. Lett. **23**, 1149.
Dupree, T. H., 1966, Phys. Fluids **9**, 1773.
Dupree, T. H., 1967, Phys. Fluids **10**, 1049.
Dupree, T. H., 1970, Phys. Rev. Lett. **25**, 789.
Dupree, T. H., 1972, Phys. Fluids **15**, 334.
Dupree, T. H., 1974, Phys. Fluids **17**, 100.
Dupree, T. H., C. E. Wagner, and W. M. Manheimer, 1975, Phys. Fluids **18**, 1167.
Edgley, P. D., R. N. Franklin, S. M. Hamberger, and R. W. Motley, 1975, Phys. Rev. Lett. **34**, 1269.
Eidman, K., and R. Sigel, 1974, in *Laser Interaction and Related Plasma Phenomena*, (Plenum, New York), Vol. 3B, p. 667.
Ellis, R. A., and M. Porkolab, 1968, Phys. Rev. Lett. **21**, 529.
Eubank, H., 1971, Phys. Fluids **14**, 2551.
Farenik, V. I., V. V. Vlasov, and A. M. Rozhkov, 1973, Zh. Eksp. Teor. Pis'ma Red. **18**, 400 [JETP Lett. **18**, 240 (1973)].
Fejer, J. A., and Y. Y. Kuo, 1972, Phys. Rev. Lett. **29**, 1667.
Fisch, N. J., and A. Bers, 1975, Phys. Rev. Lett. **35**, 373.
Flick, J., 1975, Ph.D. Thesis, Department of Astrophysical Sciences, Princeton University.
Forslund, D. W., J. M. Kindel, K. Lee, and E. L. Lindman, 1975a, Phys. Rev. Lett. **34**, 193.
Forslund, D. W., J. M. Kindel, K. Lee, E. L. Lindman, and R. L. Morse, 1975b, Phys. Rev. A **11**, 679.
Forslund, D. W., J. M. Kindel, and E. L. Lindman, 1972, Phys. Rev. Lett. **29**, 249.
Forslund, D. W., J. M. Kindel, and E. L. Lindman, 1973, Phys. Rev. Lett. **30**, 739.
Franklin, R. N., S. M. Hamberger, H. Ikezi, G. Lampis, and G. J. Smith, 1972, Phys. Rev. Lett. **28**, 1114.
Franklin, R. N., S. M. Hamberger, G. Lampis, and G. J. Smith, 1971, Phys. Rev. Lett. **27**, 1119.
Franklin, R. N., S. M. Hamberger, and G. J. Smith, 1972, Phys. Rev. Lett. **29**, 914.
Freidberg, J. P., R. W. Mitchell, R. L. Morse, and L. G. Rudsinski, 1972, Phys. Rev. Lett. **28**, 795.
Frieman, E., and P. Rutherford, 1964, Ann. Phys. (N.Y.) **28**, 134.
Galeev, A. A., 1969, Zh. Eksp. Teor. Fiz. **59**, 1361 [Sov. Phys.-JETP **30**, 737 (1970)].
Galeev, A. A., and R. Z. Sagdeev, 1973, Nucl. Fusion **13**, 603.
Gary, S. P., 1967, Phys. Fluids **10**, 570.
Gekker, I. R., and O. V. Sizukhin, 1969a, Zh. Eksp. Teor. Pis'ma Red. **9**, 408 [JETP Lett. **9**, 243 (1969)].

Gekker, I. R., 1969b, *Proceedings of the 9th International Conference on Phenomena in Ionized Gases*, Bucharest, p. 542.
Gentle, K., 1972, Radio Sci. **7**, 799.
Gentle, K. W., and J. Lohr, 1973, Phys. Rev. Lett. **30**, 75.
Gentle, K. W., and A. Malein, 1971, Phys. Rev. Lett. **26**, 625.
Gentle, K. W., and C. W. Roberson, 1971, Phys. Fluids **14**, 2780.
Goforth, R., and K. W. Gentle, 1971, Phys. Fluids **14**, 2778.
Goforth, R., and K. W. Gentle, 1972, Phys. Fluids **15**, 1974.
Goldman, M. V., 1970, Phys. Fluids **13**, 1281.
Goldman, M. V., and H. L. Berk, 1971, Phys. Fluids **14**, 801.
Gould, R. W., 1969, Am. J. Phys. **37**, 585.
Gould, R. W., T. M. O'Neil, and J. H. Malmberg, 1967, Phys. Rev. Lett. **19**, 219.
Grek, B., 1975, Ph.D. Thesis, Department of Astrophysical Sciences, Princeton University.
Grek, B., and M. Porkolab, 1973, Phys. Rev. Lett. **30**, 836.
Guillemot, M., J. Olivain, F. Perceval, A. Quemeneur, and G. Matthieussent, 1971, Phys. Fluids **14**, 2065.
Hai, F., and A. Y. Wong, 1970, Phys. Fluids **13**, 672.
Hamberger, S. M., J. Jancarik, L. E. Wharp, D. A. Aldcroft, and A. Wetherell, 1971, in *Plasma Physics and Controlled Nuclear Fusion Research* (IAEA, Vienna), Vol. II, p. 37.
Harker, K. J., and F. W. Crawford, 1970, J. Geophys. Res. **75**, 5459.
Harms, K. D., G. Hasselberg, and A. Rogister, 1974a, Nucl. Fusion **14**, 251.
Harms, K. D., G. Hasselberg, and A. Rogister, 1974b, Nucl. Fusion **14**, 657.
Hasegawa, A., 1975, *Plasma Instabilities and Nonlinear Effects* (Springer, Berlin), p. 194.
Hasegawa, A., and L. Chen, 1975, Phys. Fluids **18**, 1321.
Hendel, H. W., and J. T. Flick, 1973, Phys. Rev. Lett. **31**, 199.
Hershcovitch, A., 1977, Sc.D. Thesis, Department of Nuclear Engineering, M.I.T.
Hinton, F., and C. Oberman, 1968, Phys. Fluids **11**, 1982.
Hiroe, S., and H. Ikegami, 1967, Phys. Rev. Lett. **19**, 1414.
Ikezi, H., 1973, Phys. Fluids **16**, 1668.
Ikezi, H., T. Kamimura, M. Kako, and K. E. Lonngren, 1973, Phys. Fluids **16**, 2167.
Ikezi, H., and Y. Kiwamoto, 1971, Phys. Rev. Lett. **27**, 718.
Ikezi, H., Y. Kiwamoto, K. Nishikawa, and K. Mima, 1972, Phys. Fluids **15**, 1605.
Ikezi, H., K. Nishikawa, and K. Mima, 1974a, J. Phys. Soc. Jpn. **37**, 766.
Ikezi, H., K. Nishikawa, and K. Mima, 1974b, in the *Proceedings of the Fifth International Conference on Plasma Physics and Controlled Nuclear Fusion Research*, Tokyo (IAEA, Vienna).
Ikezi, H., and N. Takahashi, 1968, Phys. Rev. Lett. **20**, 140.
Ikezi, H., N. Takahashi, and K. Nishikawa, 1969, Phys. Fluids **12**, 853.
Ikezi, H., R. J. Taylor, and D. R. Baker, 1970, Phys. Rev. Lett. **25**, 11.
Ivanov, A. A., and V. V. Parail, 1972, Zh. Eksp. Teor. Fiz. **62**, 932 [Sov. Phys.-JETP **35**, 494 (1972)].
Ivanov, N. V., I. A. Kovan, L. I. Koslov, E. V. Los', V. S. Svishchev, and N. N. Shvindt, 1972, Zh. Eksp. Teor. Pis'ma Red. **16**, 88 [JETP Lett. **16**, 60 (1972)].
Jackson, E. A., 1967, Phys. Rev. **153**, 203.
Jahns, G., and G. Van Hoven, 1973, Phys. Rev. Lett. **31**, 436.
Jahns, G., and G. Van Hoven, 1975, Phys. Fluids **18**, 214.
Jensen, T. H., J. H. Malmberg, and T. M. O'Neil, 1969, Phys. Fluids **12**, 1728.
Johnston, S., 1976, Phys. Fluids **19**, 93.
Joyce, G., D. Montgomery, and M. Emery, 1974, Phys. Fluids **17**, 110.
Kadomtsev, B. B., 1965, *Plasma Turbulence* (Academic, New York).
Kamimura, T., 1970, J. Phys. Soc. Jpn. **28**, 495.
Karney, C. F. F., A. Bers, and J. L. Kulp, 1973, Bull. Am. Phys. Soc. **18**, 1273.
Karpman, V., 1971, Plasma Phys. **13**, 477.
Kaufman, A. N., and L. Stenflo, 1975, Phys. Scr. **11**, 269.
Kaw, P. K., 1976, Princeton Plasma Physics Laboratory Report 1208.
Kaw, P. K., C. Z. Cheng, and L. Chen, Princeton Plasma Physics Laboratory Report 1305.
Kaw, P., and J. M. Dawson, 1969, Phys. Fluids **12**, 2586.
Kharchenko, I. F., Ya. B. Fainberg, R. M. Nikolayev, E. A. Kornilov, E. I. Lutsenko, and N. S. Pedenko, 1962, Nucl. Fusion Suppl. Part 3, 1101.
Kim, H. C., R. L. Stenzel, and A. Y. Wong, 1974, Phys. Rev. Lett. **33**, 886.
Kindel, J., M. H. Okuda, and J. M. Dawson, 1972, Phys. Rev. Lett. **29**, 995.
Kitsenko, A. B., V. I. Panchenko, and K. N. Stepanov, 1973, Zh. Tekh. Fiz. **43**, 1422, 1426, 1437 [Sov. Phys. Tech. Phys. **18**, 902, 905, 911 (1974)].
Kitsenko, A. B., and K. N. Stepanov, 1973, Zh. Eksp. Teor. Fiz. **64**, 1606 [Sov. Phys.-JETP **37**, 813 (1973)].
Kittel, C., 1976, *Introduction to Solid State Physics* (Wiley, New York).
Knorr, G., 1961, Z. Naturforsch, A **16**, 1320.
Knorr, G., 1963, Z. Naturforsch, A **18**, 1304.
Kroll, N. M., 1965, J. Appl. Phys. **36**, 34.
Kruer, W. L., and J. M. Dawson, 1972, Phys. Fluids **15**, 446.
Kruer, W. L., J. M. Dawson, and R. N. Sudan, 1969, Phys. Rev. Lett. **23**, 838.
Landau, L., 1946a, J. Phys. USSR **10**, 45.
Landau, L. D., 1946b, J. Phys. USSR **10**, 25.
Landau, L. D., and E. M. Lifshitz, 1959, *Fluid Mechanics* (Pergamon, London).
Lee, A., and G. Schmidt, 1970, Phys. Fluids **13**, 2546.
Liu, C. S., P. K. Kaw, and K. Nishikawa, 1976, in *Advances in Plasma Physics*, edited by A. Simon and W. B. Thompson (Wiley, New York), Vol. 6, p. 121.
Liu, C. S., M. N. Rosenbluth, and R. B. White, 1974, Phys. Fluids **17**, 1211.
Liu, C. S., and A. Y. Wong, 1970, Phys. Rev. Lett. **25**, 1702.
Lominadze, D. G., 1972, Zh. Eksp. Teor. Fiz. **63**, 1300 [Sov. Phys.-JETP **36**, 686 (1973)].
Mah, S. Q., H. M. Skarsgard, and A. R. Strilchuk, 1970, Phys. Rev. Lett. **25**, 1409.
Malmberg, J. H., and C. B. Wharton, 1967, Phys. Rev. Lett. **19**, 775.
Malmberg, J. H., C. B. Wharton, R. W. Gould, and T. M. O'Neil, 1968a, Phys. Fluids **11**, 1147.
Malmberg, J. H., C. B. Wharton, R. W. Gould, and T. M. O'Neil, 1968b, Phys. Rev. Lett. **20**, 95.
Manheimer, W. M., and E. Ott, 1974, Phys. Fluids **17**, 1413.
Martinov, N., and A. Samain, 1974, Plasma Phys. **15**, 783.
Matthieussent and Olivain, 1975, Phys. Rev. Lett. **34**, 1610.
Maxim, B. J., and A. W. Trivelpiece, 1965, J. Appl. Phys. **36**, 481.
Mikhailovskii, A. B., V. I. Petviashvili, and A. M. Fridman, 1976, JETP Lett. **24**, 43.
Mima, K., and K. Nishikawa, 1971, J. Phys. Soc. Jpn. **30**, 1722.
Mix, L. P., and G. Bekefi, 1972, Phys. Fluids **15**, 2020.
Mizuno, K., and J. S. DeGroot, 1975, Phys. Rev. Lett. **35**, 219.
Moeller, C., 1975, Phys. Fluids **18**, 89.
Morales, G. J., and Y. C. Lee, 1975, Phys. Rev. Lett. **35**, 930.
Morales, G. J., and T. M. O'Neil, 1972, Phys. Rev. Lett. **28**, 417.
Motley, R. W., 1975, *Q. Machines* (Academic, New York).
Motley, R. W., S. Bernabei, W. M. Hooke, and D. L. Jassby, 1975, Princeton Plasma Physics Laboratory Report 1117.
Murakami, M., and L. M. Lidsky, 1970, Phys. Rev. Lett. **24**, 297.
Nicholson, D. W., and A. N. Kaufman, 1974, Phys. Rev. Lett. **33**, 1207.

Nishikawa, K., 1968, J. Phys. Soc. Jpn. **24**, 916, 1152.
Nishikawa, K., 1970, J. Phys. Soc. Jpn. **29**, 449.
Nishikawa, K., H. Hojo, and K. Mima, 1974, Phys. Rev. Lett. **33**, 148.
Nuhrenberg, J., 1971, Z. Angew. Math. Phys. **22**, 1057.
Obenschain, S. P., N. C. Luhmann, Jr., and P. T. Greiling, 1976, Phys. Rev. Lett. **36**, 1309.
Okabayashi, M., K. Chen, and M. Porkolab, 1973, Phys. Rev. Lett. **31**, 1113.
Okuda, H., C. Chu, and J. M. Dawson, 1975, Phys. Fluids **18**, 243.
Okuda, H., and J. M. Dawson, 1973, Phys. Fluids **16**, 408.
O'Neil, T. M., 1965, Phys. Fluids **8**, 2255.
O'Neil, T. M., 1968, Phys. Fluids **11**, 1761.
O'Neil, T., and R. W. Gould, 1968, Phys. Fluids **11**, 134.
Ono, M., M. Porkolab, and R. P. H. Chang, 1977, Phys. Rev. Lett. **38**, 962.
Ott, E., 1975, Phys. Fluids **18**, 566.
Ott, E., and C. T. Dum, 1971, Phys. Fluids **14**, 959.
Perkins, F. W., and J. Flick, 1971, Phys. Fluids **14**, 2012.
Pesme, D., G. Laval, and R. Pellat, 1973, Phys. Rev. Lett. **31**, 203.
Petviashvili, V. I., 1976, JETP Lett. **23**, 627.
Porkolab, M., 1969, Phys. Fluids **12**, 1330.
Porkolab, M., 1972a, Nucl. Fusion **12**, 329.
Porkolab, M., 1972b, in the *Symposium on Plasma Heating and Injection*, Varenna, Italy (Editrice Compositori, Bologna), p. 54.
Porkolab, M., 1974a, Phys. Fluids **17**, 1432.
Porkolab, M., 1974b, in the *Symposium on Plasma Heating in Toroidal Devices*, Varenna, Italy (Editrice Compositori, Bologna), pp. 28–40.
Porkolab, M., 1976, Physica C **82**, 86.
Porkolab, M., 1978, Nucl. Fusion **13**, 367.
Porkolab, M., 1977b, Phys. Fluids **20**, 2058.
Porkolab, M., V. Arunasalam, and R. A. Ellis, Jr., 1972, Phys. Rev. Lett. **29**, 1438.
Porkolab, M., V. Arunasalam, and N. C. Luhmann, Jr., 1973, in the *Electromagnetic Wave Propagation Panel Symposium*, Edinburgh, Scotland (Technical Editing and Reproduction, London), p. D8.
Porkolab, M., V. Arunasalam, and N. C. Luhmann, Jr., 1975, Plasma Phys. **17**, 405.
Porkolab, M., V. Arunasalam, N. C. Luhmann, Jr., and J. P. M. Schmitt, 1975, Princeton Plasma Physics Laboratory Report MATT–1160.
Porkolab, M., V. Arunasalam, N. C. Luhmann, Jr., and J. P. M. Schmitt, 1976, Nucl. Fusion **16**, 269.
Porkolab, M., S. Bernabei, W. M. Hooke, R. W. Motley, and T. Nagashima, 1977, Phys. Rev. Lett. **38**, 230.
Porkolab, M., and R. P. H. Chang, 1969, Phys. Fluids **12**, 1697.
Porkolab, M., and R. P. H. Chang, 1970, Phys. Fluids **13**, 2054.
Porkolab, M., and R. P. H. Chang, 1972, Phys. Fluids **15**, 283.
Porkolab, M., and G. S. Kino, 1968, Phys. Fluids **11**, 34.
Porkolab, M., and J. Sinnis, 1968, Phys. Rev. Lett. **21**, 1227.
Porkolab, M., and J. Sinnis, 1969, Princeton University Report MATT-Q-26.
Pustovalov, V. V., and V. P. Silin, 1970, Zh. Eksp. Teor. Fiz. **59**, 2215 [Sov. Phys.-JETP **32**, 1198 (1971)].
Ripin, B. H., and R. E. Pechacek, 1970, Phys. Rev. Lett. **24**, 1330.
Ripin, B. H., and R. E. Pechacek, 1972, Phys. Fluids **15**, 1980.
Ripin, B. H., and R. E. Pechacek, 1973, Phys. Fluids **16**, 572.
Roberson, C., K. W. Gentle, and P. Nielsen, 1971, Phys. Rev. Lett. **26**, 226.
Rogister, A., 1975, Phys. Rev. Lett. **34**, 80.
Rosenbluth, M. N., 1972, Phys. Rev. Lett. **29**, 565.
Rosenbluth, M. N., B. Coppi, and R. N. Sudan, 1969, Ann. Phys. (N.Y.) **55**, 248.
Rosenbluth, M. N., R. B. White, and C. S. Liu, 1973, Phys. Rev. Lett. **31**, 1190.
Ross, D. W., 1969, Phys. Fluids **12**, 613.
Rudakov, L., and V. Tsytovich, 1970, Plasma Phys. **13**, 213.
Sagdeev, R. Z., 1966, in *Reviews of Plasma Physics*, edited by M. A. Leontovitch (Consultants Bureau, New York), Vol. 4, p. 23.
Sagdeev, R. Z., and A. A. Galeev, 1969, in *Nonlinear Plasma Theory*, edited by T. M. O'Neil and D. L. Book (Benjamin, New York).
Sato, N., G. Popa, E. Mark, R. Schrittwieser, and E. Mravlag, 1976, Phys. Rev. Lett. **37**, 1684.
Sato, N., K. Sakei, and R. Hatakeyama, 1977, Phys. Rev. Lett. **38**, 1480.
Schmidt, G., 1975a, Phys. Rev. Lett. **34**, 724.
Schmidt, G., 1975b, private communication.
Seidl, M., W. Carr, D. Boyd, and R. Jones, 1976, Phys. Fluids **19**, 78.
Sen, A., 1977, private communication.
Shapiro, V. D., 1963, Zh. Eksp. Teor, Fiz. **44**, 613 [Sov. Phys.-JETP **17**, 416 (1963)].
Silin, V. P., 1965, Sov. Phys.-JETP **21**, 1127.
Sitenko, A. G., N. Van Chong, and V. N. Pavlenko, 1970, Nucl. Fusion **10**, 259.
Sleeper, A. M., J. Weinstock, and B. Bezzerides, 1973, Phys. Fluids **16**, 1508.
Sloan, L., and W. E. Drummond, 1970, Phys. Fluids **13**, 2554.
Slusher, R. E., C. M. Surko, D. R. Moler, and M. Porkolab, 1976, Phys. Rev. Lett. **36**, 674.
Spatchek, K. H., P. K. Shukla, and M. Y. Yu, 1975, Phys. Lett. A **51**, 183.
Sperling, J. L., and F. W. Perkins, 1974, Phys. Fluids **17**, 1857.
Starke, T. P., and J. H. Malmberg, 1976, Phys. Rev. Lett. **37**, 505.
Stenzel, R. L., 1975, Phys. Rev. Lett. **35**, 574.
Stenzel, R. L., 1976, Phys. Fluids **19**, 865.
Stenzel, R. L., and A. Y. Wong, 1972, Phys. Rev. Lett. **28**, 274.
Stern, R. A., and J. F. Decker, 1971, Phys. Rev. Lett. **27**, 1266.
Stern, R. A., and N. Tzoar, 1966, Phys. Rev. Lett. **17**, 903.
Su, C., and C. Oberman, 1968, Phys. Rev. Lett. **20**, 427.
Sugai, H., M. Maruyama, M. Sato, and S. Takeda, 1977, Nagoya University preprint (to be published).
Sugihara, R., T. Kamimura, 1972, J. Phys. Soc. Japan **33**, 206.
Taylor, J. B., and B. McNamara, 1971, Phys. Fluids **14**, 1492.
Taylor, R. J., D. R. Baker, and H. Ikezi, 1970, Phys. Rev. Lett. **24**, 206.
Taylor, R. J., H. Ikezi, and K. R. MacKenzie, 1969, in *Proceedings of the International Conference on Physics of Quiescent Plasmas* (Ecole Polytechnique, Paris), Part 3, p. 57.
Thomson, J. J., 1975, Nucl. Fusion **15**, 237.
Thomson, J. J., R. J. Faehl, W. L. Kruer, and S. E. Bodner, 1974, Phys. Fluids **17**, 973.
Tidman, D. A., and N. A. Krall, 1971, *Shock Waves in Collisionless Plasmas* (Wiley, New York).
Trivelpiece, A. W., and R. W. Gould, 1959, J. Appl. Phys. **30**, 1784.
Tsytovich, V. N., 1970, *Nonlinear Effects in Plasma* (Plenum, New York).
Tsytovich, V. N., 1972, *An Introduction to the Theory of Plasma Turbulence* (Pergamon, New York).
Tsytovich, V. N., 1976, Physica C **82**, 141.
Utlaut, William F., and Robert Cohen, 1971, Science **174**, 245.
Valeo, E. J., and K. G. Estbrook, 1975, Phys. Rev. Lett. **34**, 1008.
Valeo, E. J., and W. L. Kruer, 1974, Phys. Rev. Lett. **33**, 750.
Valeo, E., and C. Oberman, 1973, Phys. Rev. Lett. **30**, 1035.
Valeo, E., C. Oberman, and F. W. Perkins, 1972, Phys. Rev. Lett. **28**, 340.

Van Hoven, G., and G. Jahns, 1975, Phys. Fluids **18**, 80.
Van Wakeren, J. H. A., and H. J. Hopman, 1972, Phys. Rev. Lett. **28**, 295.
Vdovin, V. L., O. A. Zinov'ev, A. A. Ivanov, L. L. Kozorovitskii, V. V. Parail, Ya. R. Rakhimbabaev, and V. D. Rusanov, 1971, Zh. Eksp. Teor. Fiz. Pis'ma Red. **14**, 228 [JETP Lett. **14**, 149 (1971)].
Vdovin, V. L., O. A. Zinov'ev, A. A. Ivanov, L. L. Kozorovitskii, V. V. Parail, Ya. R. Rakhimbabaev, and V. D. Rusanov, 1973, Zh. Eksp. Teor. Fiz. Pis'ma Red. **17**, 4 [JETP Lett. **17**, 2 (1973)].
Vedenov, A. A., and L. I. Rudakov, 1965, Sov. Phys. Doklady 9, 1073.
Voitsenya, V. S., A. Y. Voloshko, A. V. Longinov, G. A. Miroshnickhenko, G. Y. Nizhnik, and S. I. Solodovchenko, 1972, in *Proceedings of the Fifth European Conference on Controlled Fusion and Plasma Physics*, Grenoble, Volume 1, p. 111.
Voloshko, A. Y., V. S. Voitsenya, A. V. Lanyinov, G. A. Miroschnickhenko, G. Y. Nizhnik, and S. I. Solodovchenko, 1972, Zh. Eksp. Teor. Fiz. Pis'ma Red. **16**, 80 [JETP Lett. **16**, 54 (1972)].
Weinstock, J., 1968, Phys. Fluids **11**, 1977.
Weinstock, J., 1969, Phys. Fluids **12**, 1045.
Weinstock, J., and N. Bezzerides, 1973, Phys. Fluids **16**, 2287.
Weinstock, J., and N. Bezzerides, 1974, Phys. Rev. Lett. **32**, 754.
Wharton, C. B., J. H. Malmberg, and T. M. O'Neil, 1968 Fluids **11**, 1761.
Wong, A. Y., and D. Baker, 1969, Phys. Rev. **188**, 326.
Wong, A. Y., and R. L. Stenzel, 1975, Phys. Rev. Lett. **34**, 727.
Wong, A. Y., and R. J. Taylor, 1969, Phys. Rev. Lett. **23**, 958.
Wong, A. Y., and R. J. Taylor, 1971, Phys. Rev. Lett. **27**, 644.
Wong, H. V., 1972, Phys. Fluids **15**, 632.
Zakharov, V. E., 1972, Zh. Eksp. Teor. Fiz. **62**, 1475 [Sov. Phys.-JETP **35**, 908 (1972)].
Zakharov, V. E., and E. A. Kuznetsov, 1974, Zh. Eksp. Teor. Fiz. **66**, 594 [Sov. Phys.-JETP **39**, 285 (1974)].
Zavoisky, E. K., B. A. Demidov, Yu. G. Kalinin, A. G. Plakhov, L. I. Rudakov, V. E. Rusanov, V. A. Skoryupin, G. Ye. Smolkin, A. V. Titov, S. D. Franchenko, V. V. Shapkin, G. V. Sholin, 1972, Nucl. Fusion Suppl. p. 81.

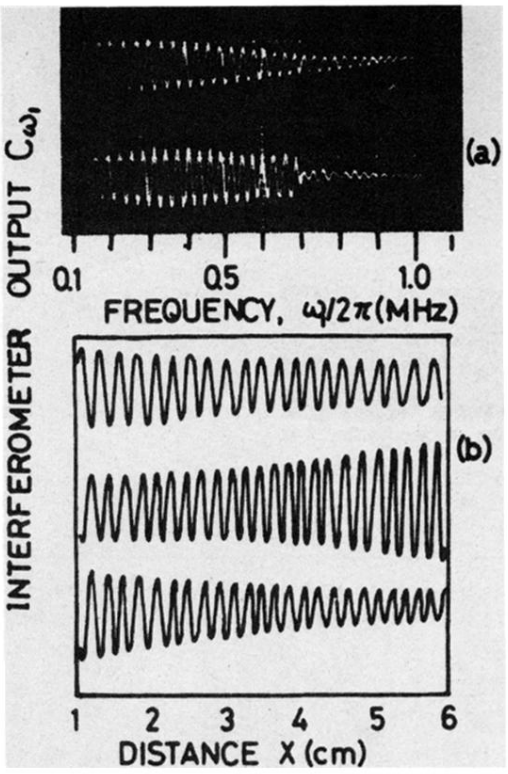

FIG. 13. (a) Interferometer output C_{ω_1} as a function of frequency ω_1. No wave ω_2 is excited in the top trace. The wave ω_2 is excited on the bottom trace and has a frequency 0.7 MHz. $\omega_{pi}/2\pi = 1.2$ MHZ. (b) Interferometer traces showing nonlinear growth and damping of wave $\omega_1/2\pi = 0.9$ MHz. Top trace, no wave ω_2. Middle trace, with wave $\omega_2/2\pi = 1.0$ MHz. Bottom trace, with wave $\omega_2/2\pi = 0.8$ MHz. $\omega_{pi}/2\pi = 1.3$ MHz. (After Ikezi and Kiwamoto, 1971.)

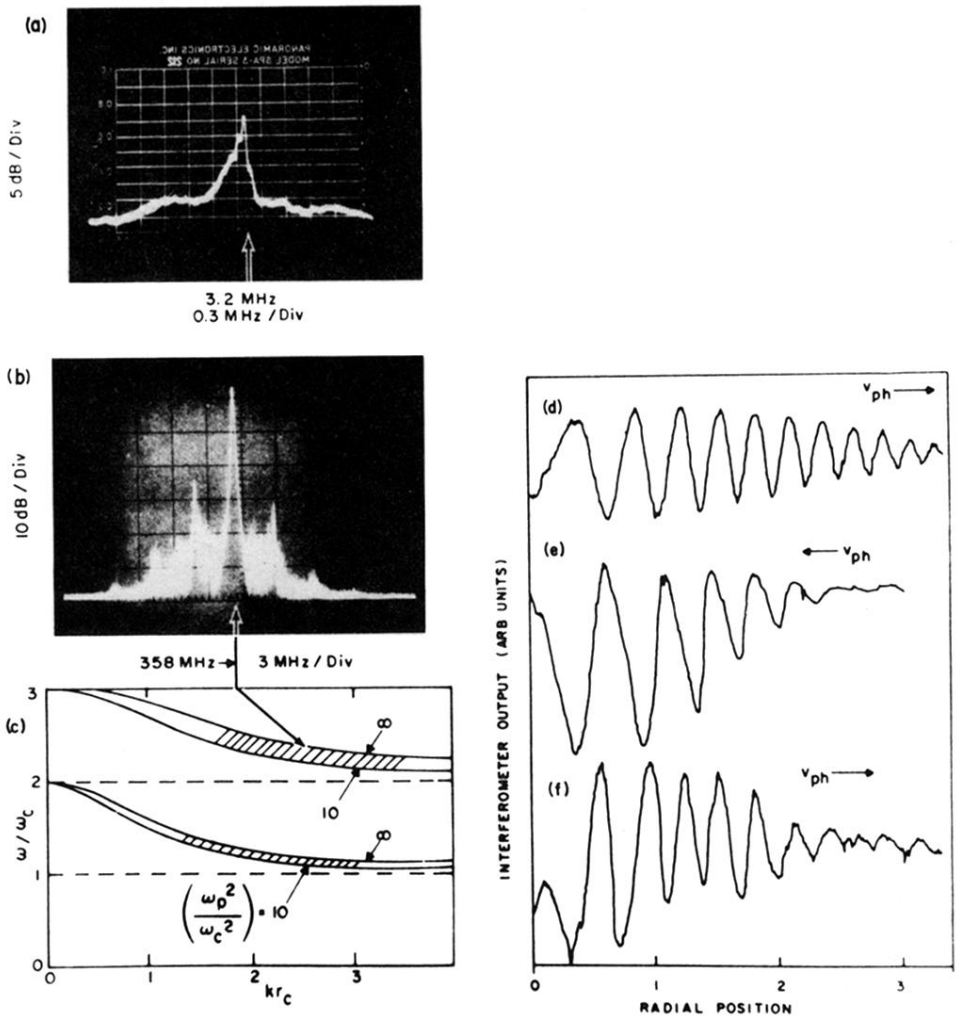

FIG. 29. Decay spectrum showing energy (frequency) conservation of: (a) low-frequency ion acoustic wave; (b) high-frequency cyclotron harmonic (Bernstein) waves, when pumped by $E_0 \perp B$ in the shaded regions of the dispersion curves of cyclotron harmonic waves. (c) The dispersion relation for the Bernstein waves. The momentum conservation is verified from the interferometer traces of the waves: (d) ion acoustic wave; (e) lower sideband (Bernstein wave); (f) upper sideband (Bernstein wave). (After Chang, Porkolab, and Grek, 1972.)

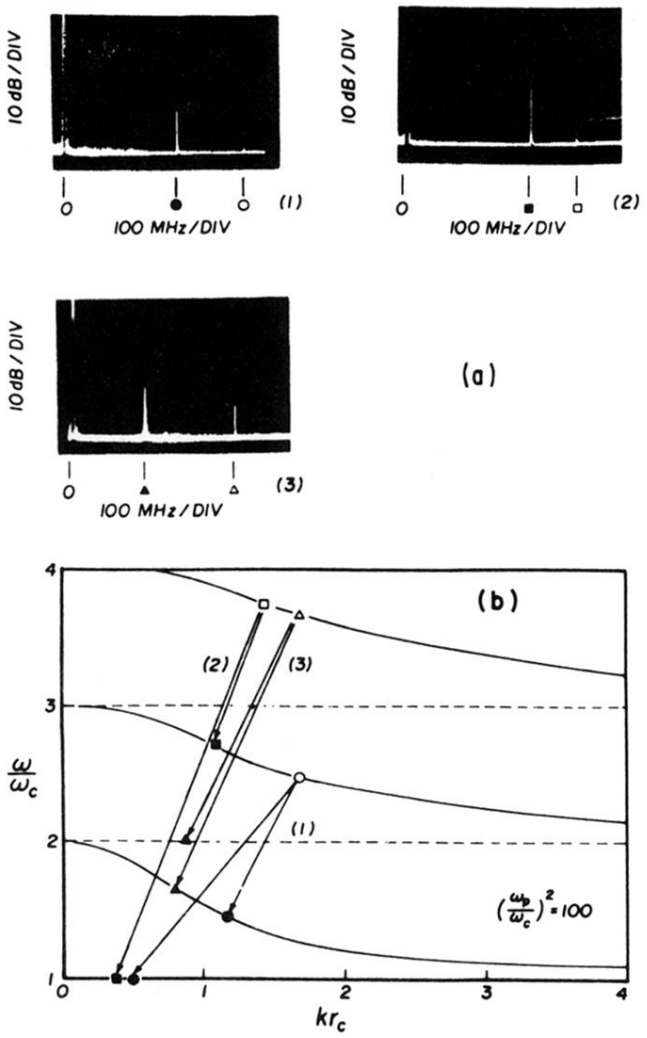

FIG. 9. (a) Spectra for three distinct cases of nonresonant decay. The finite-amplitude wave signal (hollowed symbols) is greatly attenuated by filtering. (b) Location of spectra (1), (2), and (3) on the linear dispersion diagram, with $k_{\parallel} = 0$. (In the experiment, $k_{\parallel}/k_{\perp} < 0.04$; thus these curves are a good approximation.) (After Chang and Porkolab, 1970, 1972.)